A METABOLIC SIGNAL FOR LOW BIOTIN TRANSCRIPTIONAL INDUCTION MEDIATED BY PYRUVATE CARBOXYLASE IN MYCOBACTERIUM SMEGMATIS

AND

RIP1 IN MYCOBACTERIUM TUBERCULOSIS RESPONSE TO IN VITRO AND IN VIVO STRESS

A Thesis

Presented to the Faculty of the Weill Cornell Graduate School

of Medical Sciences

in Partial Fulfillment of the Requirements for the Degree of

Doctor of Philosophy

by

Nathaniel Z. Lazar

January 2018

A METABOLIC SIGNAL FOR LOW BIOTIN TRANSCRIPTIONAL INDUCTION MEDIATED BY PYRUVATE CARBOXYLASE IN MYCOBACTERIUM SMEGMATIS

AND

RIP1 IN MYCOBACTERIUM TUBERCULOSIS RESPONSE TO IN VITRO AND IN VIVO STRESS

Nathaniel Lazar, Ph.D.

Cornell University 2018

Biotin is an essential cofactor utilized by all domains of life, but only synthesized by bacteria, fungi and plants, making biotin biosynthesis a target for antimicrobial development. We executed a genetic screen in *Mycobacterium smegmatis* and identified pyruvate carboxylase (Pyc) as required for biotin biosynthesis. *pyc*::*tn* fails to transcriptionally induce late stage biotin biosynthetic genes in low biotin conditions. Loss of the repressor *bioQ* in *pyc*::*tn* reverted biotin auxotrophy, as did reconstituting the pathway through heterologous expression of BioB and provision of DTB. The role of Pyc in biotin regulation required its catalytic activities and could be supported by *M. tuberculosis* Pyc. Pyc is the most rapidly depleted biotinylated protein after biotin withdrawal, indicating that it is a sensitive indicator of this state. Metabolomics revealed several dysregulated metabolites that could mediate BioQ derepression. Our data indicate that mycobacterial cells monitor biotin sufficiency through a metabolic signal generated by dysfunction of a biotinylated protein of central metabolism.

Rip1 is a site-2 protease required for full virulence in the mouse, but the causes of this phenotype have yet to be elucidated. We tested Δ*rip1* for defects in models of host-mediated stress and found that it is sensitive to nitric oxide (NO), hypoxia, and multiple classes of antibiotics. Further examination of the determinants of these sensitivities demonstrated differing requirements for Rip1 functions and substrates in each of these models. Δ*rip1* is not defective for induction of the DosR regulon, which links NO and hypoxia. Further, we reversed the Δ*rip1* sensitivity to antibiotics with addition of NaHS, but were unable to do so for NO or diamide.

To determine the contribution of NO to the Δ*rip1 in vivo* phenotype, we infected *nos2*$^{-/-}$ mice with Δ*rip1*. Δ*rip1* regained much of its virulence in *nos2*$^{-/-}$ mice, but did not recapitulate WT fully, indicating a partial role for NO. These mice developed granulomatous lesions, which are atypical of the murine model. Histopathological examinations demonstrated that these lesions possess numerous traits found in human pathology. We suggest that infection of *nos2*$^{-/-}$ with attenuated strains such as Δ*rip1* may be a useful model for studying the granuloma.

BIOGRAPHICAL SKETCH

Nathaniel Lazar attended Brandeis University from 2006 to 2010 and majored in Biochemistry and Biology. He joined the Immunology and Microbial Pathogenesis program at Weill Cornell Graduate School of Medical Sciences in 2010. He joined the Glickman lab in 2011, where he studied biotin biosynthesis in mycobacteria and the role of Rip1 in M. tuberculosis stress response.

ACKNOWLEDGMENTS

I would like to thank members of the Glickman lab past and present for their invaluable assistance to both the work in this thesis as well as for their positive attitudes. Particularly I would like to thank my advisor Dr. Michael Glickman, who exemplifies the ideals of science as an investigative process worth pursuing thoroughly. The contributions of everyone in the Glickman lab to my development as a researcher cannot be overstated.

I would also like to thank my family for their encouragement and unwavering belief in me.

TABLE OF CONTENTS

LIST OF FIGURES

LIST OF TABLES

LIST OF ABBREVIATIONS

ACP: acyl-carrier protein

AMP: adenosine monophosphate

ATc: anhydrotetracycline

B. subtilis: Bacillus subtilis

BC: biotin carboxylase

BCCP: biotin carboxyl carrier protein (biotin-binding domain)

CFU: colony forming unit

CO: carbon monoxide

CoA: coenzyme A

CRISPR: clustered regularly interspaced short palindromic repeats

CT: carboxytransferase

C_T: cycle threshold

DAPA: 7,8-diaminopelargonic acid

DAPI: 4,6-diamidino-2-phenylindole

DETA-NO: Diethylenetriamine-nitric oxide adduct

DNA: deoxyribonucleic acid

DTB: desthiobiotin

E. coli: *Escherichia coli*

ECF: extracytoplasmic function

EHR: enduring hypoxia response

EV: empty vector

H&E: hematoxylin and eosin

HA (tag): hemagglutinin

HRP: horseradish peroxidase

iNOS: inducible nitric oxide synthase

KAPA: 7-keto-8-aminopelargonic acid

LB: lysogeny broth

LC: liquid chromatography

M. tb: *Mycobacterium tuberculosis*

MIC: minimum inhibitory concentration

MOI: multiplicity of infection

mRNA: messenger ribonucleic acid

MS: mass spectrometry

NaHS: sodium hydrogen sulfide

NO: nitric oxide

OADC: oleic acid, albumin, dextrose, catalase supplement

OD: optical density (at 600 nm)

PBS: phosphate-buffered saline

qPCR: quantitative polymerase chain reaction

R. etli: *Rhizobium etli*

RIP: regulated intramembrane proteolysis

RPM: rotations per minute

RT: reverse transcriptase

S1P/S2P: site-1/site-2 protease

SD: Shine-Dalgarno sequence, the prokaryotic ribosome binding site

SDS: sodium dodecyl sulfate

tn: transposon

TSS: transcription start site

WT: wild type

LIST OF SYMBOLS

Δ: genetic deletion

σ: sigma (e.g. sigma factor, a bacterial transcription factor)

φ: phage, bacteriophage

~: approximate

:: : insertion

CHAPTER ONE: INTRODUCTION

Biotin biosynthesis has been incompletely characterized in *Mycobacterium smegmatis*[*]

Biotin (vitamin B7, or vitamin H) is an essential cofactor used by the carboxylase and decarboxylase family of enzymes. Whereas biotin is vital to and used by members of all domains of life, it is synthesized only by bacteria, plants, and fungi (Lin and Cronan 2011). For this reason, biotin biosynthesis has been proposed as a promising target for antibiotic development. In the human pathogen *M. tuberculosis*, depletion of the essential biotin biosynthetic protein BioA leads to bactericidality *in vitro* and clearance of *M. tuberculosis* from mice when BioA is depleted either in acute or persistent infection (Woong Park et al. 2011). The antibiotic amiclenomycin and its analogues inhibit BioA and show whole-cell activity against *M. tuberculosis* (Shi et al. 2011), and a target-based approach identified novel compounds with inhibitory activity against BioA (Park et al. 2015), many of which were also present in the diversity-oriented scaffolds (DOS) collection (Galloway, Isidro-Llobet, and Spring 2010). Further characterization of the biotin biosynthetic pathway may reveal additional antibiotic targets.

The latter stages of biotin biosynthesis are conserved among all organisms proficient for biotin biosynthesis. Pimeloyl-ACP/CoA is converted to biotin via the sequential action of four enzymes: BioF, BioA, BioD, and BioB. Thus far, no alternative pathway has been identified to perform this stage of biotin biosynthesis. In contrast, multiple different mechanisms have been shown to yield pimeloyl-ACP. In *E. coli*, the methyltransferase BioC allows malonyl-ACP

* This section is derived from: Lazar *et al* 2017 (in review)

to enter the fatty acid elongation pathway, and after two rounds of elongation, pimeloyl-ACP methyl ester exits the pathway when it is hydrolyzed by the methyl esterase BioH (Lin, Hanson, and Cronan 2010). *B. subtilis* has a cytochrome P450 enzyme (BioI) that can convert long-chain fatty acids to pimeloyl-ACP, and also possesses a pathway which converts free pimelic acid to pimeloyl-CoA using the enzyme BioW (Cryle 2010, Lin and Cronan 2011) (Summarized in Figure 1). Recent evidence indicates that BioW is the dominant pathway in *B. subtilis* (Manandhar and Cronan, 2017).

As biotin biosynthesis is an energetically costly process, many biotin prototrophs have evolved mechanisms to control the transcription of biotin biosynthetic genes such that expression is induced when exogenous biotin is not available. *E. coli* possesses a bifunctional biotin ligase BirA, which acts as a biotin ligase to covalently attach biotin to biotin-utilizing enzymes, and as a transcriptional regulator of biotin biosynthesis (Cronan 1988). In biotin-replete conditions, BirA forms a homodimer, which binds the biotin operator and represses the transcription of *bioFADBC*. In biotin-starved conditions, unbiotinylated biotin binding proteins (AccB) competitively bind to single BirA proteins to form BirA-AccB heterodimers, which do not possess repressor activity (Chakravartty and Cronan 2012, Solbiati and Cronan 2010, Weaver et al. 2001). As such, in *E. coli*, biotin biosynthesis is coupled to the accumulation of an unbiotinylated protein through the bifunctional BirA.

In contrast, *Brucella* and other *Alphaproteobacteria* utilize the GntR family protein BioR to repress expression of *bioFADBZ* and of the biotin transporter *bioY* during biotin-replete conditions (Feng, Zhang, and Cronan 2013, Feng et al. 2013). The mechanism of this repression is poorly understood, but *Brucella* (type I, or unifunctional) BirA lacks the DNA-binding domain found in *E. coli*

Figure 1: Summary of previously-characterized biotin biosynthetic pathway.

Late (green box) biotin biosynthesis is conserved in all biotin-synthesizing organisms and is catalyzed by the action of four enzymes: BioF, BioA, BioD, and BioB, which convert pimeloyl-ACP/CoA to Biotin. Synthesis of the pimeloyl-ACP moiety differs between bacteria. In E. coli (red box), BioC methylates malonyl-ACP to form malonyl-ACP methyl ester, which then enters the fatty-acid elongation pathway. BioH demethylates pimeloyl-ACP methyl ester to form pimeloyl-ACP (Lin, Hanson, and Cronan 2010). In contrast, B. subtilis (blue box) utilizes BioI to break down long-chain fatty acids into pimeloyl-ACP. A secondary pathway exists in which free pimelic acid is converted to pimeloyl-ACP by BioW (Cryle 2010).

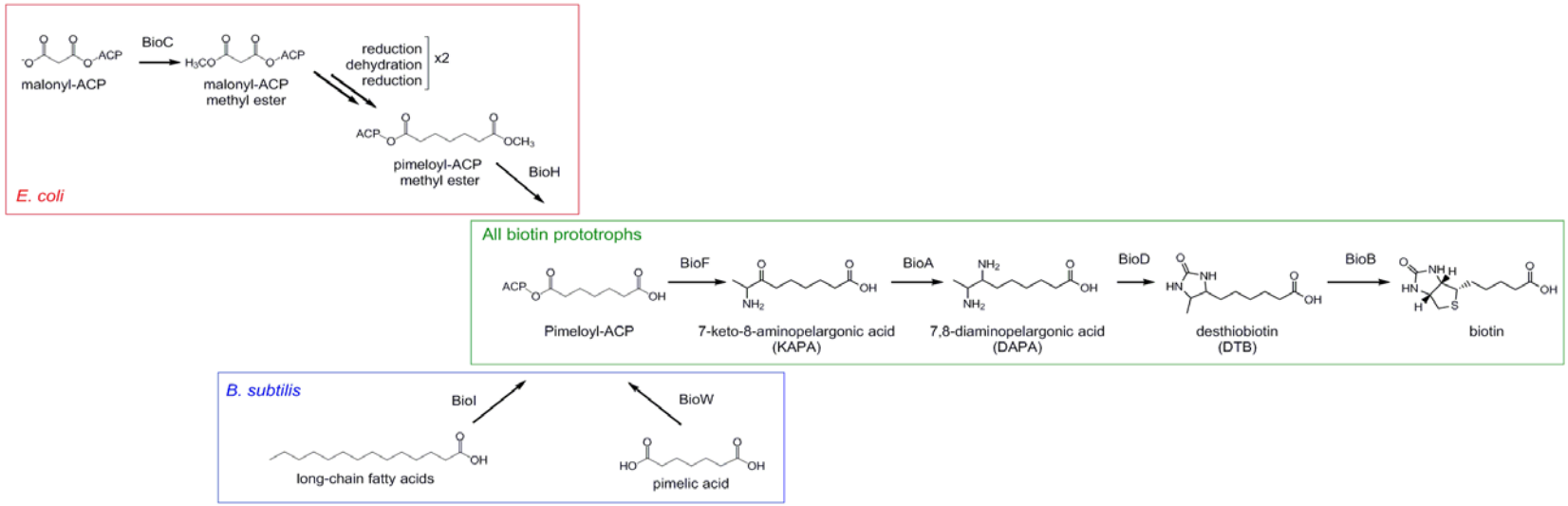
E. coli
malonyl-ACP
BioC
malonyl-ACP
methyl ester
reduction
dehydration
reduction
x2
pimeloyl-ACP
methyl ester
BioH
All biotin prototrophs
Pimeloyl-ACP
BioF
7-keto-8-aminopelargonic acid
(KAPA)
BioA
7,8-diaminopelargonic acid
(DAPA)
BioD
desthiobiotin
(DTB)
BioB
biotin
B. subtilis
BioI
long-chain fatty acids
BioW
pimelic acid

BirA (Beckett 2007). Along with many other *Actinobacteria*, *Mycobacteria* also possess a type I BirA protein, and the soil bacterium *M. smegmatis* has recently been discovered to employ the TetR family protein BioQ as a transcriptional regulator of *bioFDB* expression (Tang et al. 2014). TetR family proteins typically repress transcription in the absence of their ligand, and dissociate from DNA after ligand binding triggers a conformational shift in their helix-turn-helix DNA binding domain (Ramos et al. 2005). As is the case in *Alphaproteobacteria,* the mechanism of BioQ derepression is poorly characterized, though it has been shown that biotin itself is not the ligand of BioQ (Tang et al. 2014), suggesting that some alternate non-biotin ligand mediates BioQ release from its operator. Although TetR like repressors are abundant in *M. tuberculosis*, it lacks a predicted ortholog to BioQ and the transcriptional regulation of biotin in *M. tuberculosis* has not been elucidated (summarized in Figure 2).

In this study we undertook a genetic screen in *M. smegmatis* for biotin auxotrophs. In addition to identifying previously known late stage biotin biosynthetic genes, we identified multiple transposon insertions in pyruvate carboxylase (*pyc*) as conferring biotin auxotrophy. Analysis of *pyc* null strains supports a model in which dysfunction of Pyc during biotin depletion, itself a biotin dependent enzyme, generates a metabolic signal that stimulates BioQ derepression.

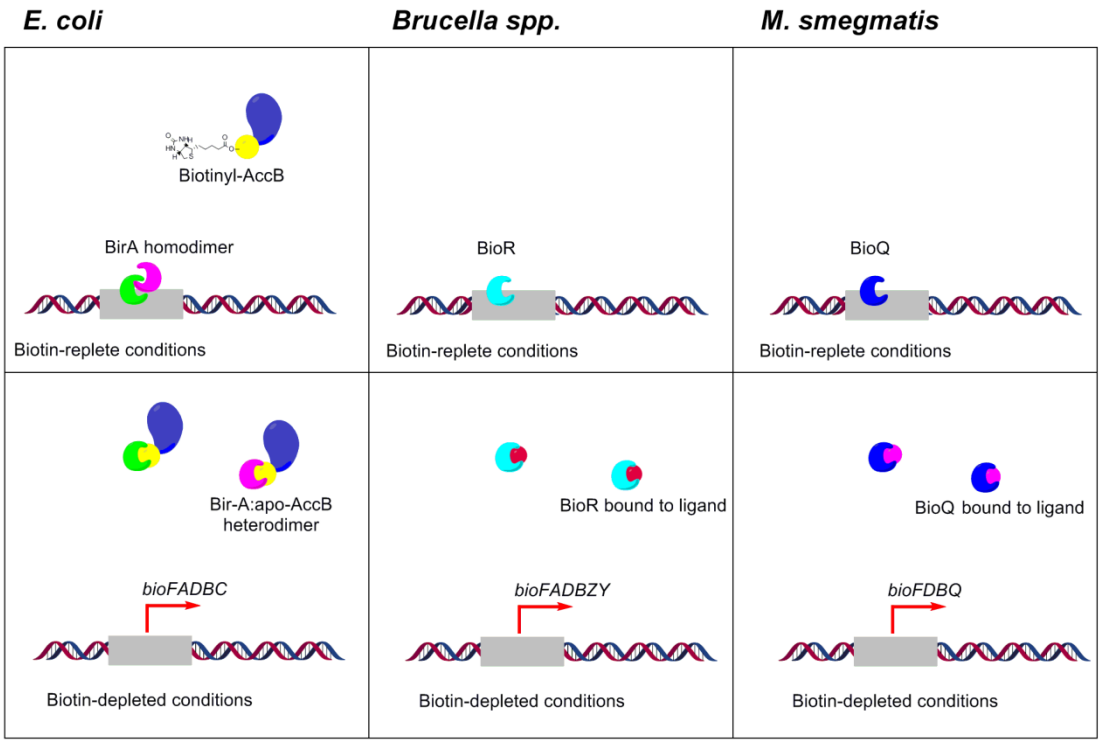

Figure 2: Summary of transcriptional regulation of biotin biosynthesis

E. coli (left) possesses a bifunctional biotin ligase (BirA) which is responsible for both the attachment of biotin to and for transcriptional regulation of biotin biosynthesis. When biotin-binding proteins are saturated with biotin BirA forms a homodimer with repressive function. When biotin is absent, unbiotinylated (*i.e.* apo-) biotin-binding proteins bind to BirA and relieve its repressive activity. (Beckett 2007) *Brucella* and *M. smegmatis* possess a biotin ligase with no repressive activity. *Brucella* (center) utilizes the repressor BioR to regulate transcription of biotin biosynthetic genes. In the absence of biotin, BioR binds its ligand and transcription is derepressed (Feng, Zhang, and Cronan 2013, Feng et al. 2013). *M. smegmatis* (right) utilizes BioQ to repress biotin transcription in the presence of biotin. In the absence of biotin, BioQ binds to its ligand and transcription is derepressed (Tang et al. 2014).

Rip1 is a site-2 protease essential for *M. tuberculosis* virulence

M. tuberculosis is a human pathogen with global health relevance (Sia and Wieland 2011, Raviglione and Sulis 2016, Zaman 2010, Gupta, Espinal, and Raviglione 2004). Upon being transmitted via the aerosol route, *M. tb* is internalized within the phagosome of the alveolar macrophage, where it is subject to numerous host-mediated stresses (van Crevel, Ottenhoff, and van der Meer 2002, Bordbar et al. 2010). Despite being localized to this environment, *M. tb* is nonetheless able to avoid killing and to establish either a latent or active infection (Goldberg, Saini, and Porcelli 2014, Behar, Divangahi, and Remold 2010, Stallings and Glickman 2010). Our interest is to examine one of the mechanisms *M. tb* utilizes to sense and to respond to host-mediated stresses.

The site-2 protease (S2P) family of proteins is utilized throughout the bacterial domain in the process of regulated intramembrane proteolysis (RIP) as part of a signal transduction pathway in order to produce a transcriptional response to stress in the periplasm or outside of the cell (Schneider and Glickman 2013, Rudner, Fawcett, and Losick 1999). S2Ps are intramembrane proteases; that is, they cleave a membrane protein at a site inside or directly adjacent to the plasma membrane (Urban 2009). Upon the initiation of stress, a site-1 protease (S1P) cleaves a membrane protein at a site in the periplasm. This proteolytic cleavage converts this membrane protein into a substrate for the site-2 protease, which then further cleaves it at a site in the plasma membrane. The cleavage event catalyzed by the site-2 protease releases the intracellular section of the membrane protein from the membrane, and with it a peripheral membrane protein which had been tethered to the membrane with it. This allows the peripheral protein to translocate to the chromosome and to

bind to its cognate promoter, where it acts as a transcription factor and drives a transcriptional response to the stress which initiated the beginning S1P cleavage event.

One of the best-studied RIP pathways is the DegS/RseP pathway in *E. coli*. The S1P DegS cleaves the anti-sigma factor anti-σ_E (RseA) in response to mislocalized membrane proteins or unfolded proteins in the periplasm (Chaba et al. 2011). RseA is then cleaved by the site-2 protease RseP (Koide, Ito, and Akiyama 2008), which releases σ_E (RpoE) from the membrane whereupon it acts as a transcription factor (Rhodius et al. 2006). RpoE is a member of the extracytoplasmic function (ECF) family of sigma factors which drives the transcription of several genes (Helmann 2002, Heinrich and Wiegert 2009). Previous work in the Glickman lab identified three members of the S2P family in *M. tb* via homology search, and further demonstrated that one of these proteins--Rip1 (Rv2869c)-- was essential for virulence, while the other two members are each dispensable (Makinoshima and Glickman 2005). A Δ*rip1* null mutant was highly attenuated for virulence in both the acute and the persistence phases of mouse infection. Further work showed that four anti-sigma factors: anti-σ_K, σ_L, σ_M, and σ_D were substrates of Rip1 (Sklar et al. 2010, Schneider, Sklar, and Glickman 2014), though genes outside the union of these four sigma factor operons remain. Additionally, a $\Delta\sigma_K/\sigma_L/\sigma_M$ triple mutant failed to recapitulate the Δ*rip1* mouse phenotype (Schneider, Sklar, and Glickman 2014). While a $\Delta\sigma_K/\sigma_L/\sigma_M/\sigma_D$ mutant has yet to be constructed or tested, these data indicate that we have yet to uncover the full mechanism of Rip1-mediated gene regulation. Additional work in the Glickman lab characterized the role of the protein-binding PDZ domain (Kroos and Akiyama

2013, Walsh et al. 2003) in both tethering substrates to Rip1 and additionally as a negative regulator of Rip1 function (Schneider et al. 2013).

Below, we describe our attempt to understand the role of Rip1 in *M. tb* virulence from a new perspective. We directly test Δ*rip1 M. tb* for defects in various *in vitro* models of host-mediated stress. We find that the Δ*rip1* strain is attenuated when treated with the nitric oxide donor DETA-NO, as well as in the Wayne model of anaerobiosis. Additionally, we found that Δ*rip1* is susceptible to multiple classes of antibiotic. We analyze the contributions of sigma factors, Rip1 catalytic activity, and the PDZ domain to these phenotypes.

The phenotype of Δ*rip1 M. tuberculosis* in *nos2*$^{-/-}$ mice

While Δ*rip1 M. tb* shows a striking defect in the mouse model of infection, this model may understate or misrepresent the role of Rip1. The granuloma—or tubercule—is the hallmark of pulmonary infection in human disease (Guirado and Schlesinger 2013, Ehlers and Schaible 2012). It is controversial whether the granuloma is a mechanism of host control of the pathogen or whether it is induced by the pathogen to enable virulence; there is growing evidence that both of these are true and that the granuloma is the result of a complex interplay between host and pathogen (Silva Miranda et al. 2012, Ramakrishnan 2012, Rubin 2009). However, it is clear that the mouse, which is not a host for *M. tuberculosis* in the wild, does not form granulomas in response to *M. tb* infection, while other models including guinea pigs, zebrafish, and nonhuman primates do develop these lesions (Pozos and Ramakrishnan 2004, Via et al. 2008). For reasons of practicality, expense, and because mouse genetics have been well-characterized—specifically with

respect to the mouse immune system—the mouse model remains one of the primary tools used to study the virulence of *M. tb* and the host immune response to it.

Human granulomas have numerous characteristics which distinguish themselves from non-granulomatous lesions. Granulomas possess a distinct organization of immune subsets from center to periphery, with the center of the lesion comprised of mostly macrophages and the periphery containing lymphocytes and dendritic cells, along with foamy macrophages (Guirado and Schlesinger 2013, Russell et al. 2009, Ehlers and Schaible 2012). Along with its immune organization, these lesions are typified by fibrosis surrounding the outside of the granuloma (Solsona Peiro, de Souza Galvao, and Altet Gomez 2014, Subbian et al. 2011). The center of the lesion may be cellular, necrotic, or cavitating (Ehlers and Schaible 2012), wit h the development of hypoxia also seen as a hallmark of the granuloma and specifically as a means of host control of the pathogen(Datta et al. 2016, Rustad et al. 2009, Via et al. 2008). Mouse models of infection which do not recapitulate hypoxia specifically may be a poor choice for elucidating certain aspects of the Δ*rip1* defect.

As we found that Δ*rip1* is susceptible to the nitric oxide donor DETA-NO in an *in vitro* model, we infected *nos2*$^{-/-}$ (iNOS knockout) mice with Δ*rip1* to determine the contribution of nitric oxide to the Δ*rip1 in vivo* phenotype. The iNOS knockout mouse has been well-studied as a means of showing the relevance of nitric oxide Δ*rip1* virulence was significantly, but not totally restored. Surprisingly, iNOS knockout mice developed granulomatous lesions rather than the non-granulomatous lesions typical of mouse infections. Further work characterizing these granulomas showed that they indeed demonstrate several aspects of pathology found in humans and non-mouse mammals.

CHAPTER TWO: A METABOLIC SIGNAL FOR LOW BIOTIN TRANSCRIPTIONAL INDUCTION MEDIATED BY PYRUVATE CARBOXYLASE IN MYCOBACTERIUM SMEGMATIS*

Disruption of *MSmeg_2412* confers biotin auxotrophy

To identify new genes involved in biotin biosynthesis in mycobacteria, we employed a forward genetics approach using the mycobacteriophage φMycoMarT7. We constructed a library of approximately 10,000 transposon insertion mutants in *M. smegmatis* mc^2155 strain, and screened these mutants for inability to grow on medium lacking biotin. This strategy identified insertions in the previously characterized biotin biosynthetic genes *bioA*, *bioB*, and *bioF* as conferring biotin auxotrophy. Three strains, each bearing independent transposon insertions in *MSmeg_2412*, were unable to grow on medium lacking biotin (Table 1). *MSmeg_2412* encodes pyruvate carboxylase, an enzyme of central carbon metabolism not previously implicated in biotin biosynthesis. Pyruvate carboxylase converts pyruvate to oxaloacetate utilizing biotin as an essential cofactor (Jitrapakdee et al. 2008, Yu et al. 2009), and has been shown to have roles in anaplerosis, gluconeogenesis, elongation of fatty acids, and branched-chain amino acid biosynthesis (Peters-Wendisch et al. 1998, Attwood 1995, Sauer and Eikmanns 2005, Owen, Kalhan, and Hanson 2002, Mukhopadhyay and Purwantini 2000)..

We proceeded to confirm that disruption of pyruvate carboxylase itself, rather than second-site mutations or polar effects, was responsible for the inability of pyruvate carboxylase insertion mutants to grow on medium lacking biotin. To do so, we complemented these strains with plasmids expressing

* This chapter is derived from: Lazar *et al* 2017 (in review)

Table 1: Biotin auxotrophic Transposon mutants.

Mutant #	**MGM #**	**gene**	**Gene length (NT)**	**Nucleotide at tn insertion**	**orientation of tn (relative to coding sequence)**
10	8001	*MSmeg_2412*	3381	2061-2062	sense
35	8002	*bioB*	3186	443-444	sense
43	8003	*bioF*	1146	132-133	antisense
67	8003	*bioF*	1146	132-133	antisense
86	8004	*bioA*	1296	1211-1212	antisense
112	8004	*bioA*	1296	1211-1212	antisense
119	8005	*MSmeg_2412*	3381	1358-1357	antisense
130	8004	*bioA*	1296	1211-1212	antisense
134	8006	*MSmeg_2412*	3381	2470-2471	antisense

MSmeg_2412 or expressing the downstream genes MSmeg_2413 and MSmeg_2414. Expression of MSmeg_2412 restored biotin prototrophy to the *pyc::tn* strain, whereas neither expression of MSmeg_2413 nor MSmeg_2414 had any effect (Figure 3A).

To further assess the biotin auxotrophy in the *pyc::tn* strain, we grew wild type *M. smegmatis*, *pyc::tn*, and *bioA::tn* in liquid medium containing decreasing

Figure 3: A transposon insertion in MSMEG_2412 (pyruvate carboxylase) impairs growth on medium lacking biotin.

(A) Growth of WT *M. smegmatis* (MGM8007), *pyc::tn* (MGM8008) *bioA::tn* (MGM8009) and *bioB::tn* (MGM8010), and *pyc::tn* complemented with MSMEG_2412 (MGM8011), MSMEG_2413 (MGM8012), or MSMEG_2414 (MGM8013) on biotin containing (left) or biotin free (right) media. Rows are ten-fold serial dilutions. EV=empty vector. **(B-D)** Growth of WT (B), *bioA::tn* (C), and *pyc::tn* (D) in biotin-replete medium (500 ng/mL, dark blue), medium with decreasing concentrations of biotin (50 ng/mL: light blue; 5 ng/mL: green; 0.5 ng/mL: yellow), and biotin-deficient medium (orange). Each line is the mean of three biological replicates. **(E)** Survival during biotin depletion. WT (circles), *bioA::tn* (squares), and *pyc::tn* (triangles) were grown in medium containing (solid lines) or lacking biotin (dashed lines), and viable CFU was assessed by culturing serial dilutions on agar media. Error bars are standard deviations of three biological replicates.

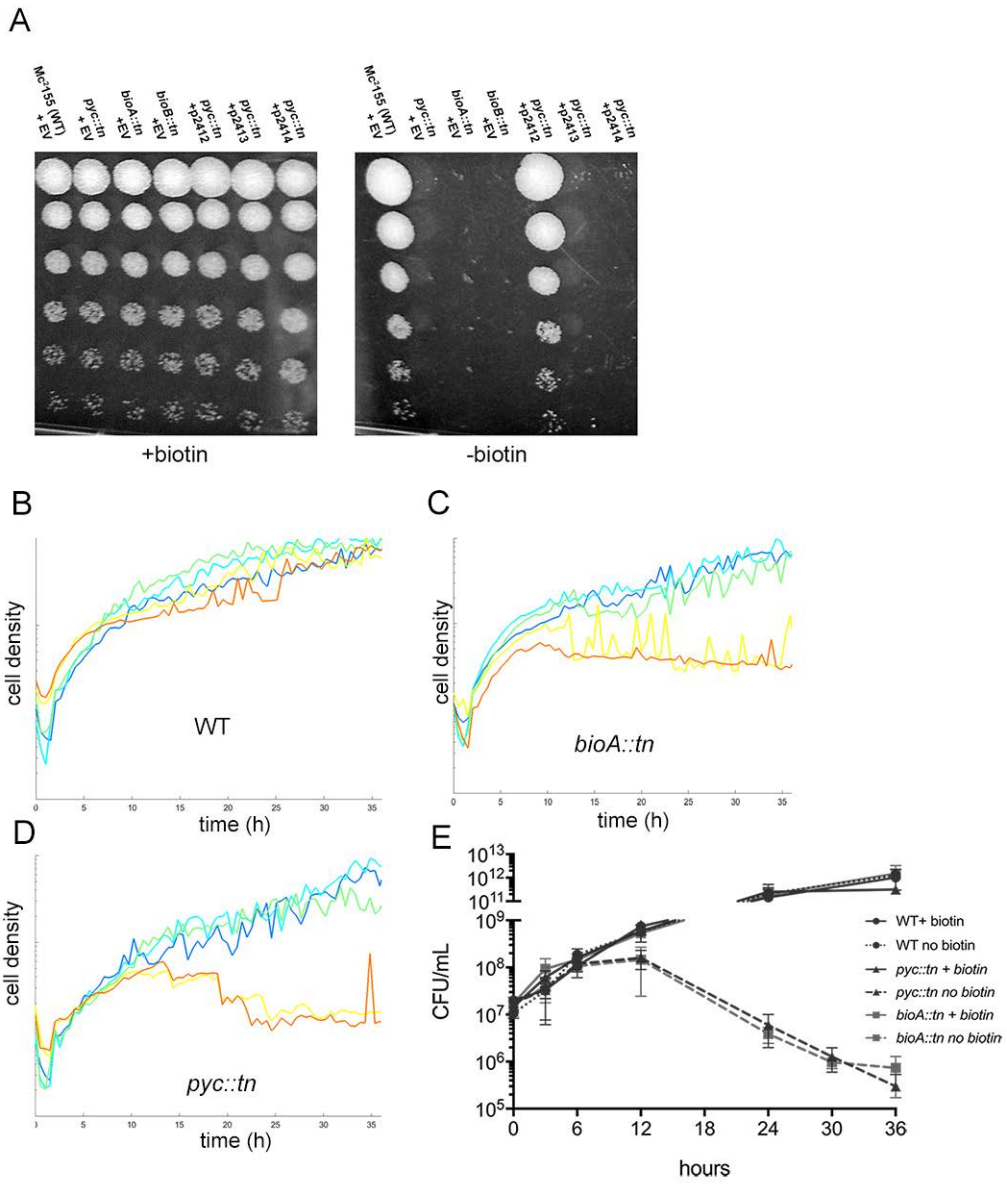
A
Mc²155 (WT) + EV
pyc::tn + EV
bioA::tn +EV
bioB::tn +EV
pyc::tn +p2412
pyc::tn +p2413
pyc::tn +p2414
+biotin
-biotin
B
cell density
WT
time (h)
C
cell density
bioA::tn
time (h)
D
cell density
pyc::tn
time (h)
E
CFU/mL
hours
WT+ biotin
WT no biotin
pyc::tn + biotin
pyc::tn no biotin
bioA::tn + biotin
bioA::tn no biotin

concentrations of biotin. Wild type *M. smegmatis* did not show an identifiable defect at any biotin concentration, whereas both *pyc::tn* and *bioA::tn* grew similarly well in medium containing 1x (500 ng/mL), 1/10x, or 1/100x biotin, but failed to grow after approximately 12 hours in medium containing either no biotin or 1/1000x biotin (Figure 3B-D). Quantitation of cell death indicated that both *pyc::tn* and *bioA::tn* lose viability with similar kinetics, beginning at 12 hours after biotin withdrawal (Figure 3E). These data indicate that loss of pyruvate carboxylase confers biotin auxotrophy in mycobacteria with a biotin requirement for viability similar to a known late stage biotin biosynthetic defect.

Pyruvate carboxylase is required for transcriptional derepression of biotin biosynthesis

Given the similar phenotype of the *pyc::tn* and *bioA::tn* mutants, we tested whether *pyc::tn* was defective in the late stages of biotin biosynthesis. Addition of desthiobiotin (DTB), the penultimate biosynthetic intermediate in the biotin biosynthetic pathway (Figure 1), was unable to restore growth to *pyc::tn*, indicating a defect in *bioB* function (Figure 4A). DTB was unsurprisingly able to restore growth to *bioA::tn* strain due to intact BioB function (Figure 4C, right panels). Expression of *bioB* restored biotin prototrophy to *pyc::tn* when the growth medium was supplemented with DTB (Figure 4C, bottom right), but only partially restored growth in the absence of DTB (Figure 4C, bottom left), indicating that the pool of DTB in the *pyc::tn* strain is limiting and implying an additional defect in the biotin biosynthetic pathway before the generation of DTB.

Biotin biosynthetic genes are transcriptionally induced in low biotin conditions such that *bioBFD* are coordinately regulated. To examine whether

Figure 4: *pyc::tn* is defective in late-stage biotin biosynthesis.

(A) pathway of late-stage biotin biosynthesis. Pimeloyl-CoA is converted to biotin via the action of four biotin biosynthetic enzymes: BioF, BioA, BioD, and BioB. Expression of *bioFD* and of *bioB*, but not of *bioA,* has been shown (Tang et al. 2014) to be repressed by the TetR-family repressor BioQ under biotin-replete conditions in *M. smegmatis*. **(B, C)** WT (MGM8019), *bioA::tn* (MGM8021), and *pyc::tn* (MGM8020) were tested for growth on medium containing (B), or lacking biotin (C, left panels) or containing the biosynthetic intermediate desthiobiotin (DTB) (C; two rightmost panels). *bioA::tn* and *pyc::tn* strains expressing *bioA* (*pyc::tn:* (MGM8034))*; bioA::tn*: (MGM8036) or *bioB* (*pyc::tn:* (MGM8035); *bioA::tn*: (MGM8037)) under the control of a heterologous promoter responsive to the inducer anhydrotetracycline (ATc) (C; ATc present in bottom panels) were also tested.

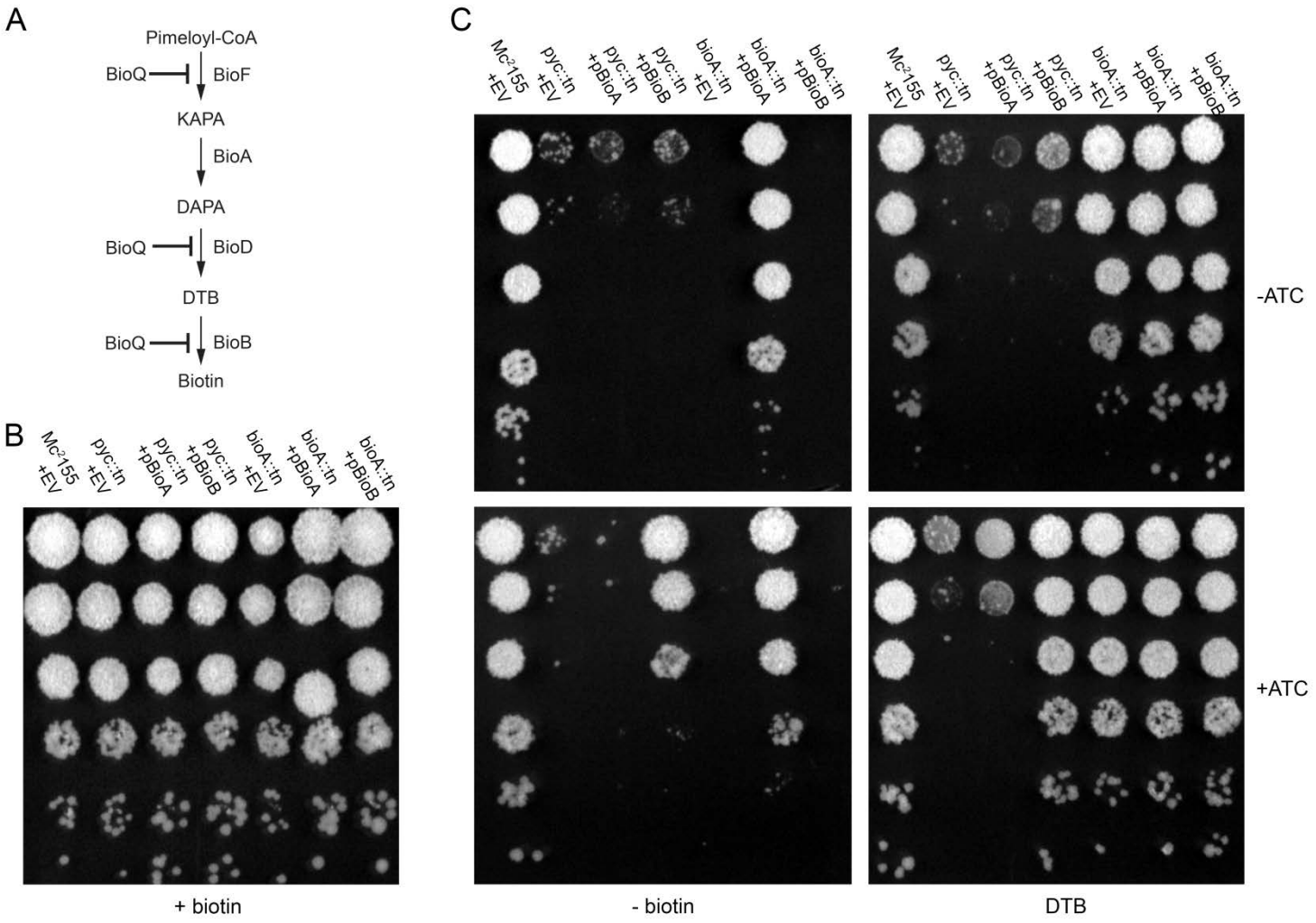
A
Pimeloyl-CoA
BioQ
BioF
KAPA
BioA
DAPA
BioQ
BioD
DTB
BioQ
BioB
Biotin
B
Mc²155 +EV
pyc::tn +EV
pyc::tn +pBioA
pyc::tn +pBioB
bioA::tn +EV
bioA::tn +pBioA
bioA::tn +pBioB
+ biotin
C
Mc²155 +EV
pyc::tn +EV
pyc::tn +pBioA
pyc::tn +pBioB
bioA::tn +EV
bioA::tn +pBioA
bioA::tn +pBioB
-ATC
+ATC
- biotin
DTB

transcriptional upregulation of these genes is defective in the *pyc::tn* strain, we quantitated the mRNAs for *bioFADB* by RT-qPCR (Figure 5A). In biotin-replete conditions, WT and *pyc::tn M. smegmatis* express similar levels of these transcripts. However, after three hours of biotin deprivation in wild type cells, we observed a 16-fold induction of *bioB* and *bioFD* (expressed as a single transcript) mRNAs (Figure 5A). We do not find *bioA* to be transcriptionally upregulated by low biotin, consistent with previous reports (Tang et al. 2014). In contrast, *pyc::tn* fails to upregulate *bioB* or *bioFD* in low biotin, potentially explaining its defect in growth in this condition (Figure 5A). Complementation of *pyc::tn* with a wild type copy of *pyc*, which complemented biotin auxotrophy (Figure 3A), restored *bioB* induction in low biotin and in fact de-repressed *bioB* even in biotin-replete conditions (Figure 5A). These data indicate that *pyc* is required for the transcriptional induction of biotin biosynthetic genes in low biotin conditions.

Previous work (Tang et al. 2014) has shown that *bioB* and *bioFD*—but not *bioA*—are repressed by the TetR like regulator BioQ, which binds to an operator in the *bioB* and *bioF* promoters which overlaps the TSS for these genes (Tang et al. 2014). BioQ dissociates from its operator in low biotin conditions, although the signal for BioQ binding or dissociation is not clear and does not appear to be biotin itself or biotinoyl-AMP (Tang et al. 2014). To test whether the biotin auxotrophy of the *pyc::tn* strain requires BioQ mediated repression, we introduced null mutations in *bioQ* in both the WT and *pyc::tn* backgrounds using homologous recombination and double counterselection

Figure 5: Pyruvate carboxylase is required for BioQ mediated derepression of *bioFDB.*

(A) Expression of the biotin biosynthetic genes *bioFADB* in WT (MGM8007), *pyc::tn* (MGM 8008) and complemented (MGM8011) strains under biotin-replete and biotin-deficient (-bio) conditions. Strains were grown for three hours with or without biotin, RNA was prepared, and RT-qPCR was performed for the indicated mRNAs. **(B)** Loss of *bioQ* suppresses the biotin auxotrophy of *pyc::tn*. Genetic deletions of *pyc* (MGM6514) and *bioQ* (MGM6516 and MGM6520) were introduced via homologous recombination and double counterselection (see strain table), and growth on medium containing or lacking biotin was assessed. **(C)** Loss of *bioQ* restores *bioB* expression to *pyc::tn*. Error bars are standard deviation of three biological replicates.

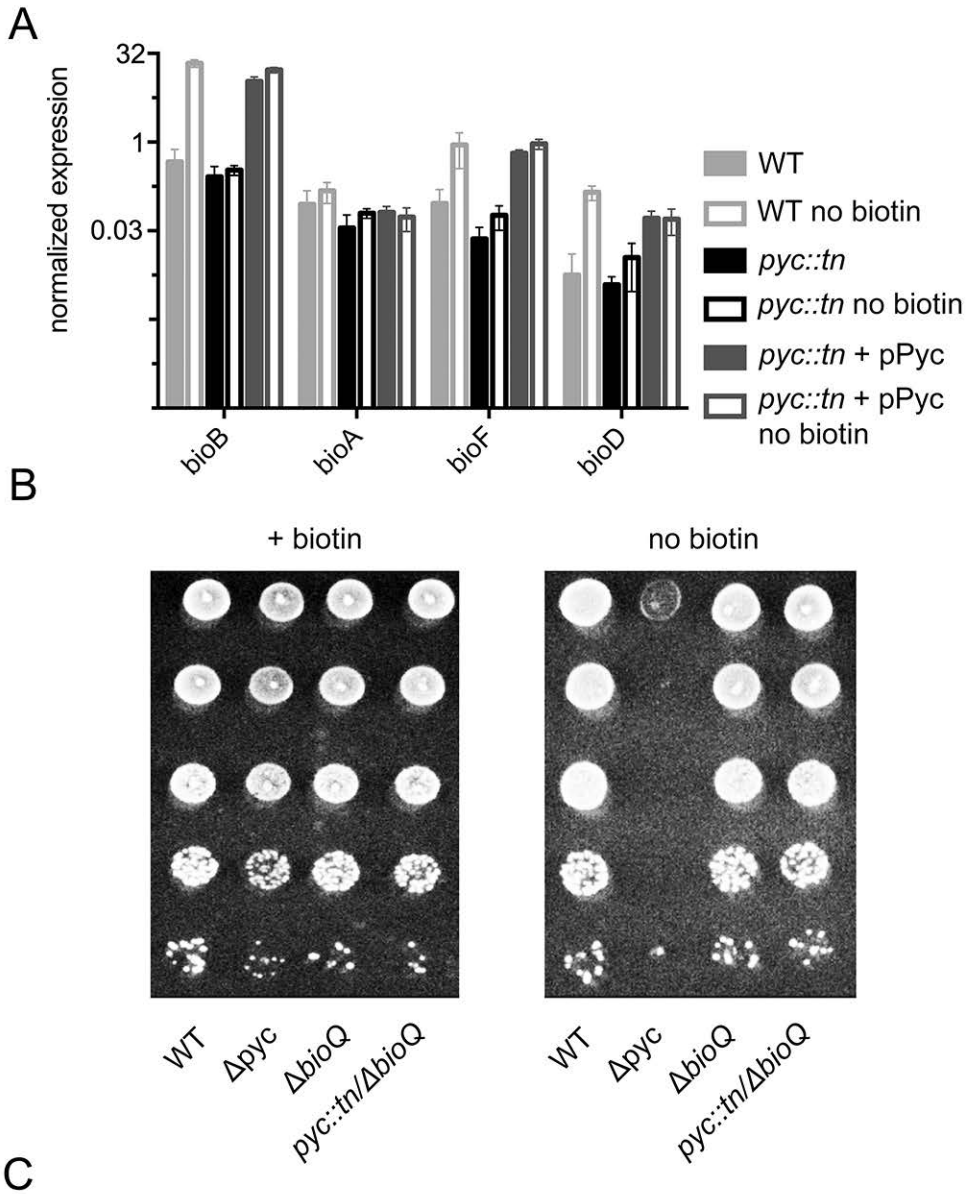
A
32
1
0.03
normalized expression
bioB
bioA
bioF
bioD
WT
WT no biotin
pyc::tn
pyc::tn no biotin
pyc::tn + pPyc
pyc::tn + pPyc no biotin
B
+ biotin
no biotin
WT
Δpyc
ΔbioQ
pyc::tn/ΔbioQ
C
normalized bioB expression
16
8
4
2
1
0.5
0.25
0.125
0.0625
Δpyc + biotin
Δpyc no biotin
ΔbioQ + biotin
ΔbioQ no biotin
pyc::tn/ΔbioQ + biotin
pyc::tn/ΔbioQ no biotin

(Barkan, Stallings, and Glickman 2011). We also constructed a null mutation of *pyc* to confirm that biotin auxotrophy was not specific to the *pyc::tn* transposon mutant.

We tested each of these strains for the ability to grow without biotin and observed that a Δ*pyc* strain was indeed a biotin auxotroph (Figure 5B) and that deletion of *bioQ* in the *pyc::tn* background restored the ability of this strain to grow without biotin (Figure 5B). We also constructed a *bioQ* null mutant via CRISPR-mediated chromosomal cleavage (see methods) in the *pyc::tn* background, (Figure 6A). We tested the ability of *pyc*::tn ∆*bioQ* and *pyc*::tn *bioQ* (frameshift) strains to grow without biotin and found that inactivation of *bioQ* reverted the biotin auxotrophy of the *pyc*::tn strain (Figure 5B and data not shown).

RT-qPCR of *bioB* mRNA showed that loss of BioQ derepressed BioB expression in wild type cells, as reported previously ((Tang et al. 2014), Figure 5C) and also restored *bioB* expression in *pyc::tn* (Figure 5C, Figure 6B). These results demonstrate that the biotin auxotrophy conferred by inactivation of pyruvate carboxylase is due to inability to derepress biotin biosynthetic genes during biotin deprivation and imply that pyruvate carboxylase is required for generation of the signal that relieves BioQ mediated repression.

Pyruvate carboxylase catalytic activity is required for its regulatory function

M. smegmatis possesses two genes predicted to code for pyruvate carboxylase enzymes: MSmeg_2412, the transposon mutant of which we analyze above, and the additional gene MSmeg_6648. Meanwhile, the predicted proteome of the pathogenic mycobacterium M. tuberculosis contains

Figure 6: Sequence alignment of mutants made in *bioQ* using CRISPR

(A) CRISPR-Cas9 was used to generate frameshift mutants in *bioQ pyc::tn*. Candidate *bioQ* sequences were sequenced and sequences were aligned to the native *bioQ* sequence (top). Identical nucleotides are shaded in gray, while nucleotides different from the reference sequence are not shaded. *bioQ* mutant #16 has a single nucleotide insertion of A at the DSB site **(B)** *pyc*::*tn bioQ* #16 restores *bioB* induction to *pyc::tn*. Error bars are standard deviation of three biological replicates.

A

```
native bioQ   1 GTGCAACTCCACAAACCCGACGTGTGTGGCTGCGGCGACGAAGATCCTCGACGACCACGGCATCGCCGACCTGACGATGCGGCGCCTGGC
mutant #16    1 -------------------ACGTGTGTGGCTGCGGCGACGAAGATCCTCGACGACCACGGCATCGCCGACCTGACGATGCGGCGCCTGGC

             90 GCGCGAGCTCGACGTCACGCCGGGCGCCCTGTACTGGCATTTCGCCAACAAA-CAGGAACTGTTGGGGGCAGTGGCCGACCACATTCTGC
             72 GCGCGAGCTCGACGTCACGCCGGGCGCCCTGTACTGGCATTTCGCCAACAAAACAGGAACTGTTGGGGGCAGTGGCCGACCACATTCTGC

            179 GCACCGCGCGCACCGACACCGCGGACCTCGCGTGGCGCGAACAGATCCACGAGTCCTGCCGCGCGTTGCGCGACGCGTTGTTGTCGCACA
            162 GCACCGCGCGCACCGACACCGCGGACCTCGCGTGGCGCGAACAGATCCACGAGTCCTGCCGCGCGTTGCGCGACGCGTTGTTGTCGCACA

            269 CCGACGGCGCCGAACTCGTGTCGGCGAGCTTCGCGTCCGGGCAGTCGGTGGTGATCACCGAGATCGTGGAGCAGCTGGGTCGCGCGGCCC
            252 CCGACGGCGCCGAACTCGTGTCGGCGAGCTTCGCGTCCGGGCAGTCGGTGGTGATCACCGAGATCGTGGAGCAGCTGGGTCGCGCGGCCC

            359 GCGCCGCCGGGGGTGAGCGACGCCGACGTCGATGCGGCCGCCCGCACCGTGATCTATTACGTGCTGGGATTCACCGTCGACGAGCAGTCCC
            342 GCGCCGCCGGGGGTGAGCGACGCCGACGTCGATGCGGCCGCCCGCACCGTGATCTATTACGTGCTGGGATTCACCGTCGACGAGCAGTCCC

            449 GGCTGCAGTGGGACGCCGTCGGCGCGCTGGGTGACGATCAGTCGATGCTCACCCGCGACGGCACCCGCCAGTTCCGCTTCGGCCTGCAGT
            432 GGCTGCAGTGGGACGCCGTCGGCGCGCTGGGTGACGATCAGTCGATGCTCACCCGCGACGGCACCCGCCAGTTCCGCTTCGGCCTGCAGT

            539 TGCTCGTCGACGGGCTGGCCGCCCACGGCGGCGGCAGTGAATTCACCGGATTTTCTTCTGCGGAGCGCTCTTTCGAGTAG
            522 TGCTCGTCGACGGGCTGGCCGCCCACGGCGGCGGCAGTGAATTCACCGGATTTTCTTCTGCGGAGCGCTCTTTCGAGTAG
```

B

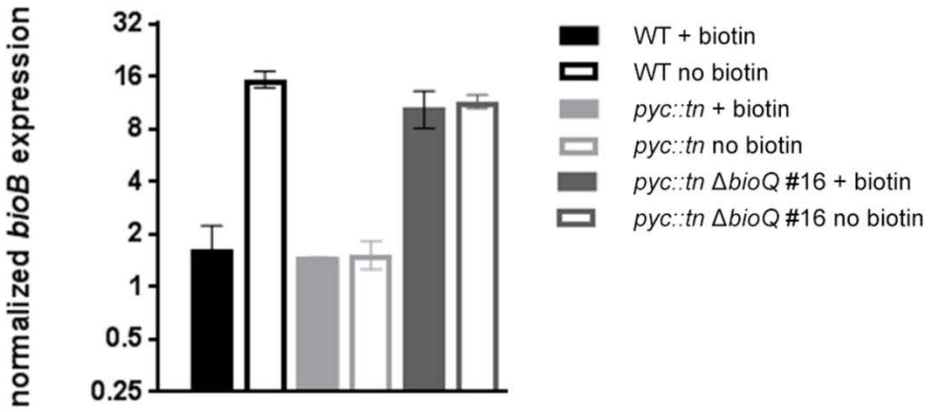

a single pyruvate carboxylase encoded by the gene Rv2967c, which is most similar in primary amino acid sequence and genomic organization to MSmeg_2412.

The two *M. smegmatis* pyruvate carboxylase proteins share a high degree of similarity (~90%) by amino acid sequence (Figure 7) with conserved amino acid residues found to be necessary for enzymatic activity (biotin carboxylase activity: E288, N290, R292 (Janiyani et al. 2001); carboxytransferase activity: (R532, D533, E566 (Yu et al. 2009, Marchler-Bauer et al. 2017, St Maurice et al. 2007)), or biotin attachment (K1093 (Polyak et al. 2001, Kim et al. 2004)). To determine whether the pyruvate carboxylases *MSmeg_6648* or *Rv2967c* can compensate for loss of *pyc* (*MSmeg_2412)*, we expressed each of these proteins in *pyc::tn*. Whereas the *M. tuberculosis* pyruvate carboxylase encoded by *Rv2967c* did complement the biotin biosynthetic defect of *pyc::tn*, *MSmeg_6648* failed to complement even when expressed under control of the inducible tet_{ON} promoter (Figure 8A). However, western blotting did not reveal a detectable protein product corresponding to *MSmeg_6648* (data not shown). These data demonstrate functional conservation between *MSmeg_2412* and *M. tuberculosis Rv2967c*.

To assess whether pyruvate carboxylase activity itself, rather than another property of *MSmeg_2412*, is required for its biotin regulatory function, we expressed truncations of *MSmeg_2412* lacking one or more predicted domains. Pyruvate carboxylase possesses three major structural domains: the N-terminal biotin carboxylase (BC), carboxytransferase (CT), and the C terminal biotin binding (BCCP). The transposon insertions we identified as conferring biotin auxotrophy were located between the BC domain and the CT

Figure 7: Primary amino acid sequence alignment of pyruvate carboxylases Rv2967c (*M. tuberculosis*) and MSMEG_2412 and 6648 (*M. smegmatis*).

Sequence alignment was performed using the Clustal Omega web form (McWilliam et al. 2013, Sievers et al. 2011). Domains were identified by homology to the *R. etli* pyruvate carboxylase (St Maurice et al. 2007). The biotin carboxylase (BC) domain is highlighted with a red line above the primary sequence, carboxytransferase (CT) with a blue line, and the biotin-binding (BCCP) with a green line. Biotin carboxylase catalytic residues (red arrows) were identified via homology with the *E. coli* biotin carboxylase, (Janiyani et al. 2001) carboxytransferase catalytic residues (blue arrows) were identified via homology with the *S. aureus* pyruvate carboxylase (Yu et al. 2009), and the biotin attachment residue (green arrow) was identified via the CDD database (Marchler-Bauer et al. 2017). Transposon insertion sites are noted with black arrows and annotated with the strain number.


A
Biotin carboxylase (BC)
119
Carboxytransferase (CT)
10
134
Biotin binding (BCCP)

domain (mutant 119) or in the CT domain (mutants 10 and 134) C-terminal to active site residues (Figure 7, black arrows). The biotin carboxylase domain adds a carboxyl group to biotin in the first step of the pyruvate carboxylase mechanism, and is essential for pyruvate carboxylase activity (Janiyani et al. 2001).

Truncations containing only the MSMEG_2412 biotin carboxylase (BC) or carboxytransferase (CT) domains failed to restore growth to *pyc::tn* on medium lacking biotin. Surprisingly, a truncation lacking the BC domain but containing both the CT domain and the biotin-binding (BCCP) domain did successfully revert the *pyc::tn* biotin phenotype (Figure 8B). However, expression of a BC catalytic mutant (E288K), which we confirmed is both expressed and biotinylated (Figure 8D), failed to restore growth to *pyc::tn* on medium lacking biotin (Figure 8C). Expression of each of these constructs in the Δ*pyc* strain, which lacks the entire Pyc protein, revealed identical requirements for complementation (Figure 8E,F).

To further address the question of whether pyruvate carboxylase activity is responsible for the requirement for pyruvate carboxylase function and relief of BioQ repression, we constructed two mutants which lack the MSMEG_2412 biotin attachment site (K1093L (Polyak et al. 2001) and K1093R (Kim et al. 2004)). As expected, expression of either of these mutants failed to restore growth to *pyc::tn* (Figure 8C), despite expression of the mutant proteins at wild type levels (Figure 8D, HA panel). We were unable to detect biotinylation of each of these mutants using streptavidin-HRP, indicating that despite their detectable expression, they each failed to be biotinylated (Figure 8D, biotin panel). As covalent linkage of biotin to the biotin-attachment lysine is required for pyruvate carboxylase activity (St Maurice et al. 2007), this experiment

Figure 8: Pyruvate carboxylase catalytic activity is required for biotin prototrophy

(A) TB Pyruvate carboxylase supports biotin biosynthesis. WT (MGM8019), *pyc::tn* (MGM8020), *bioA::tn* (MGM8021), and *pyc::tn* expressing either the annotated second pyruvate carboxylase in *M. smegmatis* (MSmeg_6648) (MGM8024) or the *M. tuberculosis* ortholog Rv2967c (MGM8025) for growth on medium lacking biotin. EV=empty vector. **(B)** Truncation of Pyc. *pyc::tn* was complemented with plasmids expressing full length pyruvate carboxylase (MGM8023), biotin carboxylase (BC) domain (MGM8026), only the carboxytransferase (CT) domain (MGM8027), or the CT domain and the biotin-binding (BCCP) domains (MGM8028). **(C)** Pyruvate carboxylase BC active site or biotin attachment sites are required for biotin prototrophy. p*yc*::t*n* was complemented with plasmids expressing full length Pyc with a BC catalytic residue mutation (E288K) (MGM8029) or the essential residue for covalent attachment of biotin (K1093L/R) (MGM8030/8031). Each strain was N-terminally HA-tagged and expressed under the control of an ATc-dependent promoter. **(D)** Each of the Pyc isoforms from (C) as well as native pyruvate carboxylase (MGM8011) were N-terminally HA tagged. Expression of each of the mutants (E288K, K1093L/R) was similar to levels of native pyruvate carboxylase (Pyc-HA+) when induced with ATc. Low levels of pyruvate carboxylase were present in the absence of induction (Pyc-HA-). Detection of protein biotinylation was performed using streptavidin-HRP. RNA polymerase subunit B (RpoB) is shown as a loading control. Native pyruvate carboxylase (Pyc-HA) is the same strain shown in Figure 3A and Figure 5A. **(E)** Δ*pyc* (MGM6521) was complemented with plasmids expressing the BC domain (MGM6522), only the CT domain (MGM6523), or the CT domain and BCCP

domains (MGM6524). **(F)** Pyruvate carboxylase BC active site or biotin attachment sites are required for biotin prototrophy. Δ*pyc* was complemented with plasmids expressing Pyc-E288K (MGM6525) or Pyc-K1093L/R (MGM6526/ 2527).

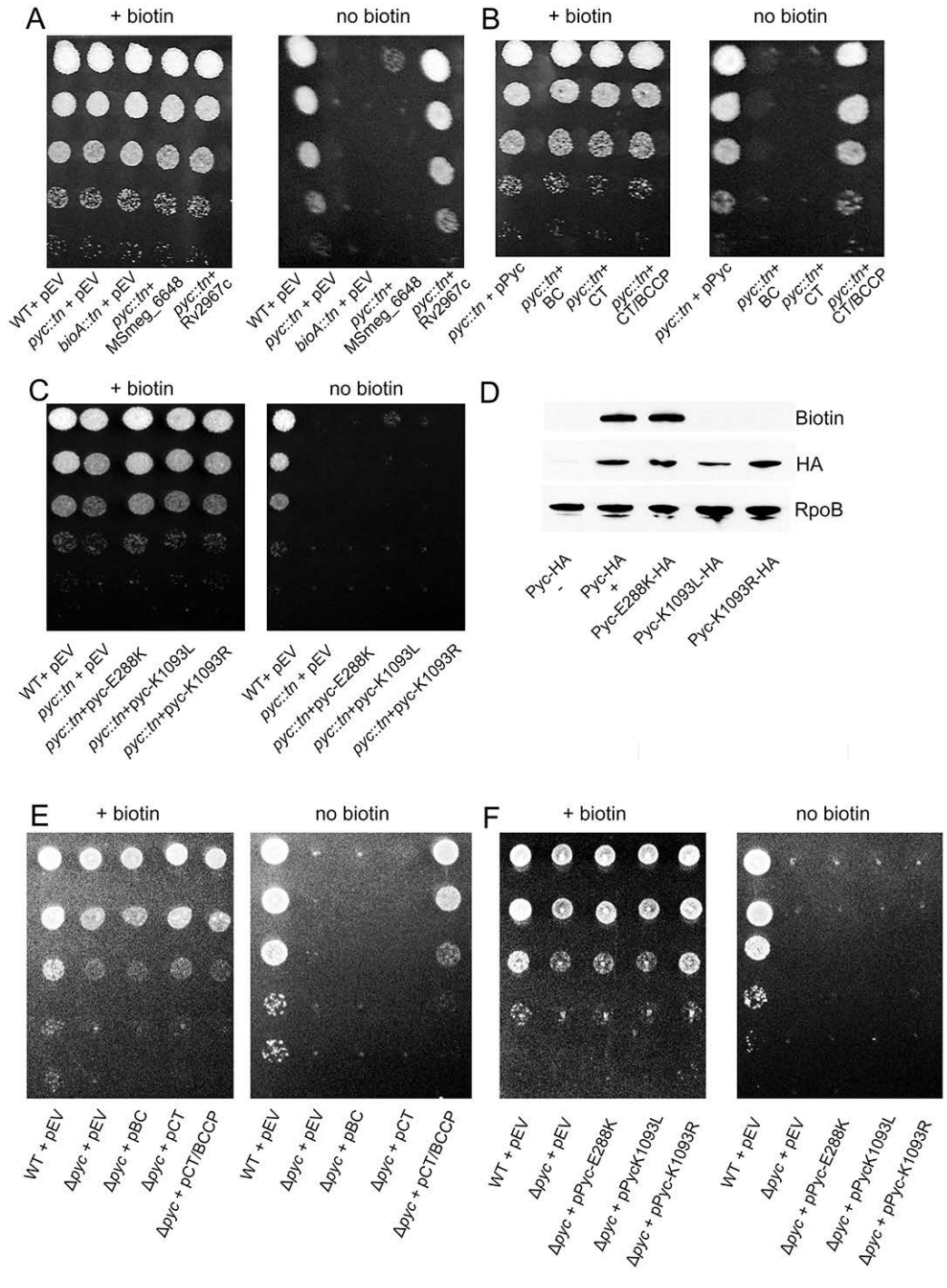
A
+ biotin
no biotin
WT+ pEV
pyc::tn + pEV
bioA::tn + pEV
pyc::tn+ MSmeg_6648
pyc::tn+ Rv2967c
B
+ biotin
no biotin
pyc::tn + pPyc
pyc::tn+ BC
pyc::tn+ CT
pyc::tn+ CT/BCCP
C
+ biotin
no biotin
WT+ pEV
pyc::tn + pEV
pyc::tn+pyc-E288K
pyc::tn+pyc-K1093L
pyc::tn+pyc-K1093R
D
Biotin
HA
RpoB
Pyc-HA -
Pyc-HA +
Pyc-E288K-HA
Pyc-K1093L-HA
Pyc-K1093R-HA
E
+ biotin
no biotin
WT + pEV
Δpyc + pEV
Δpyc + pBC
Δpyc + pCT
Δpyc + pCT/BCCP
F
+ biotin
no biotin
WT + pEV
Δpyc + pEV
Δpyc + pPyc-E288K
Δpyc + pPycK1093L
Δpyc + pPyc-K1093R

provides further evidence that pyruvate carboxylase activity of MSMEG_2412, rather than any other function of the protein or its coding sequence, is the key factor which is essential for its regulatory function. In addition, the failure of a nonbiotinylated Pyc enzyme to induce biotin biosynthesis clearly indicates that it is not simply the accumulation of a biotin free protein that is the signal for BioQ derepression.

Biotinyl-pyruvate carboxylase is depleted more quickly than other biotinylated proteins during biotin deprivation

The data presented above indicates that pyruvate carboxylase activity is required for to induce biotin biosynthetic genes through BioQ. As pyruvate carboxylase is itself a biotinylated protein, we hypothesized that loss of Pyc function, through loss of biotinylation, may be a sensitive indicator of cellular biotin starvation. To determine the effects of biotin deprivation on bacteria which cannot synthesize their own biotin, we used streptavidin-HRP to probe cellular biotinylated proteins in order to assess the kinetics of biotinylated protein depletion in WT, *pyc::tn*, and *bioA::tn M. smegmatis.* We identified biotinyl-pyruvate carboxylase (Figure 9A, top band, absent in *pyc::tn*, marked with an asterisk) as well as multiple additional biotinylated proteins. The *pyc::tn* strain lacked any gross defects in biotinylated proteins during biotin-replete (0h) conditions (other than the absence of the ~120 kDa band for pyruvate carboxylase), and showed similar rates of disappearance of biotinylated proteins when compared to the *bioA::tn* strain (Figure 9A, Figure 10). A search for homology to the Pyc biotin-binding domain within the *M. smegmatis* identified the pyruvate carboxylases MSMEG_2412 and

Figure 9: Analysis of protein biotinylation during biotin deprivation

(A) Streptavidin HRP Western blot of total biotinylated protein in WT (MGM8007), *pyc::tn* (MGM8008), and *bioA::tn* (MGM8009) during biotin deprivation for 0, 3, 6, and 12 hours. Biotinylated proteins were visualized using streptavidin-HRP with anti-RpoB as a loading control. Pyruvate carboxylase (topmost band, marked with *) was absent in *pyc::tn*, as expected, but *pyc::tn* showed no obvious deficiencies in other biotinylated proteins. The biotinylated proteins used for quantitation (see Figure 10) are marked with * or <. (**B)** Quantitation of the fraction of the indicated proteins remaining at 3 hours of biotin deprivation compared to T0 in a *bioA*::*tn* strain. Error bars are standard deviations of three biological replicates.

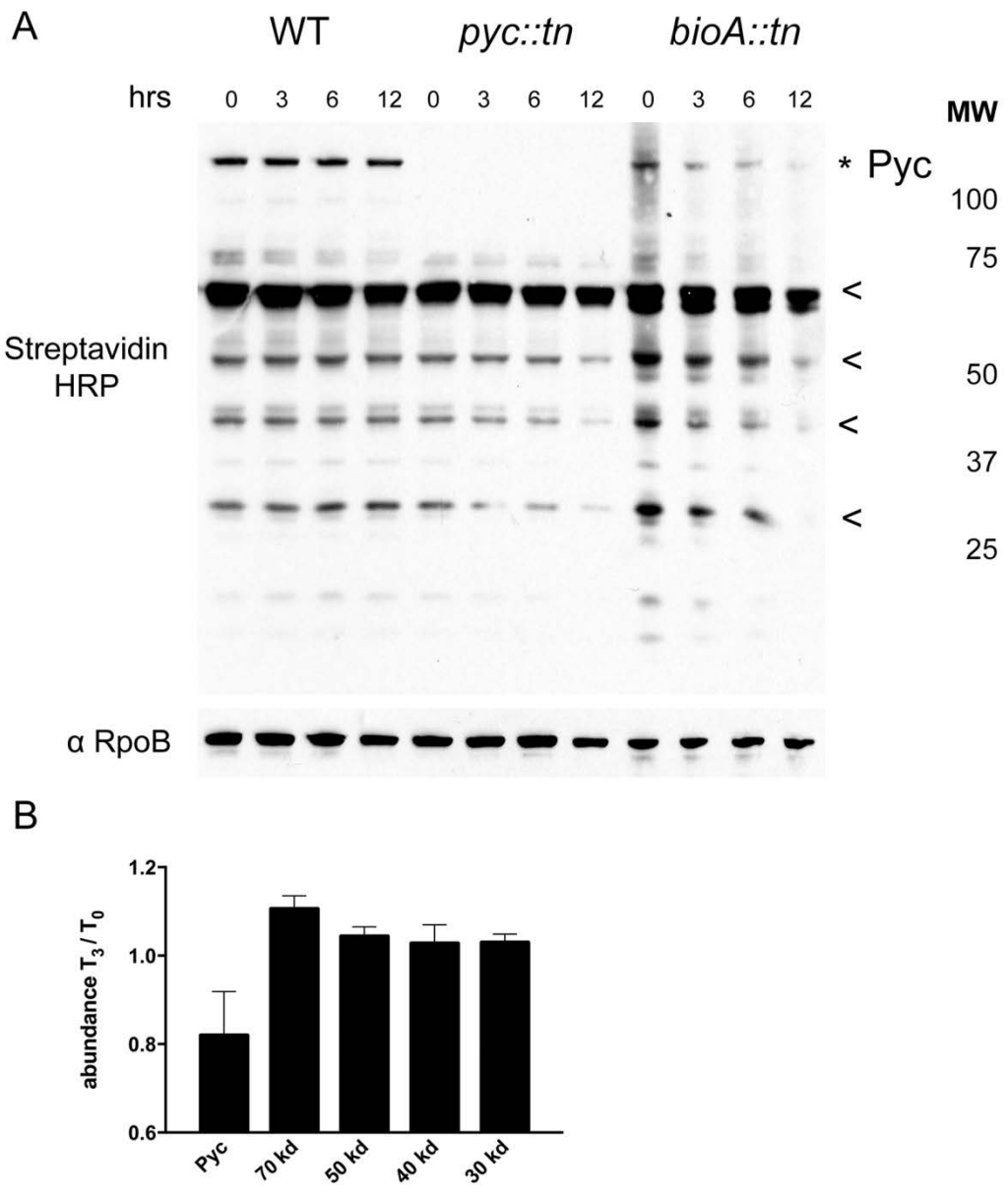
A
WT
pyc::tn
bioA::tn
hrs
0 3 6 12 0 3 6 12 0 3 6 12
MW
* Pyc
100
75
50
37
25
Streptavidin HRP
α RpoB
B
abundance T3 / T0
1.2
1.0
0.8
0.6
Pyc
70 kd
50 kd
40 kd
30 kd

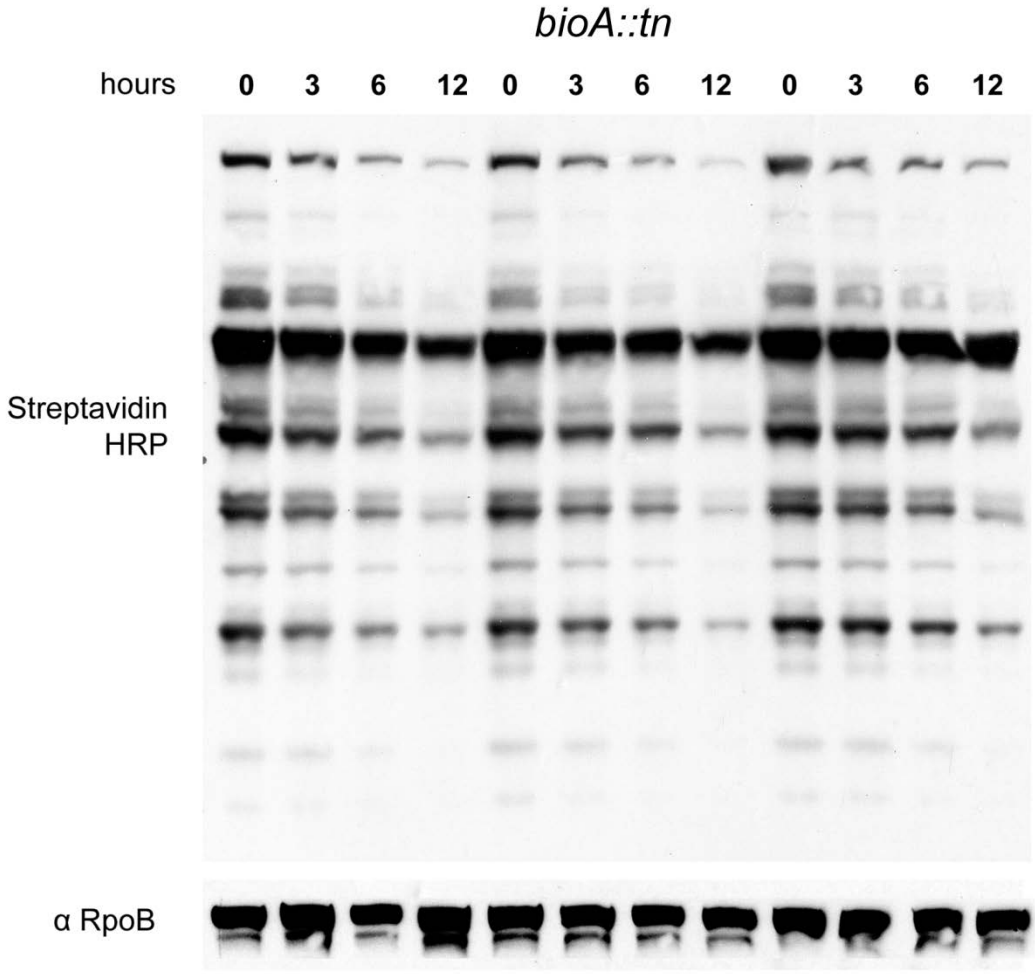

Figure 10: Triplicate Western blot analysis of *bioA*::*tn* for quantitation

Western blot of total biotinylated protein in *bioA::tn* (MGM8009) during biotin deprivation for 0, 3, 6, and 12 hours. Biotinylated proteins were visualized using streptavidin-HRP with anti-RpoB as a loading control.

MSMEG_6648, as well as the acetyl/propionyl-CoA carboxylases MSMEG_0334, 1807, 5943, and 4716. Each of these acetyl/propionyl-CoA carboxylases is predicted to have a molecular weight between 60 and 75 kDa. The biotinylated proteins we detected with molecular weights of below 60 kDa do not correspond to any protein identifiable via this method, and may either represent degradation products or uncharacterized biotinylated proteins.
We repeated this experiment in triplicate to assess the rate at which the biotin auxotroph *bioA::tn* loses biotinylated proteins (Figure 10), and quantitated the results (Figure 9B). Biotinyl-pyruvate carboxylase begins to be depleted by three hours of biotin depletion, a time point at which growth of biotin auxotrophs is comparable to WT (Figure 3C), and other biotinylated proteins have not yet declined in abundance. Depletion of the majority of biotinylated proteins is observed by six hours or more of biotin depletion, a time point that coincides with growth arrest of biotin auxotrophs (Figure 3E). We conclude that depletion of biotinyl-pyruvate carboxylase is an early marker of biotin deprivation and may generate the signal to upregulate biotin biosynthesis.

Metabolomic analysis identifies candidate inducers of BioQ dependent genes

The requirement for Pyc enzymatic function to support biotin synthesis may suggest that the signal for BioQ depression is a metabolic shift due to Pyc dysfunction. To assess this idea, we pursued a metabolomic approach. We collected metabolites from WT and *pyc::tn*, *either* in biotin-replete or biotin depleted conditions for three hours. This short period of biotin withdrawal was chosen to ensure that metabolic changes were indeed a result of biotin deprivation, rather than generalized signals of cell death, which might occur if

biotin deprivation had been lengthened until growth arrest occurs. Using this approach, we were able to identify and to quantitate the levels of approximately 150 metabolites with distinct LC-MS peaks and retention times (Figure 11). Statistical analysis identified 16 of these metabolites present at levels that were significantly different between strains and/or conditions (Figure 12A). Pyruvate, the substrate of pyruvate carboxylase, accumulated in wild type cells with biotin withdrawal, consistent with the kinetics of Pyc protein depletion, but was depleted in all conditions in *pyc::tn* cells, *i.e*. both with and without biotin (Figure 12A). Principal-component analysis (PCA) on the metabolomic data (Figure 12B) separates the samples primarily by strain on the first principal component, which explains the majority of the variation between samples. The PCA also shows that biotin withdrawal from the wild type strain causes a metabolic shift in both principal components, whereas biotin withdrawal from *pyc*::*tn* has a minimal effect (Figure 12B) Additionally, the majority of the differences between metabolites which differed between the strains (Figure 12A) or metabolites as a whole (Figure 11) are found between strains, rather than between conditions. These metabolomic data indicate that biotin withdrawal from wild type cells causes broad metabolic perturbation, including dysfunction of Pyc. In cells lacking Pyc, these metabolic changes are blunted or absent and the strain, even with biotin, has adapted to the loss of Pyc.

We performed pathway analysis (Kamburov et al. 2011) and identified alanine/aspartic acid/glutamic acid metabolism, arginine biosynthesis, lysine biosynthesis, the citric acid cycle, and pyruvate metabolism to be overrepresented within our list of significantly perturbed metabolites. However, we were unable to restore growth of *pyc::tn* on medium lacking biotin by

Figure 11 : All metabolites identified from analysis of *pyc::tn.*

We collected metabolites from three replicates of WT (MGM8007) and *pyc::tn* (MGM8008) after three hours of growth with or without biotin. Metabolite levels were normalized to total biomass measured in each replicate using a generalized linear regression model. All metabolites with identifiable signal in each replicate are summarized here. . Higher abundance for a metabolite than expected by the model given the strain's biomass is indicated in red and lower abundance in green.

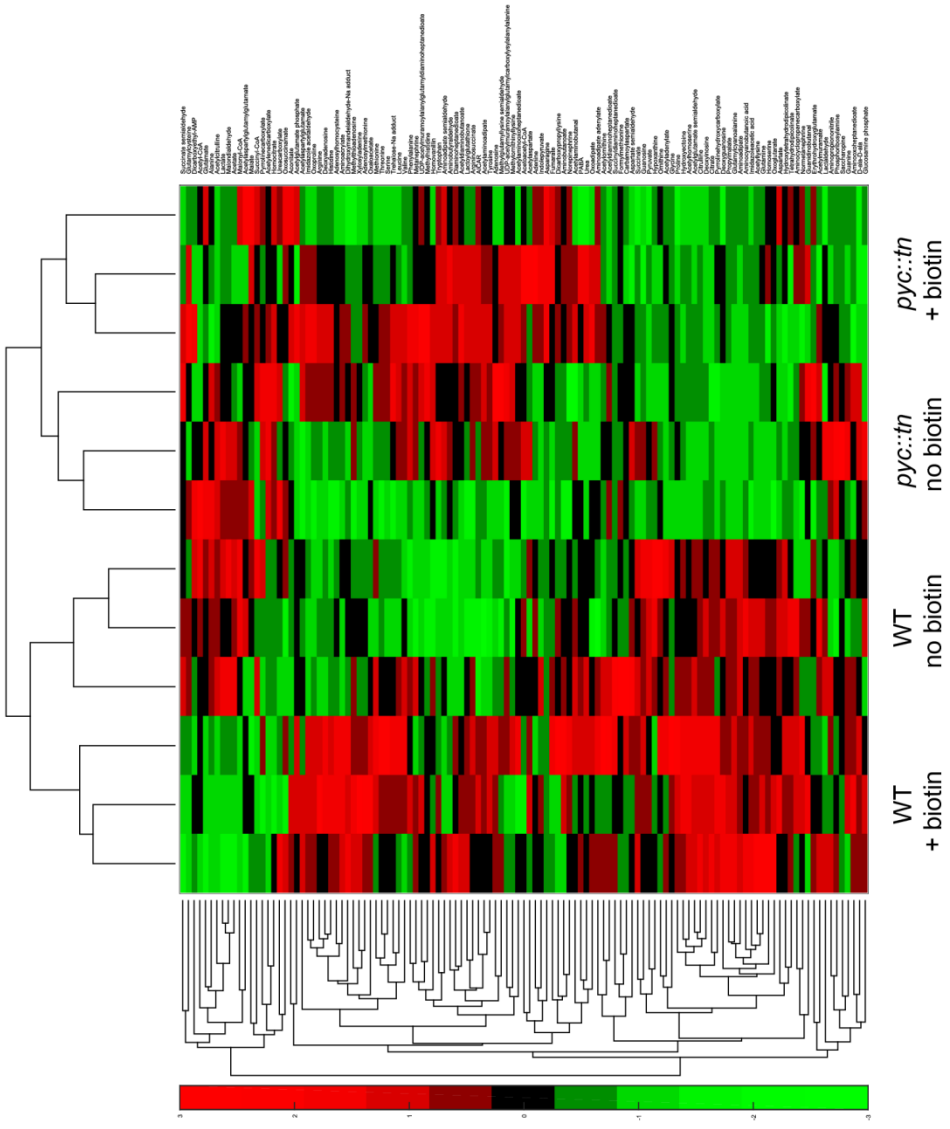
WT
+ biotin
WT
no biotin
pyc::tn
no biotin
pyc::tn
+ biotin

Figure 12: Significantly perturbed metabolites in *pyc::tn*

(A) We collected metabolites from three replicates of WT (MGM8007) and *pyc::tn* (MGM8008) after three hours of growth with or without biotin. Metabolite levels were normalized to total biomass measured in each replicate using a generalized linear regression model. Metabolites which were significantly different between strains or conditions are summarized in the heat map. Higher abundance for a metabolite than expected by the model given the strain's biomass is indicated in red, and lower abundance in green. **(B)** Principal-component analysis (PCA) of all metabolites. Each dot is one replicate of the indicated strain/biotin condition.

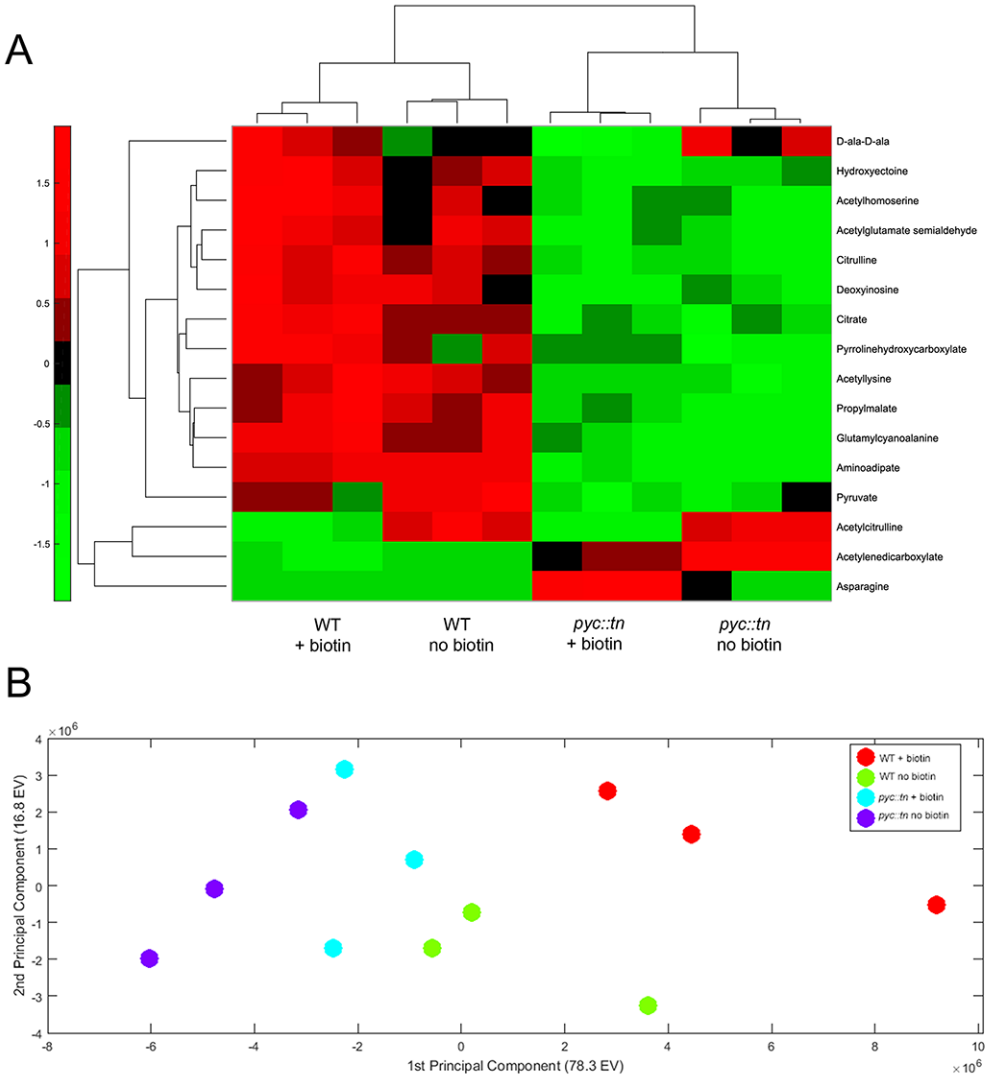
A
D-ala-D-ala
Hydroxyectoine
Acetylhomoserine
Acetylglutamate semialdehyde
Citrulline
Deoxyinosine
Citrate
Pyrrolinehydroxycarboxylate
Acetyllysine
Propylmalate
Glutamylcyanoalanine
Aminoadipate
Pyruvate
Acetylcitrulline
Acetylenedicarboxylate
Asparagine
1.5
1
0.5
0
-0.5
-1
-1.5
WT + biotin
WT no biotin
pyc::tn + biotin
pyc::tn no biotin
B
×10^6
2nd Principal Component (16.8 EV)
1st Principal Component (78.3 EV)
×10^6
WT + biotin
WT no biotin
pyc::tn + biotin
pyc::tn no biotin

supplementing the media with metabolites found at lower levels in *pyc::tn* than in WT (data not shown), possibly because these metabolites are not cell-permeable. It is also possible that the factor required to derepress biotin synthesis is a modified species of one of the accumulated metabolites or that our method failed to detect the relevant metabolite.

CHAPTER THREE: Δ*RIP1 M. TUBERCULOSIS* IS SENSITIVE TO MULTIPLE TYPES OF STRESS

Response of Δ*rip1* to *in vitro* models of stress

To determine which stresses are responsible for the virulence defect of Δrip1, we assessed its sensitivity using various previously-described *in vitro* models of host-mediated stress. We first cultured WT, Δ*rip1*, and complemented strains of *M. tuberculosis* in the presence of lysozyme (as a representative of antimicrobial peptides) (Kanetsuna 1980, Nawrocki, Crispell, and McBride 2014), the detergent SDS (Banaei et al. 2009, Vandal et al. 2009), low pH (Vandal et al. 2009, Schaible et al. 1998), hydrogen peroxide (Voskuil et al. 2011, Springer et al. 2001), and the nitric oxide donor DETA-NO (Idh et al. 2012, Voskuil et al. 2011). For each of these stresses, Δ*rip1* was killed at approximately the same frequency as WT except in the case of nitric oxide, which killed approximately 90% of Δ*rip1* bacilli at a dose which did not have an effect on the survival of WT (Figure 13A-E).

To ensure that this phenotype was not specific to the dose of stress used, we determined the minimum inhibitory concentration (MIC) of each stress for WT, Δ*rip1*, and the complemented strain. As before, Δ*rip1* showed increased sensitivity to DETA-NO, with an eight-fold lower MIC in Δ*rip1* compared to WT, though we only saw partial complementation (Figure 13F). Conversely, each of these strains had identical MICs when treated with the other stresses we had previously tested, confirming that Δ*rip1* is not attenuated in its response to these stresses.

Figure 13: Δ*rip1* is attenuated in models of nitrosative stress, hypoxia, and when treated with various antibiotics.

(A-E) Δ*rip1* is attenuated when treated with DETA-NO. CFUs were measured when WT + pEV (MGM345), Δ*rip1* + pEV (MGM349), and Δ*rip1* + pRip1 (MGM350) *M. tb* were exposed to various stresses. **(A)** 10 mM hydrogen peroxide, 4h exposure. **(B)** 2.5 mg/mL lysozyme, 2h **(C)** 0.05% SDS, 2h **(D)** acidified medium, pH 4.5, 7 d **(E)** 200 µM DETA-NO added daily, 3d. **(F)** Minimum inhibitory concentration (MIC) was measured for WT + pEV, Δ*rip1* + pEV, and Δ*rip1* + pRip1. Triplicate biological replicates were measured. **(G)** Δ*rip1* is not sensitive to gross nutrient starvation. WT + pEV, Δ*rip1* + pEV, and Δ*rip1* + pRip1 were incubated without shaking in PBS, and persistence was measured by CFU. **(H)** Δ*rip1* is attenuated in the Wayne model. WT + pEV, Δ*rip1* + pEV, and Δ*rip1* + pRip1 were tested in the Wayne model of hypoxia, growth and persistence was measured by CFU. **(I)** Δ*rip1* is effectively killed by multiple antibiotics. WT + pEV, Δ*rip1* + pEV, and Δ*rip1* + pRip1 were incubated with 40 µg/mL vancomycin, 0.1 µg/mL isoniazid, 4 µg/mL streptomycin, 0.2 µg/mL rifampicin, or no antibiotic control, and CFUs were measured at the end of 1 week. CFU counts represent a triplicate of biological replicates; error bars represent standard deviation.

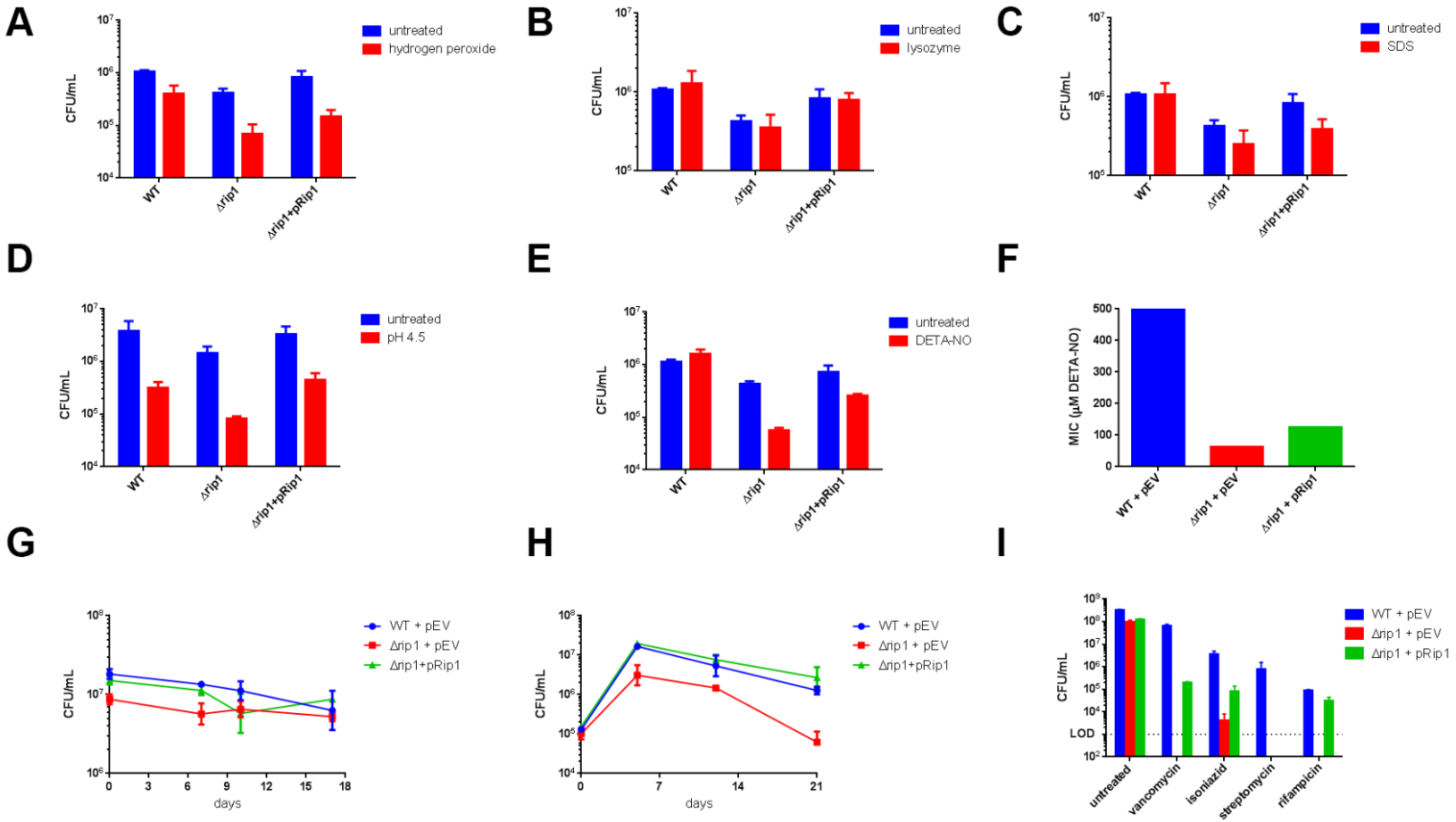
A
CFU/mL
untreated
hydrogen peroxide
WT
Δrip1
Δrip1+pRip1
B
CFU/mL
untreated
lysozyme
WT
Δrip1
Δrip1+pRip1
C
CFU/mL
untreated
SDS
WT
Δrip1
Δrip1+pRip1
D
CFU/mL
untreated
pH 4.5
WT
Δrip1
Δrip1+pRip1
E
CFU/mL
untreated
DETA-NO
WT
Δrip1
Δrip1+pRip1
F
MIC (μM DETA-NO)
WT + pEV
Δrip1 + pEV
Δrip1 + pRip1
G
CFU/mL
WT + pEV
Δrip1 + pEV
Δrip1+pRip1
days
H
CFU/mL
WT + pEV
Δrip1 + pEV
Δrip1+pRip1
days
I
CFU/mL
LOD
WT + pEV
Δrip1 + pEV
Δrip1 + pRip1
untreated
vancomycin
isoniazid
streptomycin
rifampicin

In addition to active means of killing, the host also attempts to suppress growth of *M. tuberculosis* by limiting its access to nutrients and to oxygen. To test whether Δ*rip1* is able to survive under these conditions, we utilized the Loebel model of PBS starvation (Gengenbacher et al. 2010, Loebel, Shorr, and Richardson 1933, Dietrich et al. 2015) and the Wayne model of hypoxia (Wayne and Sohaskey 2001, Wayne and Hayes 1996). Over two weeks of culture in PBS, Δ*rip1* experienced a minor drop in culturable bacilli comparable to WT and complemented strains (Figure 13G), indicating resistance to nutrient starvation. However, Δ*rip1* showed an attenuated phenotype in both early (0-7 days) and late (14-21 days) stages of hypoxia (Figure 13H).
The sensitivity of Δ*rip1* to both nitric oxide and hypoxia may indicate a general susceptibility to redox stress, though Δ*rip1* is not sensitive to hydrogen peroxide. Recent work has indicated that otherwise disparate classes of antibiotics may act via a common mechanism of inducing oxidative stress (Kohanski et al. 2007) and that the cellular response to antibiotics and to oxidative stress may be similar (Idh et al. 2012, Bulatovic et al. 2002, Nandakumar, Nathan, and Rhee 2014). We cultured WT, Δ*rip1*, and complemented strains in the presence of one of four antibiotics: vancomycin, isoniazid, rifampicin, and streptomycin. Δ*rip1* was effectively killed by each of these antibiotics, while WT *M. tb* was less susceptible.

Role of proteolysis, protein-binding PDZ domain, and σ factors in Δ*rip1* response to stress

Since identifying Rip1 as an important factor in *M. tb* virulence, the Glickman lab has attempted to elucidate the mechanism of this site-2 protease. Studies have identified the cognate anti-sigma factors for σ K, L, M (Sklar et al. 2010)

and D (Schneider, Sklar, and Glickman 2014) as substrates of Rip1. Rip1 cleaves these transmembrane anti-sigma factors, de-tethering their respective sigma factors from the cell membrane and allowing them to drive transcription of their regulons. In completing these studies, members of the Glickman lab constructed a catalytically-dead (Rip1H21A) Rip1 (Sklar et al. 2010) and a truncated Rip1 lacking its regulatory PDZ domain (Rip1ΔPDZ) (Schneider et al. 2013). To explore the mechanism of Δ*rip1* sensitivity to the previously-identified stresses, we expanded our assays to include Rip1H21A, Rip1ΔPDZ, the triple mutant $\Delta\sigma_{KLM}$, and the mutant $\Delta\sigma_{D}$.

A repeat of the previous experiment in which *M. tb* was cultured for three days in the presence of DETA-NO confirmed our prior finding that Δ*rip1* is highly sensitive to nitrosative stress. Δ*rip1* was killed at a frequency of 90% or greater at doses for which WT and the complemented strain were not killed (Figure 14A, doses > 31.25 μM; previous experiment used 200 μM). Both the $\Delta\sigma_{KLM}$, and $\Delta\sigma_{D}$ mutants were resistant to DETA-NO treatment, in concordance with the lack of *in vivo* attenuation found for these strains (Sklar and Glickman, unpublished data). Conversely, both the Rip1ΔPDZ and Rip1H21A constructs failed to complement the Δ*rip1* mutant, with expression of the H21A protein conferring even further sensitivity. The hyper-attenuation of the H21A-expressing strain confirms that Rip1 proteolytic activity is required to maintain resistance to DETA-NO. Additionally, the attenuation of the Rip1ΔPDZ-expressing mutant demonstrates that the protein-adaptor or regulatory activity of the PDZ domain is also necessary. We have been unable to construct a $\Delta\sigma_{KLMD}$ quadruple mutant to absolutely confirm that these sigma factors do not act in a redundant manner, but it seems likely that there are

Figure 14: Contribution of catalytic activity, PDZ domain, and sigma-factors to Δ*rip1* attenuation.

WT + pEV (MGM309), Δ*rip1* + pEV (MGM349), Δ*rip1* + pRip1 (MGM350), Δ*rip1* + pRip1H21A (MGM573), Δ*rip1* + pRip1ΔPDZ (MGM575), $\Delta\sigma_{KLM}$, + pEV (MGM8052), and $\Delta\sigma_{D}$ + pEV (MGM8053) were tested when treated with DETA-NO, in the Wayne model, and when treated with antibiotics. **(A)** Expression of Rip1H21A hyperattenuates Δ*rip1 in* response to DETA-NO; the PDZ domain of Rip1 is required for resistance. The above strains were treated with DETA-NO at varying concentrations for three days, with DETA-NO being refreshed daily. CFUs were measured at the end of the experiment, and survival was measured as the fraction of CFUs at each concentration of DETA-NO normalized to CFUs for the no treatment control. **(B)** Catalytic activity of Rip1 is dispensable in the Wayne model; the PDZ domain of Rip1 is required for full resistance. The above strains were tested in the Wayne model, and CFUs were measured at various points. **(C)** Catalytic activity of Rip1 and its PDZ domain are required for resistance to antibiotics. MICs were measured for he above strains for isoniazid, rifampicin, streptomycin, and vancomycin. Measurements were taken in triplicate. CFUs for this figure represent the average of three biological replicates; error bars indicate standard deviation.

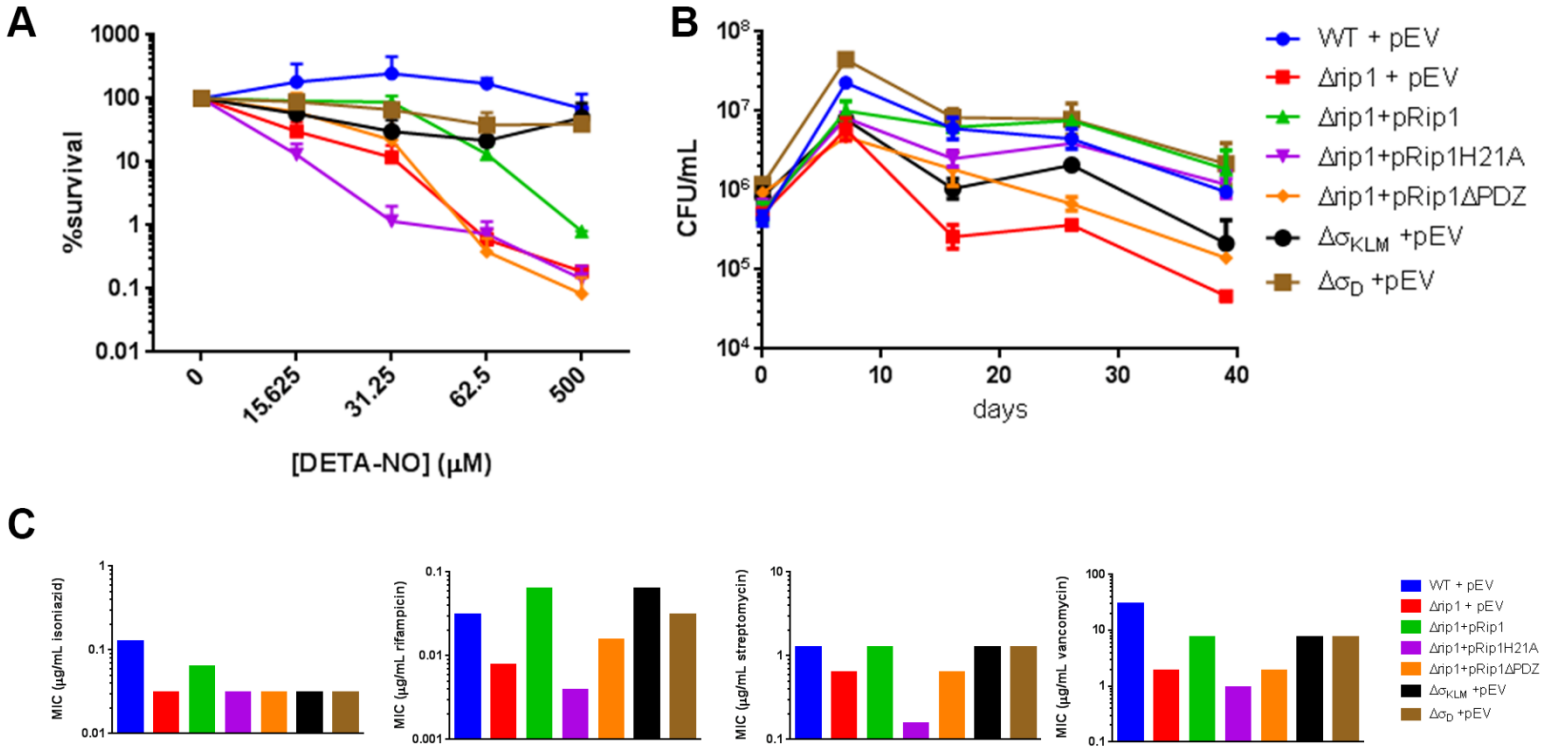
A
%survival
1000
100
10
1
0.1
0.01
0
15.625
31.25
62.5
500
[DETA-NO] (μM)
B
CFU/mL
10^8
10^7
10^6
10^5
10^4
0
10
20
30
40
days
WT + pEV
Δrip1 + pEV
Δrip1+pRip1
Δrip1+pRip1H21A
Δrip1+pRip1ΔPDZ
$\Delta\sigma_{KLM}$ +pEV
$\Delta\sigma_D$ +pEV
C
MIC (μg/mL isoniazid)
MIC (μg/mL rifampicin)
MIC (μg/mL streptomycin)
MIC (μg/mL vancomycin)
WT + pEV
Δrip1 + pEV
Δrip1+pRip1
Δrip1+pRip1H21A
Δrip1+pRip1ΔPDZ
$\Delta\sigma_{KLM}$ +pEV
$\Delta\sigma_D$ +pEV

unidentified Rip1 substrates which play a role in the Rip1-mediated response to nitrosative stress.

Addition of these strains to our Wayne model experiments did not show the same biochemical and genetic relationships between phenotypes (Figure 14B). Strikingly, while the Rip1ΔPDZ-expressing strain did show a slightly milder attenuation (compared to Δ*rip1* with an empty vector) in response to hypoxia, expression of Rip1H21A fully complemented the Δ*rip1* strain. This result demonstrates that the catalytic activity of the Rip1 protease is not required for resistance to hypoxia. Proteolysis by any enzyme may not be necessary; alternatively, expression of Rip1H21A may permit another protease to form a protein-protein complex with Rip1 and to function in the absence of Rip1 proteolysis. Δσ_{KLM} *M. tb* possessed a mild phenotype, suggesting that one or more of their anti-sigma factors are relevant Rip1 substrates in the context of hypoxia, while Δσ_D was not attenuated.

We performed MIC assays for each of the four antibiotics tested above on these strains, and found that results tended to segregate as they did in tests of DETA-NO, sensitivity, though this was not true for all of the antibiotics (Figure 14C, comparison of all phenotypes in Table 2). Expression of Rip1H21A conferred hypersensitivity in the case of streptomycin and rifampicin, while it had failed to complement Δ*rip1* in the case of isoniazid and vancomycin.

Expression of Rip1ΔPDZ partially complemented Δ*rip1* for rifampicin sensitivity, but did not complement Δ*rip1* for sensitivity to isoniazid, streptomycin, or vancomycin. Both Δσ_{KLM} and Δσ_D were resistant to rifampicin and streptomycin, sensitive to isoniazid, and had a moderate phenotype when exposed to vancomycin.

Table 2: Summary of Δ*rip1* phenotypes

Sensitivity in the Wayne model, to DETA-NO, and to antibiotics are summarized. Resistant indicates WT phenotype, sensitive indicates Δ*rip1* phenotype, hypersensitive indicates a more attenuated phenotype than Δ*rip1*, and partial indicates a phenotype between WT and Δ*rip1*.

	Wayne	DETA-NO	Rifampicin	Streptomycin	Isoniazid	Vancomycin
WT + pEV	resistant	resistant	resistant	resistant	resistant	resistant
Δ*rip1* + pEV	sensitive	sensitive	sensitive	sensitive	sensitive	sensitive
Δ*rip1* + pRip1	resistant	partial	resistant	resistant	partial	partial
Δ*rip1* + pRip1H21A	resistant	hypersensitive	hypersensitive	hypersensitive	sensitive	sensitive
Δ*rip1* + pRip1ΔPDZ	partial	sensitive	partial	sensitive	sensitive	sensitive
$\Delta\sigma_{KLM}$ + pEV	partial	resistant	resistant	resistant	sensitive	partial
$\Delta\sigma_{D}$ + pEV	resistant	resistant	resistant	resistant	sensitive	partial

We then wished to investigate whether these phenotypes illuminated novel interactors with Rip1. DosR is a response regulator which is phosphorylated by its two sensor kinases DosS/T in response to hypoxia, NO, or CO (Kumar et al. 2007). The DosR regulon has been extensively characterized (Voskuil et al. 2003, Voskuil et al. 2011), and DosR has been shown to be important in the response to hypoxia and to NO (Leistikow et al. 2010, Voskuil et al. 2011), though the extent to which it is essential is controversial (Rustad et al. 2008).

Role of DosR, Rv2625c, and NaHS-reversible oxidative stress in Δ*rip1* sensitivity to stress

To test whether Δ*rip1* is able to induce the DosR regulon, we treated WT and Δ*rip1 M. tb* with DETA-NO. Both WT and Δ*rip1* strongly induced DosR regulon genes *hspX*, *Rv2625c*, and *dosR* itself, indicating no defect in the Δ*rip1* strain for this response (Figure 15A). Neither strain induced *clpP1* transcription, as would be expected for a hypoxia-response gene which is not regulated by DosR (McGillivray, Golden, and Kaushal 2015). These remaining hypoxia-induced genes as well as the genes of the enduring hypoxia response (Rustad et al. 2008) remain to be tested. *Rv2625c*, which is induced during hypoxia and is part of the DosR regulon, is also annotated as a site-2 protease, though unlike Rip1, deletion of the gene encoding Rv2625c does not confer a growth defect (Makinoshima and Glickman 2005). As catalytic activity of Rip1 is inessential during the Wayne model, we hypothesized that Rv2625c may be acting as a protease either in parallel to Rip1 or in its stead. To test this hypothesis, we deleted *rip1* in the Δ*Rv2625c* background (confirmed by Southern blot, Figure 15B). We then tested Δ*Rv2625c* and the Δ*Rv2625c*/Δ*rip1* double mutant in the Wayne model. Δ*Rv2625c* grew and

Figure 15: Genetic interactors in Δ*rip1* sensitivity to stress and reversion of stresses with NaHS

(A) Δ*rip1*is able to induce the DosR regulon in response to NO. WT (MGM345) and Δ*rip1* (MGM349) *M. tb* were treated with NO or not treated as a control, and then RT-qPCR was performed to measure induction of DosR regulon genes (*hspX, Rv2625c*, *dosR*). *clpP1* transcript was used as a negative control. **(B)** Deletion of *Rv2625c* in the Δ*rip1* background. *Rv2625c* was deleted by specialized phage transduction, and the deletion was confirmed by Southern blot. *rip1* deletion was confirmed (left) in the double mutant, and *Rv2625c* deletion was confirmed in the Δ*Rv2625c* single mutant control (MGM705) and double mutant, double mutant. **(C)** Deletion of Rv2625c confers no additional sensitivity in the Wayne model. Δ*rip1/Rv2625c* + pEV (MGM8051) was tested for growth and persistence in the Wayne model. CFUs are the average of three biological replicates; error bars indicate standard deviation. **(D-F)** MICs were tested for WT + pEV, Δ*rip1* + pEV*,* and Δ*rip1* + pRip1 (MGM350) when treated with various stresses with no additional treatment and when 100 μM NaHS was added to counteract oxidative stress. **(D)** Δ*rip1* shows no sensitivity to diamide, and NaHS shows little effect. **(E)** NaHS does not reverse Δ*rip1* sensitivity to DETA-NO, but does improve resistance of WT and Δ*rip1* + pRip1. **(F)** NaHS reverses the sensitivity of Δ*rip1* to isoniazid, rifampicin, streptomycin, and vancomycin.

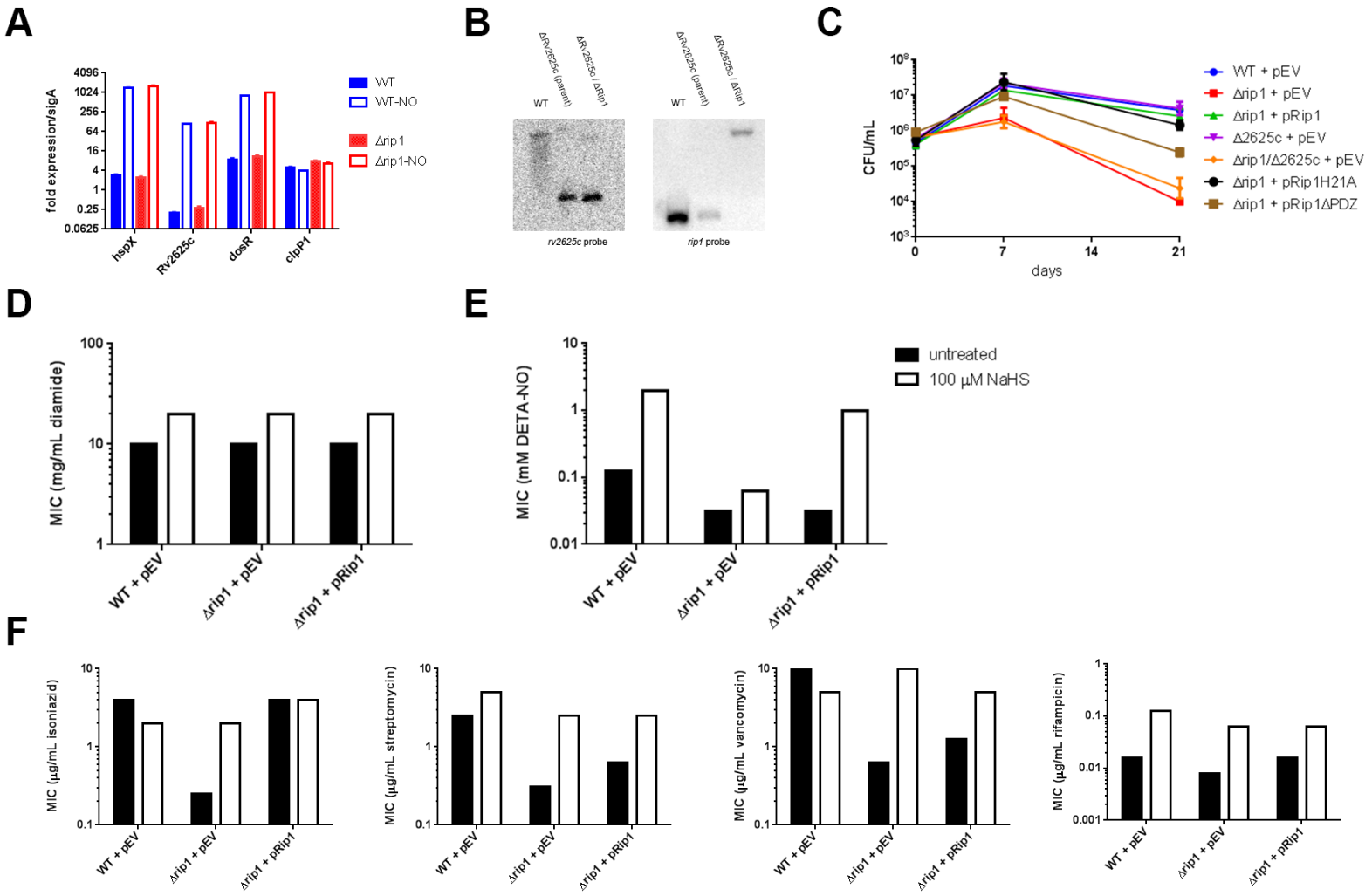
A
fold expression/sigA
4096
1024
256
64
16
4
1
0.25
0.0625
WT
WT-NO
Δrip1
Δrip1-NO
hspX
Rv2625c
dosR
clpP1
B
ΔRv2625c (parent)
ΔRv2625c::ΔRip1
WT
rv2625c probe
rip1 probe
C
CFU/mL
days
WT + pEV
Δrip1 + pEV
Δrip1 + pRip1
Δ2625c + pEV
Δrip1/Δ2625c + pEV
Δrip1 + pRip1H21A
Δrip1 + pRip1ΔPDZ
D
MIC (mg/mL diamide)
WT + pEV
Δrip1 + pEV
Δrip1 + pRip1
E
MIC (mM DETA-NO)
untreated
100 μM NaHS
F
MIC (μg/mL isoniazid)
MIC (μg/mL streptomycin)
MIC (μg/mL vancomycin)
MIC (μg/mL rifampicin)

persisted during hypoxia at a WT level, while the Δ*Rv2625c*/Δ*rip1* mutant phenocopied Δ*rip1* but conferred no additional defect (Figure 15C). As such, we concluded that Rv2625c does not act as either an additional or a backup protease along with Rip1 during the response to hypoxia.

A recent study identified Rip1 as a genetic interactor with the P-type ATPase CtpC, which responds to oxidative stress (Nambi et al. 2015). This study found that the effects of oxidative stresses like DETA-NO, or the thiol-specific oxidant diamide could be reversed with the addition of the reducing agent NaHS. Additionally, a prior study found that addition of a different reducing agent, thiourea, could reverse antibiotic-mediated killing of strains sensitive to oxidative stress (Nandakumar, Nathan, and Rhee 2014). We therefore tested the effects of NaHS during treatment with diamide, DETA-NO, and antibiotics. NaHS did increase resistance of WT, Δ*rip1*, and the complemented strain to diamide, but Δ*rip1* did not show more sensitivity to diamide than WT *M. tb*, indicating that the defect of Δ*rip1* is likely not in thiol homeostasis (Figure 15D).

Puzzlingly, addition of NaHS to media during DETA-NO treatment showed a stronger effect on WT and the complemented strain than it did on Δ*rip1* (Figure 15D). As such, we concluded that the Δ*rip1* defect in response to DETA-NO is not reversible by NaHS, which may indicate the presence of targets of NO which cannot be acted upon by NaHS, though they may be amenable to other reducing agents. Addition of NaHS during antibiotic treatment successfully increased resistance of Δ*rip1* to all four antibiotics, though it was only occasionally successful at reversing the effect of antibiotics in WT and in the complemented strain. Thus, it seems likely that Δ*rip1* sensitivity to antibiotics is mediated by oxidative stress, though we are unable

to determine whether this sensitivity is a result of greater oxidative stress at the baseline state or because of an inability to respond to oxidative stress when it occurs.

CHAPTER FOUR: Δ*RIP1 M. TUBERCULOSIS* IN *NOS2*$^{-/-}$ MICE

Δ*rip1* attenuation *in vivo* is partially attributable to nitric oxide

Based on the finding that Δ*rip1 M. tb* are susceptible to DETA-NO treatment (Figure 13E-F), we decided to investigate the contribution of nitric oxide to the *in vivo* phenotype of Δ*rip1*. Δ*rip1* is highly attenuated in the mouse model of infection (Sklar et al. 2010) in both the acute and chronic phases of infection, and is eventually cleared completely from the mouse.

The iNOS (inducible nitric oxide synthase) knockout mouse (*nos2*$^{-/-}$) is commercially available and has been used in numerous studies to determine the contribution of nitric oxide to host immunity to *M. tb* infection via infection of the mouse (MacMicking et al. 1997, Cooper et al. 2000, Scanga et al. 2001) or of macrophages derived from the iNOS knockout mice (Hu and Coates 2011, 2009). More recent work (Beisiegel et al. 2009, Mishra et al. 2017) has attempted to distinguish between the cytotoxic and immunomodulatory activities of nitric oxide.

We infected iNOS knockout mice with WT and Δ*rip1* and measured bacterial load in the lungs (Figure 16A) and spleen (Figure 16B) as well as survival of the mice over time (Figure 16C). As has been previously observed (Scanga et al. 2001), iNOS knockout mice infected with WT *M. tb* rapidly succumb to the infection in around 30 days. In comparison, Δ*rip1*-infected iNOS knockout mice began to experience lethal complications from the infection at around 70 days, and by the conclusion of the experiment (day 112), only half of the infected mice had died.

In comparison to previous experiments (Figure 16A-B, dotted lines), in which we infected WT C57Bl/6 mice with WT and Δ*rip1 M. tb*, infection of the iNOS

Figure 16: Δ*rip1* regains most but not all of its virulence when infecting iNOS knockout mice

(A-C) Infection of iNOS knockout mice with Δ*rip1* (MGM3206) and WT (EF2) (solid lines). Data from a prior infection of Bl/6 mice is superimposed (dotted lines). **(A)** Bacterial burden in the lungs. **(B)** Bacterial burden in the spleen. **(C)** Survival rate of 10 mice per strain. **(D-E)** Subsequent infection of iNOS knockout and Bl/6 mice with Δ*rip1*. **(D)** Bacterial burden in the lungs. **(E)** Bacterial burden in the spleen. CFU counts are the average of four biological replicates per organ. Error bars indicate standard deviation.

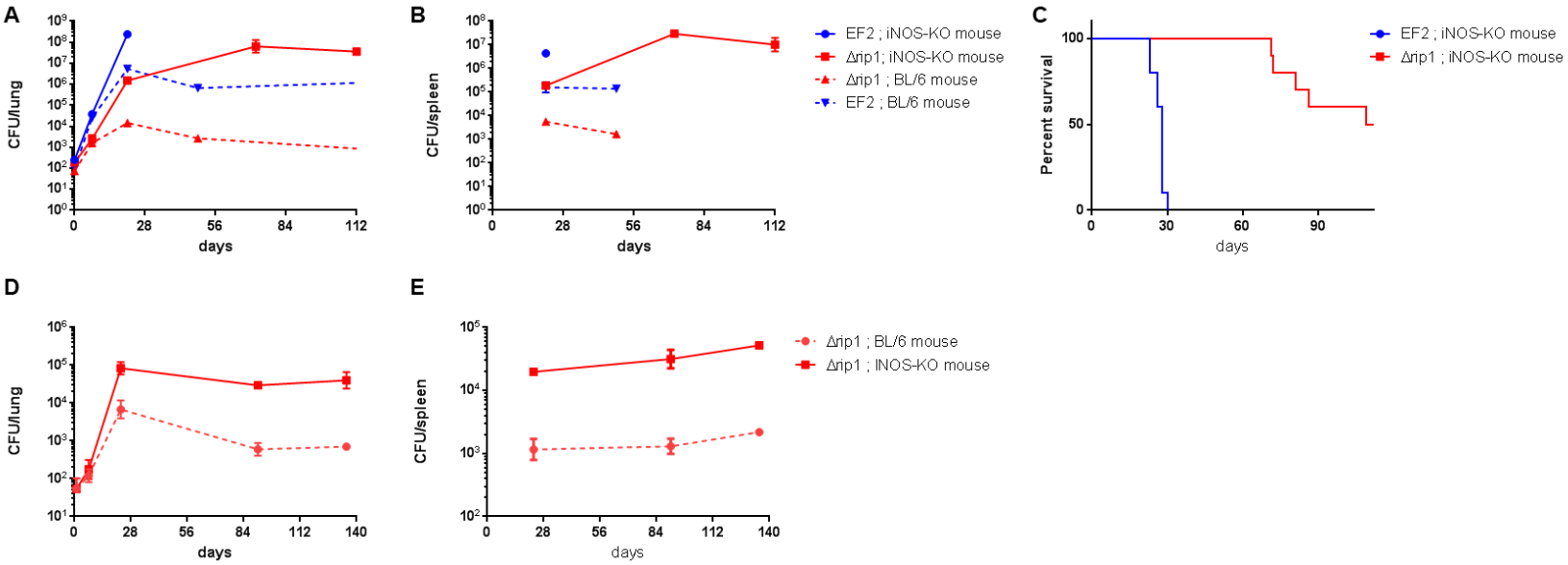
A
CFU/lung
days
B
CFU/spleen
days
EF2 ; iNOS-KO mouse
Δrip1; iNOS-KO mouse
Δrip1 ; BL/6 mouse
EF2 ; BL/6 mouse
C
Percent survival
days
EF2 ; iNOS-KO mouse
Δrip1 ; iNOS-KO mouse
D
CFU/lung
days
E
CFU/spleen
days
Δrip1 ; BL/6 mouse
Δrip1 ; INOS-KO mouse

knockout mice showed no difference before week 1. Between weeks 1 and 3, Δ*rip1* showed no defect compared to WT in the iNOS knockout mouse, while in Bl/6 mice, the virulence defect between WT and Δrip1 increased over this time period. After this time point, iNOS knockout mice established some control over the infection, albeit with a very high bacterial load (10^7-10^8 CFU/lung or spleen) which exceeded that in a chronic infection of Bl/6 mice with WT M. tb. It is also important to note that measures of bacterial burden taken at the late time points (d71 and 112) are necessarily from the fraction of mice which have established the best control over the infection, as the most-affected mice were dying or had died by these time points.

Because this infection was carried out with a high inoculum (~200-250 CFU/lung, compared to 100 CFU/lung typical of prior experiments), we decided to repeat the experiment to ensure that the result we found was not merely inoculum-dependent. To do this, we infected Bl/6 and iNOS knockout mice with Δ*rip1* (Figure 16D-E). In this experiment, we obtained a lower inoculum (~50 CFU/lung) which resulted in better host control of the infection as demonstrated by lower bacterial burden (Figure 16D-E) and no mortality. In comparison to the prior experiment, we found a smaller, though still significant difference between infection of Bl/6 and iNOS knockout mice with Δ*rip1* of about 1-2 logs in the lung and 1 log in the spleen. The restoration of virulence of Δ*rip1* in iNOS mice thus partially accounts for the defect of Δ*rip1* compared to WT M. tb in infection of Bl/6 mice (2-3 logs in the lung, 1-2 logs in the spleen) (Figure 16A-B, dotted lines). As such, we concluded that the defect of Δrip1 can be partially but not fully attributed to its sensitivity to nitric oxide. Its very early defect from the time of inoculation to week 1 is entirely independent of nitric oxide, as expected, since it comes before the induction of adaptive

immunity. Both this initial defect and the nitric oxide-independent defect Δ*rip1* shows (~1 log) after week 1 remain to be explored.

iNOS knockout mice infected with Δ*rip1* develop histopathologic features of granulomas

To further characterize the phenotype of the Δ*rip1* mutant in iNOS knockout mice, we performed histology on fixed lung sections from each infection. Hematoxylin and eosin (H&E) staining of lung sections from day 21 of the infection (Figure 17A-B) demonstrates that infection of iNOS knockout mice with WT *M. tb* (Figure 17A) yields a significant inflammatory infiltrate, with approximately 50% of the lung tissue involved, while infection of the same mouse strain with Δ*rip1* (Figure 17B) yields a more mild phenotype, with distinct sites of inflammation. These data are in accordance with the bacterial loads found in the two infections. By day 71, the Δ*rip1* infection has reached nearly the same bacterial load as the WT infection at day 21 (Figure 16A), and the pathology of the Δ*rip1*-infected mouse has similarly expanded to include a large percentage of the lung (Figure 17C). Intriguingly, this pathology includes both disorganized inflammatory infiltrates as seen in the day 21 time point as well as the beginning of more localized infiltrates. At day 112, (Figure 17D), large localized infiltrates are clearly visible, with many displaying an acellular center indicative of necrosis. Infiltrates are surrounded by a poorly-stained region which may represent foamy macrophages (Russell et al. 2009) which typically are found at the interface of necrotic regions and the surrounding lung and would be washed away during deparaffinization.

As these localized lesions appeared to share similar features with human granulomas, we decided to perform additional histological stains to further

Figure 17: Progression of pathology in WT and Δ*rip1* infected iNOS knockout mice

H&E staining of formalin-fixed, paraffin-embedded lung sections from WT **(A)** and Δ*rip1*-infected **(B-D)** iNOS knockout mice. **(A-B)** Day 21. **(C)** Day 71. **(D)** Day 112. WT-infected mice have diffuse inflammatory infiltrates at day 21, while Δ*rip1*-infected mice develop localized inflammatory infiltrates from day 71 to day 112. Signs of necrosis develop by day 112.

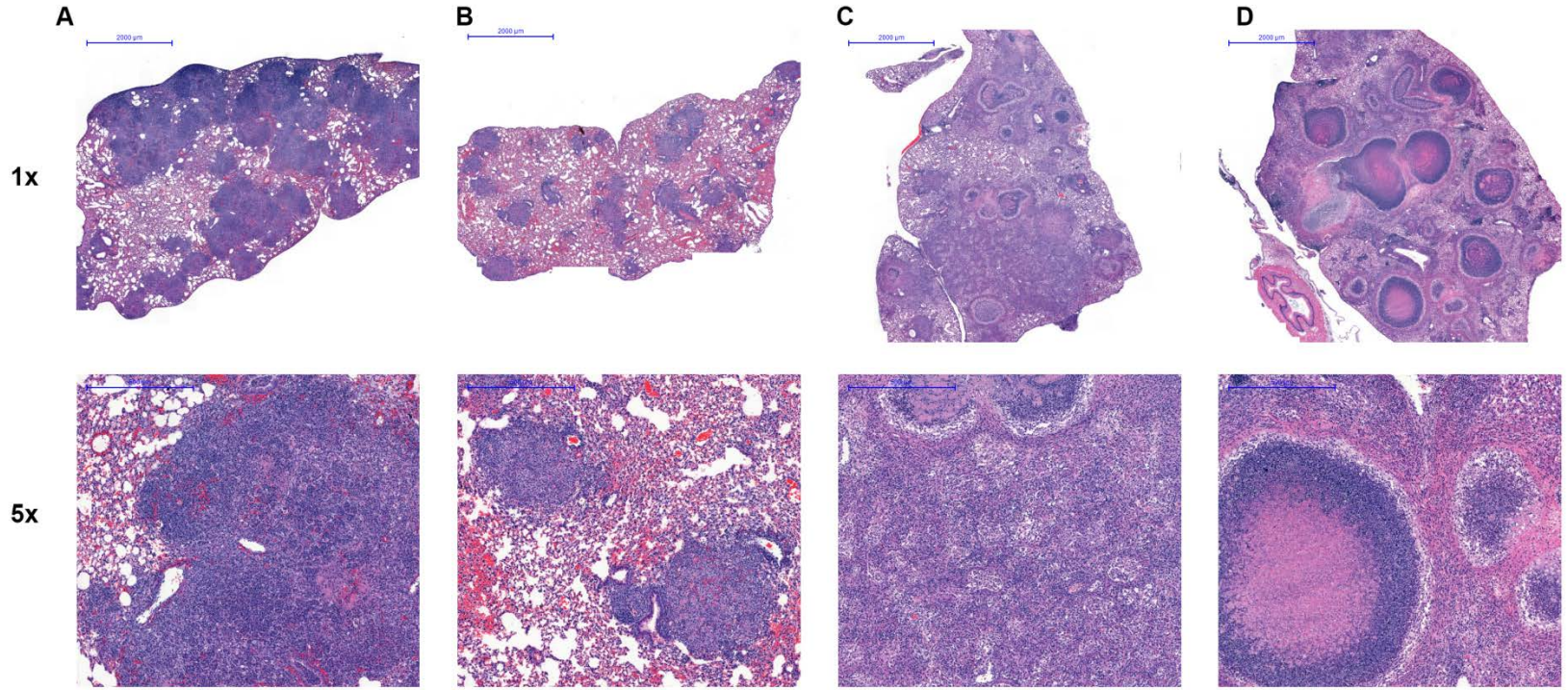
A
B
C
D
1x
5x

characterize their pathology (Figure 18). Granulomas are typically surrounded by fibrotic tissue in both human (Solsona Peiro, de Souza Galvao, and Altet Gomez 2014) and non-mouse animal models (Subbian et al. 2011) of tuberculosis infection. Masson's trichrome staining (Figure 18B-C) indicated limited fibrotic tissue (blue staining) in the border between the inflammatory infiltrate of WT-infected mice at day 21 (Figure 18B), but a fibrotic sheath forming around the granuloma of a Δ*rip1*-infected mouse at day 112 (Figure 18C; compare to H&E staining of the same lesion Figure 18A).

Additionally, we used acid-fast staining to examine the localization of *M. tb* bacilli in the lung during the infection (Figure 18D). Bacteria were largely localized inside the granulomas, with a smaller fraction of bacteria present at non-granulomatous sites of inflammation. As has been seen previously (Hoff et al. 2011), bacilli were present both in the cellular and acellular/necrotic areas of the granuloma. Bacilli were most common in the unstained area directly inside the fibrotic sheath which indicates foamy macrophages, but could also be found in the necrotic center of granulomas. Bacteria were present, but less common, in areas of the granuloma which contained cellular infiltrates, and were also less common in cellular, non-necrotic granulomas.

To assess the types of immune cells present in the inflammatory infiltrates we saw, we utilized fluorescent immunohistochemistry to stain for CD11b (macrophages/monocytes) and CD3 (T cells) (Figure 19). CD11b staining was highly evident in all samples appeared to match much of the staining of inflammatory infiltrates as seen with H&E (Figure 17), especially at early time points (Figure 19A-B). CD3 staining was far less common, with individual $CD3^+$ cells being evident in non-granulomatous tissue. Some, but not all necrotizing granulomas were characterized by a ring of $CD3^+$ cells at the

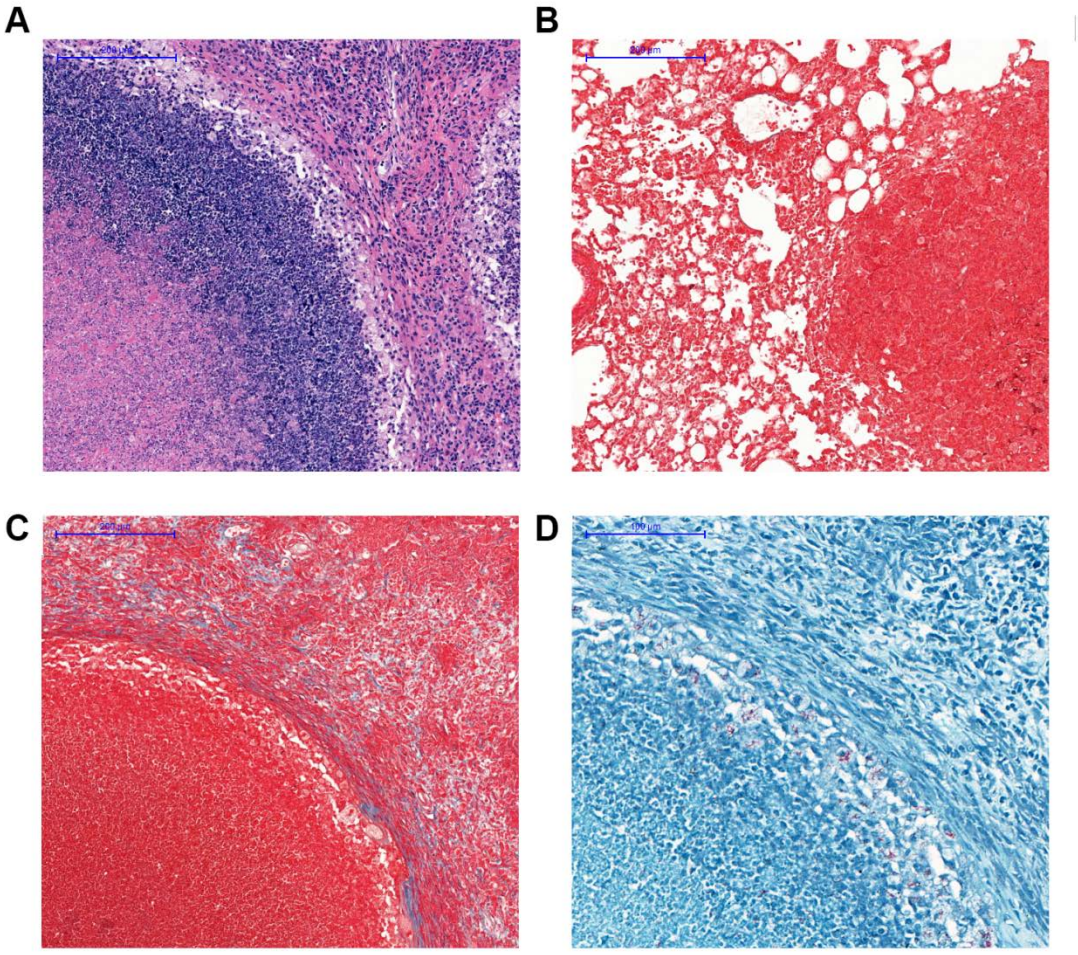

Figure 18: Comparison of H&E, Masson's trichrome, and acid-fast bacillus staining in granulomatous lesions.

(A) H&E staining of a necrotic granuloma (further zoom of lesion from Figure 17D, indicating the fibrotic, unstained, cellular, and necrotic areas of the lesion. **(B-C)** Masson's trichrome staining of **(B)** an inflammatory infiltrate from a WT-infected mouse at day 21 (further zoom of lesion from Figure 17A) and **(C)** the granuloma pictured in part A. Cytoplasm is stained red, and fibrotic tissue is stained blue. **(D)** Acid-fast bacillus staining of the granuloma from part A. Acid-fast bacilli are stained red, other tissues are stained blue. All images measured at 10x magnification.

Figure 19: Fluorescent immunohistochemistry of lung sections to detect $CD3^+$ and $CD11b^+$ cell infiltrates.

(A) Staining of WT-infected iNOS knockout mouse lung section harvested at day 21. **(B)** Δ*rip1*-infected iNOS knockout mouse lung section harvested at day 21. **(C)** day 71 **(D)** day 112. Images correspond to those taken of H&E staining in Figure 17. DAPI (cell nuclei) stained in blue, CD3 (T cells) stained in red, CD11b (macrophages and monocytes) stained in green.

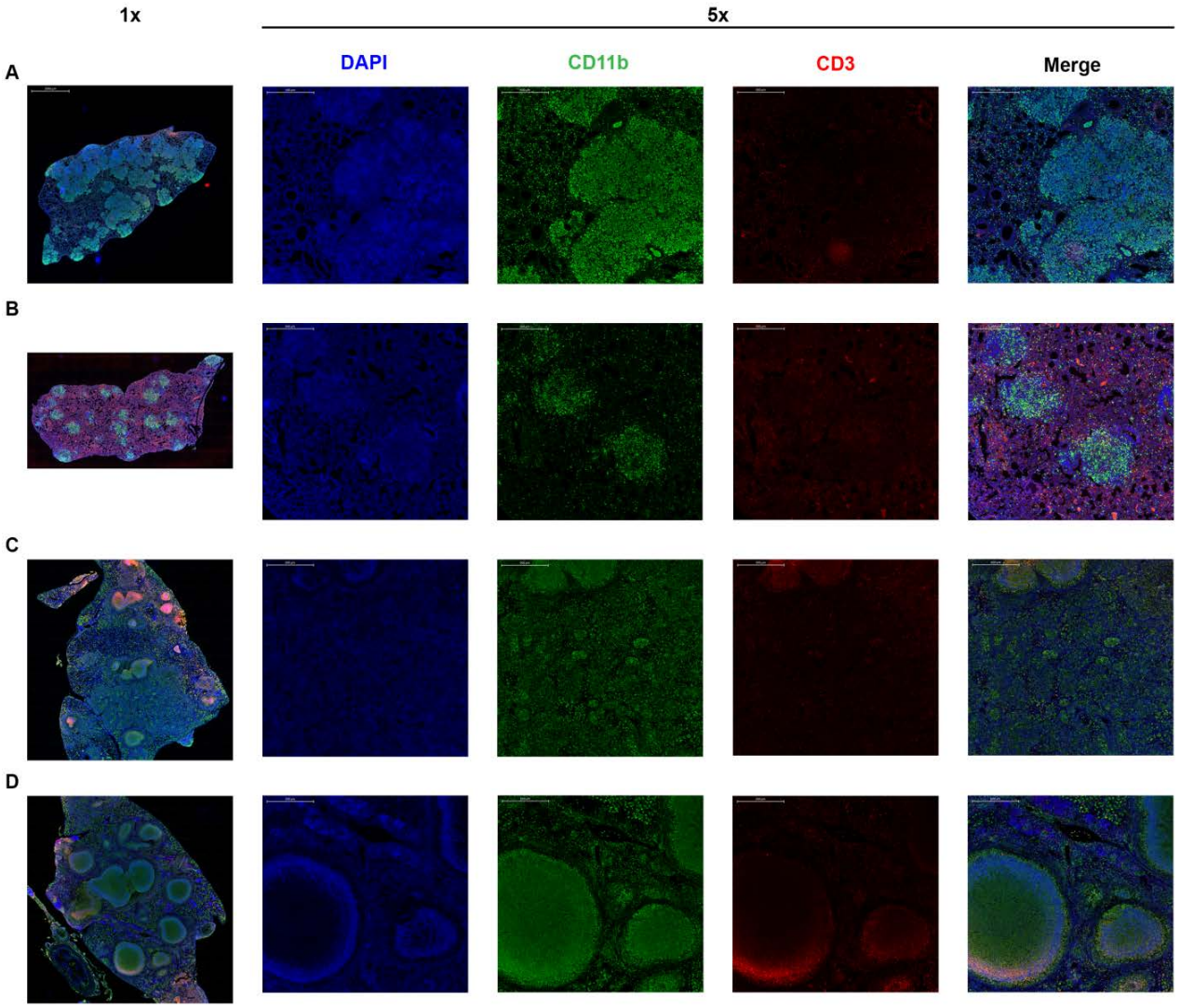
1x
5x
DAPI
CD11b
CD3
Merge
A
B
C
D

periphery of the granuloma (Figure 19D). Additionally, certain cellular granulomas did show $CD3^+$ cell infiltrates, though it is uncertain whether this is nonspecific staining, as some acellular regions and the outsides of lung sections also tended to stain as $CD3^+$.

Staining of Δ*rip1*-infected iNOS knockout mice was comparable to staining of WT-infected mice at the day 21 time point. WT-infected mice showed stronger staining for CD11b, but it is difficult to distinguish whether this is because of the differences between strains or merely because of the higher bacterial burden seen in WT-infected mice (Figure 17A).

Hypoxia is a relevant stress involved in the control of *M. tb* during infection (Rao et al. 2008, Rustad et al. 2009), but while human granulomas and non-mouse animal models of *M. tb* infection produce hypoxic lesions (Rustad et al. 2009, Via et al. 2008), this is not typically the case in infection of mice (Aly et al. 2006). Recently, the C3HeB/FeJ ("Kramnik") mouse model, which recapitulates multiple phenotypes of granulomas, has been shown to yield hypoxic lesions (Driver et al. 2012, Harper et al. 2012). As the lesions we saw in infection of iNOS knockout mice with Δ*rip1* were also granuloma-like, we decided to test these lesions for hypoxia.

Pimonidazole forms adducts with proteins in the presence of hypoxia, and has been used widely in immunohistochemistry both in the study of tuberculosis (Harper et al. 2012, Via et al. 2008) as well as in the study of tumor hypoxia (Varia et al. 1998). During our second infection (Figure 16D-E), we injected a subset of mice with pimonidazole prior to sacrifice, and then examined lesions found at late time points (day 91-135). Positive staining for pimonidazole was highly evident in both cellular (Figure 20A-B) and necrotic (Figure 20C) lesions. Unaffected parts of the lung did not show positive staining

Figure 20: Pimonidazole staining for hypoxia in granulomatous lesions

Mice were injected with pimonidazole prior to sacrifice, and sections were stained using an anti-pimonidazole adduct antibody. H&E stained lesions are shown on the left, corresponding pimonidazole staining is on the right. **(A)** 5x magnification image of a cellular lesion, showing affected and unaffected tissue. (day 135) **(B)** 10x magnification image of the same lesion **(C)** 10x magnification image of a necrotic lesion (day 135) **(D)** 10x magnification image of a necrotic lesion from a mouse not infected with pimonidazole prior to sacrifice (day 91) **(E)** Comparison of bacterial burden at day 91 from mice injected or not injected with pimonidazole prior to harvest. No change in CFU is apparent. Pimonidazole-injected groups are the average CFUs from 3 mice each, non-pimonidazole-injected groups are the average CFUs from 4 mice each. Error bars indicate standard deviation.

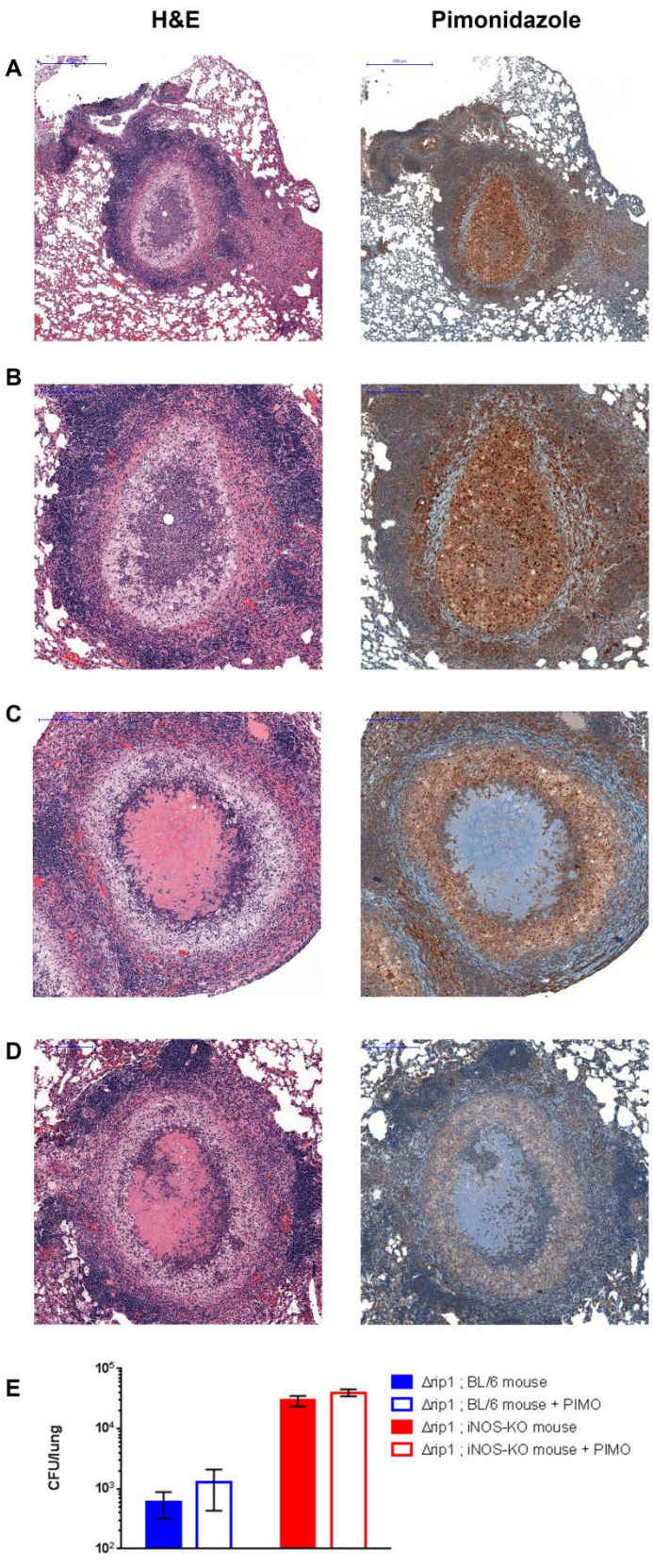
H&E
Pimonidazole
A
B
C
D
E
CFU/lung
10^5
10^4
10^3
10^2
Δrip1 ; BL/6 mouse
Δrip1 ; BL/6 mouse + PIMO
Δrip1 ; iNOS-KO mouse
Δrip1 ; iNOS-KO mouse + PIMO

(Figure 20A, bottom left area). Some nonspecific staining is likely to be present, as areas peripheral to the granuloma with strong inflammatory infiltrates also stained positive for pimonidazole (Figure 20B-C), which is not the case in rabbit granulomas (Datta et al. 2016), though this may also be a result of differences between the animal models. Lesions from mice not injected with pimonidazole did not show the same intensity of staining, though some light-brown color can be seen (Figure 20D). Finally, we assessed evident bacterial burden in mice injected or not injected with pimonidazole (Figure 20E). At both early time points (day 23, data not shown) and at time points at which hypoxia was evident (Figure 20E, day 91), both Bl/6 and iNOS mice show no change in apparent CFU when pimonidazole was injected into the host before harvest. Therefore, future experiments will not necessitate a large number of mice not be injected with pimonidazole to be used for CFU counts, and we should be able to analyze larger numbers of lesions for hypoxia.

DISCUSSION

Pyruvate carboxylase catalytic activity is required for BioQ-mediated derepression of biotin biosynthesis under low-biotin conditions[*]

We have uncovered an unanticipated role for pyruvate carboxylase in regulating biotin biosynthesis in mycobacteria. We identified transposon insertions in *MSmeg_2412*, encoding pyruvate carboxylase, as unable to grow on medium lacking biotin. The role of pyruvate carboxylase in regulating biotin biosynthesis is to mediate transcriptional induction of BioQ repressed biotin biosynthetic genes. In the absence of Pyc, these genes remain repressed, conferring biotin auxotrophy. This function of Pyc in biotin biosynthesis requires the active site residues of the Pyc enzyme as well as enzyme biotinylation, strongly suggesting that the participation of Pyc in the biotin pathway reflects its canonical enzymatic activity in central metabolism. We find that biotinyl-Pyc is the most rapidly depleted biotinylated protein upon biotin withdrawal, supporting the idea that the loss of Pyc activity is an early consequence of biotin starvation. Our primary model to explain these findings is that transient loss of pyruvate carboxylase activity caused by biotin deprivation generates the metabolic signal that derepresses BioQ-regulated genes. This metabolite could be the direct substrate of Pyc, pyruvate, which we find to accumulate with biotin withdrawal in our metabolomic studies. However, it may be unlikely that such a central metabolite, the levels of which could be affected by many factors independent of biotin starvation, would be the signal for BioQ depression. More likely is that the BioQ signal is Pyc dependent, but is a downstream conversion product of a metabolite that

[*] This section is derived from: Lazar *et al* 2017 (in review)

accumulates due to Pyc dysfunction, which we did not identify in our metabolomic studies. Further work is therefore required to identify the Pyc dependent BioQ inducer.

At first glance, it may seem paradoxical that transient loss of Pyc activity (through loss of biotinylation during biotin deprivation) induces biotin biosynthesis through BioQ, whereas permanent loss (*i.e.* genetic deletion) prevents BioQ derepression. Our data indicate that the Pyc enzyme, itself a biotinylated protein, declines rapidly in abundance during the early hours of biotin withdrawal in a strain that cannot synthesize biotin, before other biotinylated proteins have declined and before cell death occurs. Changes in metabolites caused by the transition of pyruvate carboxylase from holo- to apo- form, and its subsequent loss of catalytic activity, would be predicted to result in acute metabolic shifts that would be different from those experienced by a strain lacking pyruvate carboxylase through genetic deletion. Indeed, our metabolomic analysis strongly supports that 1) biotin withdrawal causes broad metabolic shifts in wild type cells 2) these shifts are much less dramatic or absent in Pyc deficient cells and 3) genetic deletion of *pyc* causes metabolic perturbation even in the presence of biotin such that this mutant has adapted to the metabolic shifts that accompany acute loss of Pyc function. This effect is obvious when observing the detected levels of pyruvate, the substrate of Pyc. Pyruvate accumulates in wild type cells upon biotin starvation, consistent with Pyc dysfunction. However pyruvate does not accumulate in the Pyc deficient strain in any condition, indicating that the strain has adapted to chronic loss of pyruvate carboxylase.

An alternative explanation for the role of pyruvate carboxylase in regulation of biotin biosynthesis would be that BioQ senses low levels of biotin in a manner

similar to *E. coli* BirA. When biotin levels are low, biotin-binding domains would not be saturated with biotin cofactor, and unbiotinylated BCCP domains could interact directly with BioQ to modulate BioQ's regulatory function. However, this hypothesis is unlikely to explain the mechanism by which Pyc relives BioQ-mediated repression. Expression of mutant pyruvate carboxylase enzyme lacking the biotin attachment lysine (K1093), and which we have shown is not biotinylated, is unable to restore biotin prototrophy to *pyc::tn*. As this Pyc enzyme accumulates in its unbiotinylated form, it should directly depress BioQ if the accumulation of biotin free Pyc were the signal, yet it is unable to complement the auxotrophy. Additionally, this mechanism would be atypical of TetR like repressors, which typically bind a small molecule rather than a protein as their ligand, though proteins have been shown to serve as the ligands of TetR like repressors in certain cases (Burkovski 2007).

A surprising finding of our study is that a Pyc allele lacking the N terminal biotin carboxylase domain (BC) is able to support biotin biosynthesis, yet an amino acid substitution in the BC domain active site (E288K) cannot. Our original suspicion that this effect was due to the N terminal BC fragment that may be expressed in the *pyc*::*tn* strain is belied by the ability of PycΔBC to complement the Δ*pyc* strain (in which the entire *pyc* ORF is deleted). We hypothesize that complementation with the CT+BCCP truncation may occur with the biotin carboxylase domain of another biotin-utilizing enzyme *in trans*, such as the acetyl/propionyl-CoA carboxylase alpha chain enzymes MSMEG_0334 or MSMEG_1807. Each of these proteins contains a BC and BCCP domain, but lacks a CT domain, which is present in the beta chain present on a separate polypeptide. In the E288K Pyc mutant, the presence of structurally intact but inactive BC domain in the Pyc tetramer may prevent this

in trans complementation. Prior work has demonstrated that Pyc truncations retain their enzymatic activity when alone (Sueda, Islam, and Kondo 2004) and intermediate transfer between domains has been shown to occur (St Maurice et al. 2007, Islam, Sueda, and Kondo 2005). However, full explanation of this finding will require further biochemical characterization of the mycobacterial Pyc enzyme.

In summary, we have uncovered a new mechanism of biotin regulation, which relies on the competence of a biotinylated enzyme of central metabolism as a sensor for biotin sufficiency. We anticipate that this mechanism may be applicable to other bacteria which have dissociated biotin ligase function from transcriptional regulation of biotin biosynthesis.

Δ*rip1* is sensitive to nitric oxide, hypoxia, and multiple antibiotics

We have identified nitric oxide and hypoxia as relevant host-mediated stresses which are likely to play a role in its *in vivo* phenotype. As both of these stresses are redox-related, we also tested Δ*rip1* for sensitivity to antibiotics and determined that Δ*rip1* is sensitive to multiple antibiotics with diverse biological targets and chemical makeup, which lends credence to the idea that there may be a single or small number of shared mechanisms which explain these sensitivities. However, Δ*rip1* was neither sensitive to hydrogen peroxide nor diamide, two different sources of oxidative and thiol homeostatic stress, which indicates that it is not grossly sensitive to all sources of redox stress. As Rip1 is a membrane protein and Δ*rip1* has been shown (Makinoshima and Glickman 2005) to have perturbations in its cell wall, changes in permeability may be responsible for some or all of these phenotypes; similarly, changes in efflux may also explain the pleiotropic phenotype of the Δ*rip1* mutant.

However, it seems somewhat unlikely that such a broad mechanism could account not only for the attenuation we saw but also fail to yield sensitivity to hydrogen peroxide, acid, or other mechanisms we were unable to demonstrate effectively killed Δ*rip1*. We could test Δ*rip1* for uptake of ethidium bromide (Rodrigues et al. 2013) or fluorescently-labeled vancomycin (Yang et al. 2016) along with efflux pump inhibitors to determine if Δ*rip1* has defects in permeability or efflux.

Of the Δ*rip1* stress sensitivities we identified, hypoxia in particular has been the subject of numerous studies which have elegantly examined the transcriptional response it induces. While we determined that Δ*rip1* shows no defect in inducing the DosR regulon, we did not test DosR-independent gene induction both in the early stages of hypoxia as well as in the later stages, which have been termed the enduring hypoxic response (EHR) (Rustad et al. 2008). As Δ*rip1* is attenuated in both the early and later stages of the Wayne model, a defect in induction of the EHR or other DosR-independent pathways may explain of this phenotype. In particular, the sigma factors σ_E and σ_H are known to be induced by hypoxia, but are not part of the DosR regulon. The known anti-sigma factors for σ_E and σ_H are localized to the cytoplasm, but additional anti-sigma factors or genetic interactions with Rip1 may exist.

As the Δ*rip1* phenotypes we identified are characterized by different requirements for catalytic activity and the PDZ domain as well as differing interactions with previously-identified sigma factors, it may be the case that the mechanism of Δ*rip1* sensitivity to these stresses utilizes different pathways or arms of the Rip1 regulon. While Δ*rip1*'s high degree of sensitivity to antibiotics may be an obstacle to this approach, an unbiased genetic screen for suppressors of Δ*rip1* sensitivity to antibiotics may yield novel interactors in the

Rip1 pathway. Whether or not these interactors also are active in response to nitric oxide or hypoxia would help determine whether the sensitivities we found are truly attributable to a single set of players or whether multiple arms of the Rip1 pathway are each responsible for different phenotypes.

In short, we identified three groups of stresses which show increased efficacy towards Δ*rip1.* We characterized the requirements for catalytic activity, for the PDZ domain, and for previously-discovered sigma factors in resistance towards these stresses. We are presently unsure the degree to which these stresses are linked, as they show some overlap of requirements for these factors as well as differing responses to the reducing agent NaHS. Much work remains to be done characterizing the response to these stresses in the Δ*rip1* setting, which may further elucidate the causes of this strain's attenuation.

Δ*rip1* regains a significant degree of virulence in the iNOS knockout mouse, and lesions in this host show several traits of granulomas

Based on the sensitivity of Δ*rip1* to nitric oxide described above, we infected the *nos2*$^{-/-}$ (iNOS knockout) mouse with Δ*rip1*. In the absence of this host-mediated effector, Δ*rip1* is able to grow and persist to a much greater degree in the mouse, but it does not regain the full virulence seen in the WT strain. Much of the remaining phenotype of Δ*rip1* in this setting can be attributed to a defect in the acute phase of infection present from the beginning of the infection to week 1, which is likely dominated by the innate immune system and is before iNOS is thought to be induced. Additionally, this strain—unlike the Bl/6 mouse—is able to form hypoxic lesions, which may contribute to its ability to control Δ*rip1* during chronic infection, specifically because Δ*rip1* is defective in the hypoxic stage of infection.

Strikingly, histopathology performed on lungs of iNOS mice infected with Δ*rip1* showed that lesions from these mice showed several characteristics of granulomas, including necrotic centers, an unstained ring of cells which may indicate foamy macrophages, a fibrotic sheath surrounding the wound, localization of bacteria primarily to these wounds, and positive staining for pimonidazole adducts which indicates hypoxia. This is atypical of mouse infections with *M. tb*, which has been a source of difficulty within the field given the many other advantages working with mice present. While examination of the literature does show that other infections of this mouse strain have yielded similar phenotypes (Duque-Correa et al. 2014, Cooper et al. 2000), caveats with the mode of infection (intraperitoneal, extremely low-dose aerosol) have limited the degree to which investigators have been willing to follow-up on these findings. We are currently uncertain the degree to which this is solely a phenotype of iNOS knockout mice, or whether a *rip1* deletion is required to some or any extent in order to produce the pathology we observed.

Mouse models which do show granulomatous pathology have been developed; in particular, the C3HeB/FeJ “Kramnik” mouse. This strain has been used in numerous studies (Driver et al. 2012, Harper et al. 2012, Pichugin et al. 2009, Kramnik et al. 2000) but anecdotally, issues remain, including mortality among infected mice and the tendency of these mice to form a single, central granuloma. The data we present suggests that iNOS mice infected with Δ*rip1*—or perhaps other attenuated strains—may serve not to supplant the Kramnik mouse but as a complementary model. We observed mortality in mice infected with a high dose of Δ*rip1* and variable pathology in a second, low-dose infection. A third infection is ongoing, and we hope to find that a moderate dose yields consistent pathology without the trade-off of

mortality, though the lack of robustness of this model to the infectious dose is a concern. Additionally, as Δ*rip1* has pleiotropic phenotypes, this model would likely not be particularly useful in some settings where infection with WT *M. tb* would prove helpful, such as killing of bacteria with antibiotics in a hypoxic setting or at a lower dose mediated by poor diffusion across a fibrous barrier.

To further explore the contribution of Rip1 during infection as well as to improve the relevance of the iNOS/ Δ*rip1* model, we propose to infect these mice with a Δ*rip1* knockout which conditionally expresses Rip1. We can then demonstrate the role of Rip1 at various phases of infection by choosing when to induce or not to induce expression of the complementing plasmid. Expression of Rip1 must be tightly regulated, as previous attempts at complementation of Δ*rip1* under an inducible promoter failed to show a Δ*rip1* phenotype under uninduced conditions, likely because of low-level transcription without the inducer. We must also demonstrate that phenotypes we wish to investigate in this *in vivo* model are fully complemented by expression of Rip1 under this promoter, as we have repeatedly seen incomplete or partial complementation of Rip1. However, if Rip1 can be induced at late time points without causing mortality in the host and development of granulomas proceeds as seen in Δ*rip1* infections, we would then be able to consider this model with fewer caveats.

To summarize briefly, we assessed the role of nitric oxide stress as a mediator of attenuation of the Δ*rip1* strain by infecting iNOS knockout mice with Δ*rip1.* Infection of these mice restored a significant degree of virulence to Δ*rip1*, though it still failed to recapitulate the full extent of virulence seen in infection with WT *M. tb*. We also found that because this strain was attenuated, it allowed infection of iNOS mice to proceed further than would usually happen

when infecting this generally *M. tb*-susceptible strain. As such, we were able to observe development of lesions in the lung which possess histopathological traits of human granulomas, which is atypical of the mouse model. Beyond its use as a tool for studying Δ*rip1*, we believe infection of iNOS knockout mice possesses significant potential as a model for studying the ways in which pathological traits common to human disease affect the development of *M. tb* infection.

METHODS*

Growth of mycobacteria

M. smegmatis was grown aerobically in liquid culture in 7H9 broth (Difco) supplemented with 0.5% dextrose, 0.5% glycerol, and either 0.05% Tween 80 or 0.02% Tyloxapol (7H9/smeg) and on 7H10 (Remel) agar plates supplemented with 0.5% dextrose and 0.5% glycerol (7H10/smeg). 7H9 lacking biotin was made according to the listed ingredients: ammonium sulfate 500 mg/L, monopotassium phosphate 1 g/L, disodium phosphate 2.5 g/L, sodium citrate 100 mg/L, magnesium sulfate 50 mg/L, calcium chloride 500 µg/L, zinc sulfate 1 mg/L, copper sulfate 1 mg/L, L-glutamic acid 500 mg/L, ferric ammonium citrate 40 mg/L, pyridoxine hydrochloride 1 mg/L and supplemented with dextrose, glycerol, and Tween 80/Tyloxapol as above. 7H10 lacking biotin was made according to the listed ingredients: ammonium sulfate 500 mg/L, monopotassium phosphate 1.5 g/L, disodium phosphate 1.5 g/L, sodium citrate 400 mg/L, magnesium sulfate 25 mg/L, calcium chloride 500 µg/L, zinc sulfate 1 mg/L, copper sulfate 1 mg/L, L-glutamic acid 500 mg/L, ferric ammonium citrate 40 mg/L, pyridoxine hydrochloride 1 mg/L, malachite green 250 µg/L, agar 15 g/L and supplemented with dextrose and glycerol as above.

M. tuberculosis was grown aerobically in liquid culture in 7H9 broth supplemented with 0.5% glycerol, 0.05% Tween 80, and 10% OADC (7H9/TB). OADC was made according to the listed ingredients and was adjusted to pH 7: sodium chloride 8.5 g/L, bovine serine albumin fraction V

* This chapter is partially derived from: Lazar *et al* 2017 (in review)

(Roche) 50 g/L, dextrose 20 g/L, oleic acid 600 µL/L, catalase 30 mg/L (Sigma). Cultures were grown as 50 mL cultures in a 490 cm^2 roller bottle (Corning) rolled at 2 RPM.*M. tuberculosis* was grown on 7H10 agar plates (7H10/TB) supplemented with 0.5% glycerol and 10% OADC.
Antibiotics were added at the following concentrations for mycobacteria: 20 µg/mL kanamycin, 20 µg/mL streptomycin, 50 µg/mL hygromycin.
Supplements were added at the following concentrations: 50 ng/mL anhydrotetracycline (ATc), 500 ng/mL desthiobiotin (DTB), 500 ng/mL biotin, 1 µg/mL avidin.

Transposon insertional mutagenesis

A library of transposon insertion mutants in *M. smegmatis* was generated as described previously (Siegrist and Rubin 2009). Briefly, a 50 mL culture of mc^2155 *M. smegmatis* was grown aerobically to log phase (OD 0.5-1) in (7H9/smeg). The culture was washed twice in 50 mL of mycobacteriophage buffer (MP Buffer) (50mM Tris [pH 8.0], 150 mM NaCl, 10mM $MgCl_2$, 2 mM $CaCl_2$), and then resuspended in 5mL MP buffer at 37°C. Cells were transduced with φMycoMarT7 at a multiplicity of infection (MOI) of 10 for one hour, and then were transferred to 150 mm diameter 7H10/smeg plates supplemented with kanamycin and incubated for three days at 37°C. A small aliquot was serially diluted 10-fold and cultured on 7H10/smeg plates with kanamycin to determine the overall frequency of tn mutagenesis in the library. 10,000 kanamycin resistant tn mutants were pooled and then frozen at -80°C.

Screening and transposon insertion mapping

Aliquots of the transposon insertional mutant library generated above were diluted to a cell density to yield single colonies on 150 mm 7H10/smeg plates supplemented with kanamycin. Individual colonies were patched onto 7H10/smeg medium lacking biotin but with 1 µg/mL avidin and onto 7H10/smeg medium with biotin. tn mutants which grew on medium containing biotin but not on medium lacking biotin were retested for biotin auxotrophy and confirmed auxotrophs were processed for transposon mapping as described previously (Siegrist and Rubin 2009). Briefly, biotin auxotrophs were grown to log phase and genomic DNA was prepared. Genomic DNA was digested with *Sac*II restriction endonuclease (NEB) overnight and fragments were self-ligated using T4 DNA ligase (NEB) overnight. The reaction was dialyzed, transformed into competent DH5α *λpir E. coli*, plated on LB agar supplemented with 40 µg/mL kanamycin, and incubated overnight at 37°C. A single colony was picked and used to inoculate a 5 mL culture of liquid LB broth supplemented with kanamycin. Plasmid DNA was prepared, and the insertion site was sequenced using primers (oNZL003/004) which anneal to the transposon sequence.

Growth of on solid medium lacking biotin

Strains were grown in 7H9/smeg medium with appropriate antibiotics to log phase, then washed three times in 7H9/smeg, with avidin substituted for biotin. ODs were normalized to a starting OD of 0.1, and then serial dilutions were spotted onto solid medium (spots 2-5 µL). Agar media cultures were incubated at 37°C for three days.

Growth in liquid medium lacking biotin

Strains were grown in 7H9/smeg medium with appropriate antibiotics to log phase, then washed three times in 7H9/smeg reconstituted using its components, but omitting biotin. Cultures were inoculated to a starting OD of 0.075 at 150 µL per well in a 96 well flat-bottomed clear microplate (Corning) in medium containing 1x (500 ng/mL), 1/10x, 1/100x, 1/1000x, or 0 biotin. Each strain/condition was repeated in triplicate. The microplate was incubated at 37°C for 36 hours in a Tecan M1000 plate reader constantly shaking at a 6 mm amplitude in orbital mode. OD600 readings were taken every 30 minutes for the duration of the experiment.

Sequence alignment

Sequence alignment was performed using the Clustal Omega web form (McWilliam et al. 2013, Sievers et al. 2011). Biotin carboxylase catalytic residues were identified via homology with the *E. coli* biotin carboxylase, (Janiyani et al. 2001) carboxytransferase catalytic residues were identified via homology with the *S. aureus* pyruvate carboxylase (Yu et al. 2009), and the biotin attachment residue was identified via the CDD database (Marchler-Bauer et al. 2017). Domain architecture was identified by homology to the *R. etli* pyruvate carboxylase (St Maurice et al. 2007).

Western blot analysis

Protein lysates were made from *M. smegmatis* cultures grown to mid-log OD_{600}, then washed three times in 7H9/smeg broth made without biotin but including avidin, then resuspended to various ODs such that the culture would reach OD 0.6 after biotin deprivation (OD 0.3 for 3h deprivations and 0.15 for 6

and 12 hour deprivations). Cultures were pelleted by centrifugation at 3000g for ten minutes, then supernatant was aspirated and the pellets were frozen overnight at -80°C. Pellets were resuspended in lysis buffer (50 mM Tris-HCl [pH 8.0], 50 mM NaCl, 2% SDS, 2 mM EDTA, 1 mM DTT, 1 mM PMSF) and lysed by bead beating with 0.1 mm zirconia beads in a Biospec Mini-Beadbeater-16 3 times for 45s each. Samples were centrifuged at 3000g for 10 minutes and soluble protein concentration in the supernatant was quantified by absorbance at 280 nm in a NanoDrop 1000 (Thermo). Samples were added 1:1 to 2x SDS sample buffer (20% glycerol, 125 mM Tris [pH 6.8], 4% SDS, 0.2% bromphenol blue, 100 mM DTT), boiled for 10 minutes, then cooled on ice before loading equal quantities of protein into a 4-12% NuPage Bis-Tris protein gradient gel (Thermo Fisher). Gels were run using MOPS SDS running buffer (Thermo Fisher) for 80 minutes at 150 V before being transferred to a Protran nitrocellulose membrane (Whatman) using a Trans-Blot semi-dry apparatus (Bio-Rad). Biotinylated protein was detected using streptavidin-HRP

Metabolomics

Metabolites were detected using LC-MS on samples prepared from *M. smegmatis* cultures grown on nitrocellulose filters as performed previously (Puckett et al. 2017, Eoh and Rhee 2013, de Carvalho et al. 2010). Strains were grown to mid-log OD in 7H9/smeg and then inoculated onto 0.22 µM nitrocellulose filters under vacuum filtration. Experiments were done in triplicate. Filters were placed on top of 7H10/smeg agar plates and allowed to grow at 37°C for two days, followed by transfer to 7H10/smeg agar plates made with biotin or without biotin and with avidin for three hours. Filters were

transferred to methanol/acetonitrile/water (2:2:1) precooled on dry ice to metabolically quench the bacteria and bacteria were scraped off of filters. Cells were lysed by bead beating with zirconia beads, centrifuged, and supernatants were filtered across 0.22 µM filters. LC-MS was performed with an Agilent Accurate Mass 6220 TOF coupled with an Agilent 1200 Liquid Chromatography system using a Cogent Diamond Hydride Type C as described previously (Eoh and Rhee 2013). Metabolites were identified based on unique accurate mass-retention time identifiers for masses exhibiting the expected distribution of accompanying isotopomers.

Metabolites were normalized to overall biomass using a generalized linear regression model which takes into account that most metabolites remain unchanged (Boyle et al. under review). Statistical analysis was performed using ANOVA for fixed effects on a linear mixed-effects model. The threshold of significance was adjusted for multiple hypotheses testing using the Bonferroni correction.

Reverse transcription-quantitative PCR

Relative mRNA levels were identified using reverse transcriptase-quantitative PCR (RT-qPCR). *M. smegmatis* cultures were grown to mid log OD and either not treated (+ biotin) or washed three times in 7H9/smeg lacking biotin and containing avidin before being resuspended in medium lacking biotin. All cultures were inoculated in triplicate to an OD of 0.3 and incubated at 37°C for three hours before being centrifuged at 3000g. The supernatant was aspirated and cells were frozen overnight at -80°C. Cells were lysed and RNA prepared using a GeneJET RNA Purification kit (Thermo) following the bacteria total RNA purification protocol with alterations. Before lysis, cells were resuspended

in 200 µL Tris-EDTA (TE) buffer supplemented with 1 mg/mL lysozyme. Cells were disrupted by beat beating with zirconia beads, and protein was digested with proteinase K for 5 minutes at room temperature. Lysis buffer was added and the mixture was vortexed, then ethanol was added and the mixture was centrifuged at 3000g. The supernatant was added to a GeneJET RNA purification column and the protocol followed as written.

M. tuberculosis cultures were grown to mid-log OD and were treated with 50 µM DETA-NO for 40 minutes (or not treated). Treatment was performed in triplicate. Cultures were centrifuged at 3000g and the supernatant was aspirated. Pellets were resuspended in Trizol reagent (Invitrogen). Cells were disrupted mechanically by bead beating with zirconia beads. RNA was extracted with chloroform, precipitated with isopropanol, washed with 70% ethanol, and then dried before being resuspended in water.

cDNA was synthesized using a Thermo Maxima First Strand cDNA synthesis kit with dsDNAse, using 500 ng of RNA per sample. qPCR was performed using a Thermo Scientific DyNAmo Flash Probe qPCR kit and TaqMan reagents on an Applied Biosystems 7500 quantitative PCR machine. Single amplifications were confirmed by the presence of a melting curve with a single peak, and the absence of contaminating genomic DNA was confirmed by the absence of amplification in control cDNA synthesis reactions performed without RT. The cycle threshold (C_T) value observed for each sample was normalized to the endogenous control value observed for the housekeeping gene *sigA* using the formula $\Delta C_T = C_{T;\,gene} - C_{T;\,sigA.}$ Normalized expression levels for each gene and condition were calculated using the formula $2^{(-\Delta C_T)}$.

Construction of mutants using CRISPR

Human codon-optimized Cas9 from pX330 (Cong et al. 2013) was cloned using a “dual control” system (Kim et al. 2013) under a tight anhydrotetracycline-dependent promoter with a mutated ribosome-binding site (SD5) (Woong Park et al. 2011) to produce an inducible plasmid (pAJF658) and integrated into the *M. smegmatis* genome at the L5 phage *attB* site. crRNA containing 20 nucleotides of homology to the desired cut site was fused to tracrRNA present on an episomal plasmid (pAJF619) to form a single guide RNA (sgRNA). The resultant vector was transformed into strains already containing pAJF658. Parent strains containing both pAJF658 and pAJF619 were grown to mid-log OD, induced with ATc for three hours or not induced for controls, and was cultured on 7H10/smeg plates containing and lacking ATc. Individual surviving colonies were picked for inductions which produced approximately 10-fold or more killing and colony PCR was performed to amplify the genomic DNA region surrounding the sgRNA targeted site. PCR products were treated with ExoSAP-IT (Thermo) and sequenced.

Construction of mutants using homologous recombination and double counterselection

Mutants were constructed using the method described in (Barkan, Stallings, and Glickman 2011). Briefly, plasmids were constructed containing 500 bp flanking regions 5’ and 3’ of the gene to be deleted. Plasmids also contained a hygromycin resistance cassette, as well as *galK* and *sacB* genes to be used for double counterselection. The plasmids lacked a mycobacterial origin of replication to prevent replication of the plasmid without integration via homologous recombination. Plasmids were transformed into parent strains

and intermediates were selected by resistance to hygromycin. Integrated plasmids were counterselected using 0.2% 2-deoxy-galactose (2-DOG) and 5% sucrose. Recombinations which produced genetic deletions were confirmed via southern blot.

Tests of sensitivity to in vitro stresses

M. tb cultures were grown to mid-log OD before being exposed to stresses, or not exposed as a control: 10 mM hydrogen peroxide, 4h exposure. 2.5 mg/mL lysozyme, 2h. 0.05% SDS, 2h. Acidified 7H9/TB medium, pH 4.5, 7d**.** 200 µM DETA-NO (Cayman Chemical) added daily, 3d. Cultures were exposed to stresses as 10 mL cultures in 30 mL PETG inkwell bottles (Nalgene) shaking at 150 RPM. Cultures were plated on 7H10/TB plates and incubated at 37^{o}C for 3 weeks before CFUs were enumerated. Exposures were performed in triplicates.

MIC Determination

Cultures were grown to mid-log OD before being exposed to stress or antibiotic. Cultures were diluted to OD 0.01 in 96-well plates with 200 µL culture volumes, excluding the outer wells, which were filled with water to minimize the effect of evaporation. Stress was added over a range of 2-fold dilutions. Cultures were exposed in triplicate. Plates were wrapped in parafilm and then added to a sealable plastic container before being incubated at 37^{o}C without shaking for one week. MICs were determined as the minimum concentration of stress or antibiotic necessary to prevent a visible pellet from forming. Strains were added to plates in triplicate.

Loebel model

Cultures were grown to mid-log OD before being washed three times in PBS. Cultures were resuspended in PBS at OD 0.05, and then added as 50 mL cultures in 650 mL suspension culture flasks incubated at 37^{o}C on their sides. Cultures were grown in triplicates. Cultures were plated on 7H10/TB plates and incubated at 37^{o}C for 3 weeks before CFUs were enumerated.

Wayne model

Wayne model experiments were performed as previously described (Wayne and Hayes 1996) with alterations. Briefly, cultures were grown to mid-log OD. Cultures were diluted to OD 0.005 in 7H9/TB. 17mL of cultures was added to sterile 20x125mm borosilicate glass tubes (Fisher) with a 1.5x8mm Teflon-coated stir bar (Fisher). 9 µg/mL methylene blue was added to one of three replicates to indicate hypoxia via decolorization. Tubes were tightly sealed with a rubber stopper, placed in a tube rack, and then stirred using a Wheaton Biostir stirring at 150 RPM and incubated at 37^{o}C.

To remove culture from the tube without introducing air, we withdrew culture using a 1 mL tuberculin syringe and an intradermal bevel 26Gx 3/8 precision glide needle (BD). Culture was plated on 7H10/TB plates and incubated at 37^{o}C for 3 weeks before CFUs were enumerated.

Construction of mutants

Mutants in *M. tb* were constructed using specialized transduction using the temperature sensitive phage phAE87 (Bardarov et al. 1997, Barkan et al. 2009). *Rip1* was deleted by allelic exchange with hyg^{R}. *M. tb* Δ*Rv2625c* was grown to OD 0.8 and then infected with phage at an MOI of 10 for 4h at 37^{o}C.

Hygromycin-resistant colonies were selected and genomic DNA was prepared for screening by Southern blotting.

Infection of mice

Strains were grown to mid-log OD, washed twice in PBS/0.05% Tween 80, and sonicated to disperse clumps, before being diluted in sterile water to OD 0.016. Mice were exposed to 4×10^7 CFU in a Middlebrook Inhalation Exposure System (Glas-Col). This dose of bacteria delivers 100 CFU per animal. Bacterial burden was determined by plating lung or spleen homogenates on 7H10/TB plates. Organs were homogenized using a Bullet Blender 5E homogenizer to bead beat organs in 2-4 mL of PBS/0.05% Tween 80 in 5mL tubes. Lungs were homogenized for 4 minutes at speed 8; spleens were homogenized for 8 minutes at speed 8. For histology, lungs were fixed in 10% phosphate buffered formalin for 24 hours at 4^oC before being washed in water, washed in ethanol, embedded in paraffin and stained.

Injection with pimonidazole

Mice were injected with 100 µL 15 mg/mL pimonidazole (Hypoxyprobe) suspended in water via the intraperitoneal route with a 1/2 cc U-100 insulin syringe with a permanently attached 28G ½ (0.36mm x 13mm) needle (BD). Mice were sacrificed 1-1.5 hours after injection, and embedded lung sections were stained with an anti-pimonidazole antibody conjugated to HRP and counterstained with hematoxylin.

APPENDIX A: LIST OF OLIGONUCLEOTIDES

Name	**Sequence**	**Relevant Features**
oNZL003	GCCTTCTTGACGAGTTCTTCTGAG	sequencing of transposon insertions (F direction)
oNZL004	CCGAGATAGGGTTGAGTGTTGTTC	sequencing of transposon insertions (R direction)
oCrBioQ-1F	CACCCTGGCATTTCGCCAACAAAC	crRNA deletion of *bioQ*
oCrBioQ-1R	AAACGTTTGTTGGCGAAATGCCAG	crRNA deletion of *bioQ*
oCrBioQ-2F	CACCGAGATCGTGGAGCAGC	crRNA deletion of *bioQ*
oCrBioQ-2R	AAACGCTGCTCCACGATCTCGGTG	crRNA deletion of *bioQ*
oBioF-F	CACCCGACATCGTGATGAC	primer for qPCR amplification of *bioF* (F direction)
oBioF-R	CGGTGTCGAAGATGAAC	primer for qPCR amplification of *bioF* (R direction)
oBioF-taq	CACGACGCTGTCGAAAGCACTG	taqMan probe for qPCR quantitation of *bioF*
oBioA-F	CTGGACACGGTGTTCTTC	primer for qPCR amplification of *bioA* (F direction)
oBioA-R	TCATCAACCGGTGCTTGG	primer for qPCR amplification of *bioA* (R direction)
oBioA-taq	TGGAGGTCGCGGTGAAGATG	taqMan probe for qPCR quantitation of *bioA*
oBioD-F	ACCGCATTGACCCTCGAAG	primer for qPCR amplification of *bioD* (F direction)
oBioD-R	ATCCAGTCTGCGTCAAAC	primer for qPCR amplification of *bioD* (R direction)
oBioD-taq	CGAACGCTTCGAGGCGTTGAG	taqMan probe for qPCR quantitation of *bioD*
oBioB-F	CATCATCAGCCTCAAGAC	primer for qPCR amplification of *bioB* (F direction)
oBioB-R	TTCGGTGGCACCGGTCTTTG	primer for qPCR amplification of *bioB* (R direction)
oBioB-taq	TGCCACTTCTGCTCGCAGT	taqMan probe for qPCR quantitation of *bioB*
oSigA-F	TGAGGTGACCGACGATCT	primer for qPCR amplification of *M. smegmatis sigA* (F direction)
oSigA-R	GGCATCAGCTTCTTCTTCCT	primer for qPCR amplification of *M. smegmatis sigA* (R direction)
oSigA-taq	AAGACACCGACCTGGAACTCG	taqMan probe for qPCR quantitation of *M. smegmatis sigA*
oTBSigA-F	CGACGAAGACCACGAAGAC	primer for qPCR amplification of *M. tuberculosis sigA* (F direction)
oTBSigA-R	TTTCGGTGGGTTCAGCGATCTCC	primer for qPCR amplification of *M. tuberculosis sigA* (R direction)
oTBSigA-taq	CGTCTTCATCCCAGACGAAATC	taqMan probe for qPCR quantitation of *M. tuberculosis sigA*
o2625c-F	TCTTGATCGCGTTGGGATTG	primer for qPCR amplification of *Rv2625c* (F direction)

APPENDIX A (continued)

o2625c-taq	CGAAGACGCCAGCAAGGACATCAG	taqMan probe for qPCR quantitation of *Rv2625c*
o2625c-R	CCCGGCGAATTGATGTAGAG	primer for qPCR amplification of *Rv2625c* (R direction)
oDosR-F	TCTGATCCTCACGTCCTACAC	primer for qPCR amplification of *dosR* (F direction)
oDosR-taq	TGCCAGCGGATATGTCGTCAAAG	taqMan probe for qPCR quantitation of *dosR*
oDosR-R	AGCGCCCACATCTTTGAC	primer for qPCR amplification of d*osR* (R direction)
oHspX-F	GAATTCGCGTACGGTTCCTTC	primer for qPCR amplification of *hspX* (F direction)
oHspX-taq	ATTAAGGCCACCTACGACAAGGG	taqMan probe for qPCR quantitation of *hspX*
oHspX-R	GCCACCGACACAGTAAGAATG	primer for qPCR amplification of *hspX* (R direction)
oClpP1-F	GTTATGCGCTCAGATTCTGC	primer for qPCR amplification of *clpP1* (F direction)
oClpP1-taq	CGAAGACGCCAGCAAGGACATCAG	taqMan probe for qPCR quantitation of *clpP1*
oClpP1-R	CCCGGCGAATTGATGTAGAG	primer for qPCR amplification of *clpP1* (R direction)

APPENDIX B: LIST OF PLASMIDS

Name	**Relevant Features**
pMSG419	TET-ON dependent expression vector with a polylinker for N-terminal HA fusions *hygR oriM oriE*
pNZL035	pMSG419 / MSMEG_2412
pNZL036	pMSG419 / MSMEG_2413
pNZL037	pMSG419 / MSMEG_2414
pNZL106	TET-ON dependent expression vector with a polylinker for N-terminal HA fusions *strepR oriM oriE*
pNZL035.strep	pNZL106 / MSMEG_2412 (pyruvate carboxylase)
pNZL065	pNZL106 / MSMEG_6648 (other annotated *M. smegmatis* pyruvate carboxylase)
pNZL070	pNZL106 / Rv2967c (*M. tuberculosis pyc*)
pNZL107	pNZL106 / MSMEG_2412 biotin carboxylase (BC) domain (2412 residues 1-441)
pNZL108	pNZL106 / MSMEG_2412 carboxytransferase (CT) domain (2412 residues 498-965)
pNZL109	pNZL106 / MSMEG_2412 CT + biotin binding (BCCP) domain (2412 residues 498-1128)
pNZL154	pNZL106 / MSMEG_2412 E288K biotin carboxylase catalytic site mutant
pNZL163	pNZL106 / MSMEG_2412 K1093L biotin attachment site mutant
pNZL164	pNZL106 / MSMEG_2412 K1093R biotin attachment site mutant
pNZL156	pNZL106 / MSMEG_3188 (BioA)
pNZL159	pNZL106 / MSMEG_3194 (BioB)
pAJF658	TET-ON dependent expression vector with a DAS tag for Dual Control / hCas9 *hygR oriE int attP*
pAJF619	tracrRNA parent plasmid *strepR oriE oriM*
pBioQ-1	pAJF619 fused to oCrBioQ-1F/R via oligonucleotide ligation
pBioQ-2	pAJF619 fused to oCrBioQ-2F/R via oligonucleotide ligation
pMV261.kan	Episomal mycobacterial vector *kanR oriM oriE*
pHMG121	pMV261.kan / Rip1 (*Rv2869c)*
pHMG221	pMV261.kan / Rip1H21A
pMSG395	pMV261.kan / Rip1ΔPDZ

APPENDIX C: LIST OF STRAINS

Strain number	**Description**	**Genotype/ Relevant Features**	**Reference**
MGM8000	WT	Wild Type *M. smegmatis* mc2155	Laboratory collection
MGM8001	m10	Mc2155 *MSMEG_2412::tn*	this work
MGM8002	m35	Mc2155 *bioB::tn*	this work
MGM8003	m43	Mc2155 *bioF::tn*	this work
MGM8004	m86	Mc2155 *bioA::tn*	this work
MGM8005	m119	Mc2155 *MSMEG_2412::tn*	this work
MGM8006	m134	Mc2155 *MSMEG_2412::tn*	this work
MGM8007	WT + EV	Mc2155 / pMSG419	this work
MGM8008	*pyc::tn* + EV	MGM8006 / pMSG419	this work
MGM8009	*bioA::tn* + EV	MGM8004 / pMSG419	this work
MGM8010	*bioB::tn* + EV	MGM8002 / pMSG419	this work
MGM8011	*pyc::tn* + pPyc	MGM8006 / pNZL035	this work
MGM8012	*pyc::tn* + p2413	MGM8006 / pNZL036	this work
MGM8013	*pyc::tn* + p2414	MGM8006 / pNZL037	this work
MGM8019	WT + EV	Mc2155 / pNZL106	this work
MGM8020	*pyc::tn* + EV	MGM8006 / pNZL106	this work
MGM8021	*bioA::tn* + EV	MGM8004 / pNZL106	this work
MGM8023	*pyc::tn* + pPyc	MGM8006 / pNZL035.strep	this work
MGM8024	*pyc::tn* + p6648	MGM8006/ pNZL065	this work
MGM8025	*pyc::tn* + pRv2967c	MGM8006/ pNZL070	this work
MGM8026	*pyc::tn* + pPyc (BC domain)	MGM8006 / pNZL107	this work
MGM8027	*pyc::tn* + pPyc (CT domain)	MGM8006 / pNZL108	this work
MGM8028	*pyc::tn* + pPyc (CT + BCCP domains)	MGM8006 / pNZL109	this work
MGM8029	*pyc::tn* + pPyc-E288K	MGM8006 / pNZL154	this work
MGM8030	*pyc::tn* + pPyc-K1093L	MGM8006 / pNZL163	this work
MGM8031	*pyc::tn* + pPyc-K1093R	MGM8006 / pNZL164	this work
MGM8034	*pyc::tn* + pBioA	MGM8006 / pNZL156	this work
MGM8035	*pyc::tn* + pBioB	MGM8006 / pNZL159	this work
MGM8036	*bioA::tn* + pBioA	MGM8004 / pNZL156	this work
MGM8037	*bioA::tn* + pBioB	MGM8004 / pNZL159	this work
MGM8041	*bioQ* mutant #16	MGM8006 *bioQ* frameshift 138-139 A	this work
MGM8050	Δrip1/ΔRv2625c	EF2 Δrip1::loxP ΔRv2625c:: hyg	this work
MGM8051	Δrip1/ΔRv2625c + pEV	MGM8050 / pMV261.kan	this work
MGM8052	ΔσKLM + pEV	MGM3256 / pMV261.kan	this work
MGM8053	ΔσD + pEV	MGM-JSS005 / pMV261.kan	this work
MGM6514	Δ*pyc*	Mc2155 *MSMEG_2412::hyg*	this work
MGM6516	Δ*bioQ*	Mc2155 *bioQ::hyg*	this work
MGM6520	*pyc::tn* / Δ*bioQ*	MGM8006 *bioQ::hyg*	this work
MGM6521	Δ*pyc* + EV	MGM6514 / pNZL106	this work

APPENDIX C (continued)

MGM6522	Δpyc + pNZL107	MGM6514 / pNZL107	this work
MGM6523	Δpyc + pNZL108	MGM6514 / pNZL108	this work
MGM6524	Δpyc + pNZL109	MGM6514 / pNZL109	this work
MGM6525	Δpyc + pNZL154	MGM6514 / pNZL154	this work
MGM6526	Δpyc + pNZL163	MGM6514 / pNZL163	this work
MGM6527	Δpyc + pNZL164	MGM6514 / pNZL164	this work
EF2	WT	M. tuberculosis Erdman	Laboratory collection
MGM309	Δrip1	EF2 Δrip1::hyg	(Makinoshima and Glickman 2005)
MGM345	WT + pEV	EF2 / pMV261.kan	(Sklar et al. 2010)
MGM349	Δrip1 + pEV	EF2 Δrip1::hyg / pMV261.kan	(Sklar et al. 2010)
MGM350	Δrip1 + pRip1	EF2 Δrip1::hyg / pHMG121	(Sklar et al. 2010)
MGM705	ΔRv2625c + pEV	EF2 ΔRv2625c::hyg / pMV261.kan	(Sklar et al. 2010)
MGM573	Δrip1 + pRip1-H21A	EF2 Δrip1::hyg / pHMG221	(Sklar et al. 2010)
MGM575	Δrip1 + pRip1ΔPDZ	EF2 Δrip1::hyg / pMSG395	(Schneider et al. 2013)
MGM3256	ΔσKLM	EF2 ΔσL::loxP ΔσM::hyg ΔσK::zeo	(Schneider, Sklar, and Glickman 2014)
MGM-JSS005	ΔσD	EF2 ΔσD::hyg	(Schneider, Sklar, and Glickman 2014)
MGM3206	Δrip1 cured	EF2 Δrip1::loxP	(Schneider, Sklar, and Glickman 2014)

REFERENCES

Aly, S., K. Wagner, C. Keller, S. Malm, A. Malzan, S. Brandau, F. C. Bange, and S. Ehlers. 2006. "Oxygen status of lung granulomas in Mycobacterium tuberculosis-infected mice." *J Pathol* 210 (3):298-305. doi: 10.1002/path.2055.

Attwood, P. V. 1995. "The structure and the mechanism of action of pyruvate carboxylase." *Int J Biochem Cell Biol* 27 (3):231-49.

Banaei, N., E. Z. Kincaid, S. Y. Lin, E. Desmond, W. R. Jacobs, Jr., and J. D. Ernst. 2009. "Lipoprotein processing is essential for resistance of Mycobacterium tuberculosis to malachite green." *Antimicrob Agents Chemother* 53 (9):3799-802. doi: 10.1128/AAC.00647-09.

Bardarov, S., J. Kriakov, C. Carriere, S. Yu, C. Vaamonde, R. A. McAdam, B. R. Bloom, G. F. Hatfull, and W. R. Jacobs, Jr. 1997. "Conditionally replicating mycobacteriophages: a system for transposon delivery to Mycobacterium tuberculosis." *Proc Natl Acad Sci U S A* 94 (20):10961-6.

Barkan, D., Z. Liu, J. C. Sacchettini, and M. S. Glickman. 2009. "Mycolic acid cyclopropanation is essential for viability, drug resistance, and cell wall integrity of Mycobacterium tuberculosis." *Chem Biol* 16 (5):499-509. doi: 10.1016/j.chembiol.2009.04.001.

Barkan, D., C. L. Stallings, and M. S. Glickman. 2011. "An improved counterselectable marker system for mycobacterial recombination using galK and 2-deoxy-galactose." *Gene* 470 (1-2):31-6. doi: 10.1016/j.gene.2010.09.005.

Beckett, D. 2007. "Biotin sensing: universal influence of biotin status on transcription." *Annu Rev Genet* 41:443-64. doi: 10.1146/annurev.genet.41.042007.170450.

Behar, S. M., M. Divangahi, and H. G. Remold. 2010. "Evasion of innate immunity by Mycobacterium tuberculosis: is death an exit strategy?" *Nat Rev Microbiol* 8 (9):668-74. doi: 10.1038/nrmicro2387.

Beisiegel, M., M. Kursar, M. Koch, C. Loddenkemper, S. Kuhlmann, U. Zedler, M. Staber, R. Hurwitz, and S. H. Kaufmann. 2009. "Combination of host susceptibility and virulence of Mycobacterium tuberculosis determines dual role of nitric oxide in the protection and control of inflammation." *J Infect Dis* 199 (8):1222-32. doi: 10.1086/597421.

Bordbar, A., N. E. Lewis, J. Schellenberger, B. O. Palsson, and N. Jamshidi. 2010. "Insight into human alveolar macrophage and M. tuberculosis interactions via metabolic reconstructions." *Mol Syst Biol* 6:422. doi: 10.1038/msb.2010.68.

Boyle, K. E., H. T. Monaco, M. Deforet, J. Yan, W. Wang, K. Y. Rhee, and J. B. Xavier. under review. "Metabolism and the evolution of social behavior."Submitted.

Burkovski, A. 2007. "Nitrogen control in Corynebacterium glutamicum: proteins, mechanisms, signals." *J Microbiol Biotechnol* 17 (2):187-94.

Chaba, R., B. M. Alba, M. S. Guo, J. Sohn, N. Ahuja, R. T. Sauer, and C. A. Gross. 2011. "Signal integration by DegS and RseB governs the σ E-mediated envelope stress response in Escherichia coli." *Proc Natl Acad Sci U S A* 108 (5):2106-11. doi: 10.1073/pnas.1019277108.

Chakravartty, V., and J. E. Cronan. 2012. "Altered regulation of Escherichia coli biotin biosynthesis in BirA superrepressor mutant strains." *J Bacteriol* 194 (5):1113-26. doi: 10.1128/JB.06549-11.

Cong, L., F. A. Ran, D. Cox, S. Lin, R. Barretto, N. Habib, P. D. Hsu, X. Wu, W. Jiang, L. A. Marraffini, and F. Zhang. 2013. "Multiplex genome engineering using CRISPR/Cas systems." *Science* 339 (6121):819-23. doi: 10.1126/science.1231143.

Cooper, A. M., J. E. Pearl, J. V. Brooks, S. Ehlers, and I. M. Orme. 2000. "Expression of the nitric oxide synthase 2 gene is not essential for early control of Mycobacterium tuberculosis in the murine lung." *Infect Immun* 68 (12):6879-82.

Cronan, J. E., Jr. 1988. "Expression of the biotin biosynthetic operon of Escherichia coli is regulated by the rate of protein biotination." *J Biol Chem* 263 (21):10332-6.

Cryle, M. J. 2010. "Selectivity in a barren landscape: the P450(BioI)-ACP complex." *Biochem Soc Trans* 38 (4):934-9. doi: 10.1042/BST0380934.

Datta, M., L. E. Via, W. Chen, J. W. Baish, L. Xu, C. E. Barry, 3rd, and R. K. Jain. 2016. "Mathematical Model of Oxygen Transport in Tuberculosis Granulomas." *Ann Biomed Eng* 44 (4):863-72. doi: 10.1007/s10439-015-1415-3.

de Carvalho, L. P., S. M. Fischer, J. Marrero, C. Nathan, S. Ehrt, and K. Y. Rhee. 2010. "Metabolomics of Mycobacterium tuberculosis reveals compartmentalized co-catabolism of carbon substrates." *Chem Biol* 17 (10):1122-31. doi: 10.1016/j.chembiol.2010.08.009.

Dietrich, J., S. Roy, I. Rosenkrands, T. Lindenstrom, J. Filskov, E. M. Rasmussen, J. Cassidy, and P. Andersen. 2015. "Differential influence of nutrient-starved Mycobacterium tuberculosis on adaptive immunity results in progressive tuberculosis disease and pathology." *Infect Immun* 83 (12):4731-9. doi: 10.1128/IAI.01055-15.

Driver, E. R., G. J. Ryan, D. R. Hoff, S. M. Irwin, R. J. Basaraba, I. Kramnik, and A. J. Lenaerts. 2012. "Evaluation of a mouse model of necrotic

granuloma formation using C3HeB/FeJ mice for testing of drugs against Mycobacterium tuberculosis." *Antimicrob Agents Chemother* 56 (6):3181-95. doi: 10.1128/AAC.00217-12.

Duque-Correa, M. A., A. A. Kuhl, P. C. Rodriguez, U. Zedler, S. Schommer-Leitner, M. Rao, J. Weiner, 3rd, R. Hurwitz, J. E. Qualls, G. A. Kosmiadi, P. J. Murray, S. H. Kaufmann, and S. T. Reece. 2014. "Macrophage arginase-1 controls bacterial growth and pathology in hypoxic tuberculosis granulomas." *Proc Natl Acad Sci U S A* 111 (38):E4024-32. doi: 10.1073/pnas.1408839111.

Ehlers, S., and U. E. Schaible. 2012. "The granuloma in tuberculosis: dynamics of a host-pathogen collusion." *Front Immunol* 3:411. doi: 10.3389/fimmu.2012.00411.

Eoh, H., and K. Y. Rhee. 2013. "Multifunctional essentiality of succinate metabolism in adaptation to hypoxia in Mycobacterium tuberculosis." *Proc Natl Acad Sci U S A* 110 (16):6554-9. doi: 10.1073/pnas.1219375110.

Feng, Y., J. Xu, H. Zhang, Z. Chen, and S. Srinivas. 2013. "Brucella BioR regulator defines a complex regulatory mechanism for bacterial biotin metabolism." *J Bacteriol* 195 (15):3451-67. doi: 10.1128/JB.00378-13.

Feng, Y., H. Zhang, and J. E. Cronan. 2013. "Profligate biotin synthesis in alpha-proteobacteria - a developing or degenerating regulatory system?" *Mol Microbiol* 88 (1):77-92. doi: 10.1111/mmi.12170.

Galloway, W. R., A. Isidro-Llobet, and D. R. Spring. 2010. "Diversity-oriented synthesis as a tool for the discovery of novel biologically active small molecules." *Nat Commun* 1:80. doi: 10.1038/ncomms1081.

Gengenbacher, M., S. P. Rao, K. Pethe, and T. Dick. 2010. "Nutrient-starved, non-replicating Mycobacterium tuberculosis requires respiration, ATP synthase and isocitrate lyase for maintenance of ATP homeostasis and viability." *Microbiology* 156 (Pt 1):81-7. doi: 10.1099/mic.0.033084-0.

Goldberg, M. F., N. K. Saini, and S. A. Porcelli. 2014. "Evasion of Innate and Adaptive Immunity by Mycobacterium tuberculosis." *Microbiol Spectr* 2 (5). doi: 10.1128/microbiolspec.MGM2-0005-2013.

Guirado, E., and L. S. Schlesinger. 2013. "Modeling the Mycobacterium tuberculosis Granuloma - the Critical Battlefield in Host Immunity and Disease." *Front Immunol* 4:98. doi: 10.3389/fimmu.2013.00098.

Gupta, R., M. A. Espinal, and M. C. Raviglione. 2004. "Tuberculosis as a major global health problem in the 21st century: a WHO perspective." *Semin Respir Crit Care Med* 25 (3):245-53. doi: 10.1055/s-2004-829520.

Harper, J., C. Skerry, S. L. Davis, R. Tasneen, M. Weir, I. Kramnik, W. R. Bishai, M. G. Pomper, E. L. Nuermberger, and S. K. Jain. 2012. "Mouse

model of necrotic tuberculosis granulomas develops hypoxic lesions." *J Infect Dis* 205 (4):595-602. doi: 10.1093/infdis/jir786.

Heinrich, J., and T. Wiegert. 2009. "Regulated intramembrane proteolysis in the control of extracytoplasmic function sigma factors." *Res Microbiol* 160 (9):696-703. doi: 10.1016/j.resmic.2009.08.019.

Helmann, J. D. 2002. "The extracytoplasmic function (ECF) sigma factors." *Adv Microb Physiol* 46:47-110.

Hoff, D. R., G. J. Ryan, E. R. Driver, C. C. Ssemakulu, M. A. De Groote, R. J. Basaraba, and A. J. Lenaerts. 2011. "Location of intra- and extracellular M. tuberculosis populations in lungs of mice and guinea pigs during disease progression and after drug treatment." *PLoS One* 6 (3):e17550. doi: 10.1371/journal.pone.0017550.

Hu, Y., and A. R. Coates. 2009. "Acute and persistent Mycobacterium tuberculosis infections depend on the thiol peroxidase TpX." *PLoS One* 4 (4):e5150. doi: 10.1371/journal.pone.0005150.

Hu, Y., and A. R. Coates. 2011. "Mycobacterium tuberculosis acg gene is required for growth and virulence in vivo." *PLoS One* 6 (6):e20958. doi: 10.1371/journal.pone.0020958.

Idh, J., M. Mekonnen, E. Abate, W. Wedajo, J. Werngren, K. Angeby, M. Lerm, D. Elias, T. Sundqvist, A. Aseffa, O. Stendahl, and T. Schon. 2012. "Resistance to first-line anti-TB drugs is associated with reduced nitric oxide susceptibility in Mycobacterium tuberculosis." *PLoS One* 7 (6):e39891. doi: 10.1371/journal.pone.0039891.

Islam, M. N., S. Sueda, and H. Kondo. 2005. "Construction of new forms of pyruvate carboxylase to assess the allosteric regulation by acetyl-CoA." *Protein Eng Des Sel* 18 (2):71-8. doi: 10.1093/protein/gzi011.

Janiyani, K., T. Bordelon, G. L. Waldrop, and J. E. Cronan, Jr. 2001. "Function of Escherichia coli biotin carboxylase requires catalytic activity of both subunits of the homodimer." *J Biol Chem* 276 (32):29864-70. doi: 10.1074/jbc.M104102200.

Jitrapakdee, S., M. St Maurice, I. Rayment, W. W. Cleland, J. C. Wallace, and P. V. Attwood. 2008. "Structure, mechanism and regulation of pyruvate carboxylase." *Biochem J* 413 (3):369-87. doi: 10.1042/BJ20080709.

Kamburov, A., R. Cavill, T. M. Ebbels, R. Herwig, and H. C. Keun. 2011. "Integrated pathway-level analysis of transcriptomics and metabolomics data with IMPaLA." *Bioinformatics* 27 (20):2917-8. doi: 10.1093/bioinformatics/btr499.

Kanetsuna, F. 1980. "Effect of lysozyme on mycobacteria." *Microbiol Immunol* 24 (12):1151-62.

Kim, H. S., U. Hoja, J. Stolz, G. Sauer, and E. Schweizer. 2004. "Identification of the tRNA-binding protein Arc1p as a novel target of in vivo biotinylation in Saccharomyces cerevisiae." *J Biol Chem* 279 (41):42445-52. doi: 10.1074/jbc.M407137200.

Kim, J. H., K. M. O'Brien, R. Sharma, H. I. Boshoff, G. Rehren, S. Chakraborty, J. B. Wallach, M. Monteleone, D. J. Wilson, C. C. Aldrich, C. E. Barry, 3rd, K. Y. Rhee, S. Ehrt, and D. Schnappinger. 2013. "A genetic strategy to identify targets for the development of drugs that prevent bacterial persistence." *Proc Natl Acad Sci U S A* 110 (47):19095-100. doi: 10.1073/pnas.1315860110.

Kohanski, M. A., D. J. Dwyer, B. Hayete, C. A. Lawrence, and J. J. Collins. 2007. "A common mechanism of cellular death induced by bactericidal antibiotics." *Cell* 130 (5):797-810. doi: 10.1016/j.cell.2007.06.049.

Koide, K., K. Ito, and Y. Akiyama. 2008. "Substrate recognition and binding by RseP, an Escherichia coli intramembrane protease." *J Biol Chem* 283 (15):9562-70. doi: 10.1074/jbc.M709984200.

Kramnik, I., W. F. Dietrich, P. Demant, and B. R. Bloom. 2000. "Genetic control of resistance to experimental infection with virulent Mycobacterium tuberculosis." *Proc Natl Acad Sci U S A* 97 (15):8560-5. doi: 10.1073/pnas.150227197.

Kroos, L., and Y. Akiyama. 2013. "Biochemical and structural insights into intramembrane metalloprotease mechanisms." *Biochim Biophys Acta* 1828 (12):2873-85. doi: 10.1016/j.bbamem.2013.03.032.

Kumar, A., J. C. Toledo, R. P. Patel, J. R. Lancaster, Jr., and A. J. Steyn. 2007. "Mycobacterium tuberculosis DosS is a redox sensor and DosT is a hypoxia sensor." *Proc Natl Acad Sci U S A* 104 (28):11568-73. doi: 10.1073/pnas.0705054104.

Leistikow, R. L., R. A. Morton, I. L. Bartek, I. Frimpong, K. Wagner, and M. I. Voskuil. 2010. "The Mycobacterium tuberculosis DosR regulon assists in metabolic homeostasis and enables rapid recovery from nonrespiring dormancy." *J Bacteriol* 192 (6):1662-70. doi: 10.1128/JB.00926-09.

Lin, S., and J. E. Cronan. 2011. "Closing in on complete pathways of biotin biosynthesis." *Mol Biosyst* 7 (6):1811-21. doi: 10.1039/c1mb05022b.

Lin, S., R. E. Hanson, and J. E. Cronan. 2010. "Biotin synthesis begins by hijacking the fatty acid synthetic pathway." *Nat Chem Biol* 6 (9):682-8. doi: 10.1038/nchembio.420.

Loebel, R. O., E. Shorr, and H. B. Richardson. 1933. "The Influence of Foodstuffs upon the Respiratory Metabolism and Growth of Human Tubercle Bacilli." *J Bacteriol* 26 (2):139-66.

MacMicking, J. D., R. J. North, R. LaCourse, J. S. Mudgett, S. K. Shah, and C. F. Nathan. 1997. "Identification of nitric oxide synthase as a protective locus against tuberculosis." *Proc Natl Acad Sci U S A* 94 (10):5243-8.

Makinoshima, H., and M. S. Glickman. 2005. "Regulation of Mycobacterium tuberculosis cell envelope composition and virulence by intramembrane proteolysis." *Nature* 436 (7049):406-9. doi: 10.1038/nature03713.

Marchler-Bauer, A., Y. Bo, L. Han, J. He, C. J. Lanczycki, S. Lu, F. Chitsaz, M. K. Derbyshire, R. C. Geer, N. R. Gonzales, M. Gwadz, D. I. Hurwitz, F. Lu, G. H. Marchler, J. S. Song, N. Thanki, Z. Wang, R. A. Yamashita, D. Zhang, C. Zheng, L. Y. Geer, and S. H. Bryant. 2017. "CDD/SPARCLE: functional classification of proteins via subfamily domain architectures." *Nucleic Acids Res* 45 (D1):D200-D203. doi: 10.1093/nar/gkw1129.

McGillivray, A., N. A. Golden, and D. Kaushal. 2015. "The Mycobacterium tuberculosis Clp gene regulator is required for in vitro reactivation from hypoxia-induced dormancy." *J Biol Chem* 290 (4):2351-67. doi: 10.1074/jbc.M114.615534.

McWilliam, H., W. Li, M. Uludag, S. Squizzato, Y. M. Park, N. Buso, A. P. Cowley, and R. Lopez. 2013. "Analysis Tool Web Services from the EMBL-EBI." *Nucleic Acids Res* 41 (Web Server issue):W597-600. doi: 10.1093/nar/gkt376.

Mishra, B. B., R. R. Lovewell, A. J. Olive, G. Zhang, W. Wang, E. Eugenin, C. M. Smith, J. Y. Phuah, J. E. Long, M. L. Dubuke, S. G. Palace, J. D. Goguen, R. E. Baker, S. Nambi, R. Mishra, M. G. Booty, C. E. Baer, S. A. Shaffer, V. Dartois, B. A. McCormick, X. Chen, and C. M. Sassetti. 2017. "Nitric oxide prevents a pathogen-permissive granulocytic inflammation during tuberculosis." *Nat Microbiol* 2:17072. doi: 10.1038/nmicrobiol.2017.72.

Mukhopadhyay, B., and E. Purwantini. 2000. "Pyruvate carboxylase from Mycobacterium smegmatis: stabilization, rapid purification, molecular and biochemical characterization and regulation of the cellular level." *Biochim Biophys Acta* 1475 (3):191-206.

Nambi, S., J. E. Long, B. B. Mishra, R. Baker, K. C. Murphy, A. J. Olive, H. P. Nguyen, S. A. Shaffer, and C. M. Sassetti. 2015. "The Oxidative Stress Network of Mycobacterium tuberculosis Reveals Coordination between Radical Detoxification Systems." *Cell Host Microbe* 17 (6):829-37. doi: 10.1016/j.chom.2015.05.008.

Nandakumar, M., C. Nathan, and K. Y. Rhee. 2014. "Isocitrate lyase mediates broad antibiotic tolerance in Mycobacterium tuberculosis." *Nat Commun* 5:4306. doi: 10.1038/ncomms5306.

Nawrocki, K. L., E. K. Crispell, and S. M. McBride. 2014. "Antimicrobial Peptide Resistance Mechanisms of Gram-Positive Bacteria." *Antibiotics (Basel)* 3 (4):461-92. doi: 10.3390/antibiotics3040461.

Owen, O. E., S. C. Kalhan, and R. W. Hanson. 2002. "The key role of anaplerosis and cataplerosis for citric acid cycle function." *J Biol Chem* 277 (34):30409-12. doi: 10.1074/jbc.R200006200.

Park, S. W., D. E. Casalena, D. J. Wilson, R. Dai, P. P. Nag, F. Liu, J. P. Boyce, J. A. Bittker, S. L. Schreiber, B. C. Finzel, D. Schnappinger, and C. C. Aldrich. 2015. "Target-based identification of whole-cell active inhibitors of biotin biosynthesis in Mycobacterium tuberculosis." *Chem Biol* 22 (1):76-86. doi: 10.1016/j.chembiol.2014.11.012.

Peters-Wendisch, P. G., C. Kreutzer, J. Kalinowski, M. Patek, H. Sahm, and B. J. Eikmanns. 1998. "Pyruvate carboxylase from Corynebacterium glutamicum: characterization, expression and inactivation of the pyc gene." *Microbiology* 144 (Pt 4):915-27. doi: 10.1099/00221287-144-4-915.

Pichugin, A. V., B. S. Yan, A. Sloutsky, L. Kobzik, and I. Kramnik. 2009. "Dominant role of the sst1 locus in pathogenesis of necrotizing lung granulomas during chronic tuberculosis infection and reactivation in genetically resistant hosts." *Am J Pathol* 174 (6):2190-201. doi: 10.2353/ajpath.2009.081075.

Polyak, S. W., A. Chapman-Smith, T. D. Mulhern, J. E. Cronan, Jr., and J. C. Wallace. 2001. "Mutational analysis of protein substrate presentation in the post-translational attachment of biotin to biotin domains." *J Biol Chem* 276 (5):3037-45. doi: 10.1074/jbc.M003968200.

Pozos, T. C., and L. Ramakrishnan. 2004. "New models for the study of Mycobacterium-host interactions." *Curr Opin Immunol* 16 (4):499-505. doi: 10.1016/j.coi.2004.05.011.

Puckett, S., C. Trujillo, Z. Wang, H. Eoh, T. R. Ioerger, I. Krieger, J. Sacchettini, D. Schnappinger, K. Y. Rhee, and S. Ehrt. 2017. "Glyoxylate detoxification is an essential function of malate synthase required for carbon assimilation in Mycobacterium tuberculosis." *Proc Natl Acad Sci U S A* 114 (11):E2225-E2232. doi: 10.1073/pnas.1617655114.

Ramakrishnan, L. 2012. "Revisiting the role of the granuloma in tuberculosis." *Nat Rev Immunol* 12 (5):352-66. doi: 10.1038/nri3211.

Ramos, J. L., M. Martinez-Bueno, A. J. Molina-Henares, W. Teran, K. Watanabe, X. Zhang, M. T. Gallegos, R. Brennan, and R. Tobes. 2005. "The TetR family of transcriptional repressors." *Microbiol Mol Biol Rev* 69 (2):326-56. doi: 10.1128/MMBR.69.2.326-356.2005.

Rao, S. P., S. Alonso, L. Rand, T. Dick, and K. Pethe. 2008. "The protonmotive force is required for maintaining ATP homeostasis and viability of hypoxic, nonreplicating Mycobacterium tuberculosis." *Proc Natl Acad Sci U S A* 105 (33):11945-50. doi: 10.1073/pnas.0711697105.

Raviglione, M., and G. Sulis. 2016. "Tuberculosis 2015: Burden, Challenges and Strategy for Control and Elimination." *Infect Dis Rep* 8 (2):6570. doi: 10.4081/idr.2016.6570.

Rhodius, V. A., W. C. Suh, G. Nonaka, J. West, and C. A. Gross. 2006. "Conserved and variable functions of the sigmaE stress response in related genomes." *PLoS Biol* 4 (1):e2. doi: 10.1371/journal.pbio.0040002.

Rodrigues, L., C. Villellas, R. Bailo, M. Viveiros, and J. A. Ainsa. 2013. "Role of the Mmr efflux pump in drug resistance in Mycobacterium tuberculosis." *Antimicrob Agents Chemother* 57 (2):751-7. doi: 10.1128/AAC.01482-12.

Rubin, E. J. 2009. "The granuloma in tuberculosis--friend or foe?" *N Engl J Med* 360 (23):2471-3. doi: 10.1056/NEJMcibr0902539.

Rudner, D. Z., P. Fawcett, and R. Losick. 1999. "A family of membrane-embedded metalloproteases involved in regulated proteolysis of membrane-associated transcription factors." *Proc Natl Acad Sci U S A* 96 (26):14765-70.

Russell, D. G., P. J. Cardona, M. J. Kim, S. Allain, and F. Altare. 2009. "Foamy macrophages and the progression of the human tuberculosis granuloma." *Nat Immunol* 10 (9):943-8. doi: 10.1038/ni.1781.

Rustad, T. R., M. I. Harrell, R. Liao, and D. R. Sherman. 2008. "The enduring hypoxic response of Mycobacterium tuberculosis." *PLoS One* 3 (1):e1502. doi: 10.1371/journal.pone.0001502.

Rustad, T. R., A. M. Sherrid, K. J. Minch, and D. R. Sherman. 2009. "Hypoxia: a window into Mycobacterium tuberculosis latency." *Cell Microbiol* 11 (8):1151-9. doi: 10.1111/j.1462-5822.2009.01325.x.

Sauer, U., and B. J. Eikmanns. 2005. "The PEP-pyruvate-oxaloacetate node as the switch point for carbon flux distribution in bacteria." *FEMS Microbiol Rev* 29 (4):765-94. doi: 10.1016/j.femsre.2004.11.002.

Scanga, C. A., V. P. Mohan, K. Tanaka, D. Alland, J. L. Flynn, and J. Chan. 2001. "The inducible nitric oxide synthase locus confers protection against aerogenic challenge of both clinical and laboratory strains of Mycobacterium tuberculosis in mice." *Infect Immun* 69 (12):7711-7. doi: 10.1128/IAI.69.12.7711-7717.2001.

Schaible, U. E., S. Sturgill-Koszycki, P. H. Schlesinger, and D. G. Russell. 1998. "Cytokine activation leads to acidification and increases maturation of Mycobacterium avium-containing phagosomes in murine macrophages." *J Immunol* 160 (3):1290-6.

Schneider, J. S., and M. S. Glickman. 2013. "Function of site-2 proteases in bacteria and bacterial pathogens." *Biochim Biophys Acta* 1828 (12):2808-14. doi: 10.1016/j.bbamem.2013.04.019.

Schneider, J. S., S. P. Reddy, H. Y. E, H. W. Evans, and M. S. Glickman. 2013. "Site-2 protease substrate specificity and coupling in trans by a PDZ-substrate adapter protein." *Proc Natl Acad Sci U S A* 110 (48):19543-8. doi: 10.1073/pnas.1305934110.

Schneider, J. S., J. G. Sklar, and M. S. Glickman. 2014. "The Rip1 protease of Mycobacterium tuberculosis controls the SigD regulon." *J Bacteriol* 196 (14):2638-45. doi: 10.1128/JB.01537-14.

Shi, C., T. W. Geders, S. W. Park, D. J. Wilson, H. I. Boshoff, O. Abayomi, C. E. Barry, 3rd, D. Schnappinger, B. C. Finzel, and C. C. Aldrich. 2011. "Mechanism-based inactivation by aromatization of the transaminase BioA involved in biotin biosynthesis in Mycobaterium tuberculosis." *J Am Chem Soc* 133 (45):18194-201. doi: 10.1021/ja204036t.

Sia, I. G., and M. L. Wieland. 2011. "Current concepts in the management of tuberculosis." *Mayo Clin Proc* 86 (4):348-61. doi: 10.4065/mcp.2010.0820.

Siegrist, M. S., and E. J. Rubin. 2009. "Phage transposon mutagenesis." *Methods Mol Biol* 465:311-23. doi: 10.1007/978-1-59745-207-6_21.

Sievers, F., A. Wilm, D. Dineen, T. J. Gibson, K. Karplus, W. Li, R. Lopez, H. McWilliam, M. Remmert, J. Soding, J. D. Thompson, and D. G. Higgins. 2011. "Fast, scalable generation of high-quality protein multiple sequence alignments using Clustal Omega." *Mol Syst Biol* 7:539. doi: 10.1038/msb.2011.75.

Silva Miranda, M., A. Breiman, S. Allain, F. Deknuydt, and F. Altare. 2012. "The tuberculous granuloma: an unsuccessful host defence mechanism providing a safety shelter for the bacteria?" *Clin Dev Immunol* 2012:139127. doi: 10.1155/2012/139127.

Sklar, J. G., H. Makinoshima, J. S. Schneider, and M. S. Glickman. 2010. "M. tuberculosis intramembrane protease Rip1 controls transcription through three anti-sigma factor substrates." *Mol Microbiol* 77 (3):605-17. doi: 10.1111/j.1365-2958.2010.07232.x.

Solbiati, J., and J. E. Cronan. 2010. "The switch regulating transcription of the Escherichia coli biotin operon does not require extensive protein-protein interactions." *Chem Biol* 17 (1):11-7. doi: 10.1016/j.chembiol.2009.12.007.

Solsona Peiro, J., M. L. de Souza Galvao, and M. N. Altet Gomez. 2014. "Inactive fibrotic lesions versus pulmonary tuberculosis with negative bacteriology." *Arch Bronconeumol* 50 (11):484-9. doi: 10.1016/j.arbres.2013.07.009.

Springer, B., S. Master, P. Sander, T. Zahrt, M. McFalone, J. Song, K. G. Papavinasasundaram, M. J. Colston, E. Boettger, and V. Deretic. 2001. "Silencing of oxidative stress response in Mycobacterium tuberculosis: expression patterns of ahpC in virulent and avirulent strains and effect

of ahpC inactivation." *Infect Immun* 69 (10):5967-73. doi: 10.1128/IAI.69.10.5967-5973.2001.

St Maurice, M., L. Reinhardt, K. H. Surinya, P. V. Attwood, J. C. Wallace, W. W. Cleland, and I. Rayment. 2007. "Domain architecture of pyruvate carboxylase, a biotin-dependent multifunctional enzyme." *Science* 317 (5841):1076-9. doi: 10.1126/science.1144504.

Stallings, C. L., and M. S. Glickman. 2010. "Is Mycobacterium tuberculosis stressed out? A critical assessment of the genetic evidence." *Microbes Infect* 12 (14-15):1091-101. doi: 10.1016/j.micinf.2010.07.014.

Subbian, S., L. Tsenova, P. O'Brien, G. Yang, M. S. Koo, B. Peixoto, D. Fallows, J. B. Zeldis, G. Muller, and G. Kaplan. 2011. "Phosphodiesterase-4 inhibition combined with isoniazid treatment of rabbits with pulmonary tuberculosis reduces macrophage activation and lung pathology." *Am J Pathol* 179 (1):289-301. doi: 10.1016/j.ajpath.2011.03.039.

Sueda, S., M. N. Islam, and H. Kondo. 2004. "Protein engineering of pyruvate carboxylase: investigation on the function of acetyl-CoA and the quaternary structure." *Eur J Biochem* 271 (7):1391-400. doi: 10.1111/j.1432-1033.2004.04051.x.

Tang, Q., X. Li, T. Zou, H. Zhang, Y. Wang, R. Gao, Z. Li, J. He, and Y. Feng. 2014. "Mycobacterium smegmatis BioQ defines a new regulatory network for biotin metabolism." *Mol Microbiol*. doi: 10.1111/mmi.12817.

Urban, S. 2009. "Making the cut: central roles of intramembrane proteolysis in pathogenic microorganisms." *Nat Rev Microbiol* 7 (6):411-23. doi: 10.1038/nrmicro2130.

van Crevel, R., T. H. Ottenhoff, and J. W. van der Meer. 2002. "Innate immunity to Mycobacterium tuberculosis." *Clin Microbiol Rev* 15 (2):294-309.

Vandal, O. H., J. A. Roberts, T. Odaira, D. Schnappinger, C. F. Nathan, and S. Ehrt. 2009. "Acid-susceptible mutants of Mycobacterium tuberculosis share hypersusceptibility to cell wall and oxidative stress and to the host environment." *J Bacteriol* 191 (2):625-31. doi: 10.1128/JB.00932-08.

Varia, M. A., D. P. Calkins-Adams, L. H. Rinker, A. S. Kennedy, D. B. Novotny, W. C. Fowler, Jr., and J. A. Raleigh. 1998. "Pimonidazole: a novel hypoxia marker for complementary study of tumor hypoxia and cell proliferation in cervical carcinoma." *Gynecol Oncol* 71 (2):270-7. doi: 10.1006/gyno.1998.5163.

Via, L. E., P. L. Lin, S. M. Ray, J. Carrillo, S. S. Allen, S. Y. Eum, K. Taylor, E. Klein, U. Manjunatha, J. Gonzales, E. G. Lee, S. K. Park, J. A. Raleigh, S. N. Cho, D. N. McMurray, J. L. Flynn, and C. E. Barry, 3rd. 2008. "Tuberculous granulomas are hypoxic in guinea pigs, rabbits, and

nonhuman primates." *Infect Immun* 76 (6):2333-40. doi: 10.1128/IAI.01515-07.

Voskuil, M. I., I. L. Bartek, K. Visconti, and G. K. Schoolnik. 2011. "The response of mycobacterium tuberculosis to reactive oxygen and nitrogen species." *Front Microbiol* 2:105. doi: 10.3389/fmicb.2011.00105.

Voskuil, M. I., D. Schnappinger, K. C. Visconti, M. I. Harrell, G. M. Dolganov, D. R. Sherman, and G. K. Schoolnik. 2003. "Inhibition of respiration by nitric oxide induces a Mycobacterium tuberculosis dormancy program." *J Exp Med* 198 (5):705-13. doi: 10.1084/jem.20030205.

Walsh, N. P., B. M. Alba, B. Bose, C. A. Gross, and R. T. Sauer. 2003. "OMP peptide signals initiate the envelope-stress response by activating DegS protease via relief of inhibition mediated by its PDZ domain." *Cell* 113 (1):61-71.

Wayne, L. G., and L. G. Hayes. 1996. "An in vitro model for sequential study of shiftdown of Mycobacterium tuberculosis through two stages of nonreplicating persistence." *Infect Immun* 64 (6):2062-9.

Wayne, L. G., and C. D. Sohaskey. 2001. "Nonreplicating persistence of mycobacterium tuberculosis." *Annu Rev Microbiol* 55:139-63. doi: 10.1146/annurev.micro.55.1.139.

Weaver, L. H., K. Kwon, D. Beckett, and B. W. Matthews. 2001. "Competing protein:protein interactions are proposed to control the biological switch of the E coli biotin repressor." *Protein Sci* 10 (12):2618-22. doi: 10.1110/ps.32701.

Woong Park, S., M. Klotzsche, D. J. Wilson, H. I. Boshoff, H. Eoh, U. Manjunatha, A. Blumenthal, K. Rhee, C. E. Barry, 3rd, C. C. Aldrich, S. Ehrt, and D. Schnappinger. 2011. "Evaluating the sensitivity of Mycobacterium tuberculosis to biotin deprivation using regulated gene expression." *PLoS Pathog* 7 (9):e1002264. doi: 10.1371/journal.ppat.1002264.

Yang, D., F. Ding, K. Mitachi, M. Kurosu, R. E. Lee, and Y. Kong. 2016. "A Fluorescent Probe for Detecting Mycobacterium tuberculosis and Identifying Genes Critical for Cell Entry." *Front Microbiol* 7:2021. doi: 10.3389/fmicb.2016.02021.

Yu, L. P., S. Xiang, G. Lasso, D. Gil, M. Valle, and L. Tong. 2009. "A symmetrical tetramer for S. aureus pyruvate carboxylase in complex with coenzyme A." *Structure* 17 (6):823-32. doi: 10.1016/j.str.2009.04.008.

Zaman, K. 2010. "Tuberculosis: a global health problem." *J Health Popul Nutr* 28 (2):111-3.